Molecular Dynamics Simulation Studies on Counteraction of Temperature-Induced and Urea-Conferred Protein Denaturation by Trehalose Molecules

A Thesis Submitted

in Partial Fulfillment of the Requirements

for the Degree of

DOCTOR OF PHILOSOPHY

by

Subrata Paul

to the

Department of Chemistry

Indian Institute of Technology Guwahati, India

2015

Dedicated to
my beloved parents and brother

Declaration

I hereby declare that the matter manifested in this thesis "*Molecular Dynamics Simulation Studies on Counteraction of Temperature-Induced and Urea-Conferred Protein Denaturation by Trehalose Molecules*" is the result of research carried out by me in the Department of Chemistry, Indian Institute of Technology Guwahati, India under the supervision of Dr. Sandip Paul.

In keeping with the general practice of reporting scientific observations, due acknowledgement has been made wherever the work described is based on the findings of other investigators.

Subrata Paul
IIT Guwahati

Certificate

It is certified that the work contained in this thesis entitled, "*Molecular Dynamics Simulation Studies on Counteraction of Temperature-Induced and Urea-Conferred Protein Denaturation by Trehalose Molecules*" has been carried out by Subrata Paul for the Degree of Doctor of Philosophy under my supervision and the same has not been submitted elsewhere for a degree.

Dr. Sandip Paul
Thesis Supervisor
Department of Chemistry
Indian Institute of Technology Guwahati
Guwahati-781039, India

Preface

Over the past few years, trehalose has generated considerable research interest to the community of biophysicists and biochemists for its ability to stabilize proteins and biomembranes from heat and chemical denaturation. It has been widely used for long term preservation of therapeutic proteins, foods, and cosmetics industries. Although trehalose's protein protecting ability under harsh environmental conditions is well-established and interest in how trehalose exerts its stabilizing effect has remained very active, what is still unknown is the mechanism by which trehalose exactly stabilizes proteins and offset temperature- and urea-conferred protein denaturation. The entitled thesis seeks to address this issue by means of classical molecular dynamics simulation

It is my great pleasure to express here few words of appreciation to the people who actually made this thesis a reality and an unforgettable experience for me. I wish, in particular, to express profound gratitude and sincere respect to my thesis supervisor Dr. Sandip Paul for his excellent guidance, constant encouragement, unstinting inspiration, and amicable cooperation during the course of this work. In my countless discussion sessions with him which I am going to treasure forever, he not only showed how science and its challenges could be made interesting to ease out a solution, but also taught me the way this fun conveyed to the others. I am indebted to Prof. Anumita Paul, Prof. Aiyagari Ramesh and Dr. Lal Mohon Kundu for periodically assessing my work and providing valuable suggestions for its improvement. My sincere thanks go to all other faculty members in the department for their kind help at various stages of my doctoral work.

I am grateful to Dhruba Da (Dr. Dhruba Jyoti Kalita), Renjith (Dr. Renjith B) and Somnath Da (currently in France), for their help and cheerful association, which were very much available in times of need. No words will be sufficient to express my feelings to labmates Dr. Rahul Sarma, Bhanita, Gargi, Shubhadip, Krishna and Srijita, whom I consider a part of my life. I am truly grateful to them for taking the time to listen to many questions arising in my mind and sharing their knowledge about computer simulations. They read several parts of the thesis and made suggestions for its betterment. I owe a lot to my friends Aswini, Apurba, Jiban, Naba, Jayanta, Subrata (Nath), Suraj, Paramartha

Sukanya, Pankaj, Sukhamoy, Satya, Arghya, Harikrishna, and Debashis and all other research scholars in the department for their lively company during my stay in IITG.

I take this opportunity to express my sincere thanks to all my teachers in school, college, and university days for helping and encouraging me in various aspects of life and academics. All of my learning from them will be an asset in every walk of my life. I am grateful to the institute and also Center for Development of Advanced Computing (CDAC) for the computational support.

Many thanks go at last but certainly not the least to my family for their understanding, encouragement, and patience in my every endeavor. This thesis would not have seen the light of this day without their great wishes, immense patience, and great sacrifice. A famous quote reads- "Every journey begins with a single step"- and today, only because of my family, I move a step uphill towards my zenith.

Subrata Paul

2015

"A scientific truth does not triumph by convincing its opponents and making them see the light, but rather because its opponents eventually die and a new generation grows up that is familiar with it."

– Max Planck

Outline of the Thesis

Chapter 1

Introduction

"Protein unfolding simulations are coming of age. They can be expected to fairly reliably depict protein folding/unfolding transition states, intermediate states, and denatured states, provided explicit solvent and good simulation techniques are employed. Simulations provide a molecular framework for the interpretation of experimental protein folding studies, and they are readily amenable to validation by comparison with experiment."

– V. Daggett *Chem. Rev.* **106**, 1898 (2006)

■ PROTEIN DENATURATION AND COUNTERACTION

Proteins are essential to all kinds of life on this planet and are found in all the living organisms and viruses known to us. Usually in all biological systems, proteins function as enzymes or as the building blocks of biological matter. The function of proteins depends on the specific three dimensional structure of the protein. Protein is a polypeptide chain, which contains sequence of amino acids. The specific sequence and the spatial arrangement of a peptide chain determine its three-dimensional structure. This three-dimensional structure remains in folded conformation in all living cells under so-called native conditions. However, under some non-native conditions, an alternative folding pathways can be accessed that sometimes result the total loss of structure. Such changes on the molecular level can lead to systemic malfunction and disease in the organisms.

Some physico-chemical conditions that are known to affect the folding of biomolecules are temperature, pressure, pH, solvent, co-solvent or salt concentration etc. As demonstrated by both experiments and simulations, a temperature change can significantly affect the protein folding [1-3] as well as the the stability of the native protein. Protein folding/unfolding equilibrium depends on melting temperature (T_m). A native protein is stable at melting temperature and can unfold upon cooling and heating [4-7]. Protein unfolding can be defined as a process where the spatial arrangement of the polypeptide chains within the biomolecule changes from the native protein to more disordered one *i.e.* alteration of three-dimensional structure [4]. In temperature induced protein denaturation, some bonds in a protein molecule are weakened. First, it affects the long range interaction, which is responsible for the stability of the tertiary structure. Because of the weakening of this interaction, protein becomes more flexible and internal groups are more exposed to the solvent. And, consequently, it breaks the hydrogen bonds of a helix upon heating and amide nitrogen and carbonyl oxygen form hydrogen bonds with the solvent molecules. Since, temperature is high, the short range interactions that initially direct protein folding are greatly weakened and the resulting structures are very different from the native structure [8]. An important consequence of these changes is the breaking of the subtle balance between hydrophobic and hydrophilic interactions in proteins.

In recent Raman spectroscopy and modulated differential scanning calorimetry (MDSC) investigation on lysozyme, Hédoux and co-workers [9] describe the two stage process of thermal denaturation of protein. Firstly, they reported that due to the breaking of hydrogen bond network of water, water molecules penetrate into the tertiary structure of

proteins and the tertiary structure becomes more flexible with out a conformational change in the secondary structure. This breaking of hydrogen bond network of water induced a predenaturational stage of protein with intact secondary structure. Such intermediate stage is also observed in previous investigations on different proteins [10-13]. This transformation from native to transient tertiary structure is characterized by decreased hydrophobic interactions in the protein interiors and which appears to be the precursor to the second stage of thermal denaturation, *i.e.* the unfolding process of the secondary structure.

Protein denaturation also occurs in the presence of chemical denaturant urea. It has been known for many years that a high concentration of urea can cause protein denaturation in solution [14, 15] and hence inhibit many important biological activities. Based on numerous experimental and theoretical studies, two mechanisms namely *direct* and *indirect* mechanism have been proposed for urea-conferred protein denaturation. According to *direct* mechanism, urea molecules interact directly by forming hydrogen bonds with the protein backbone or side chains and stabilize the unfolded state of protein [16-30]. The *indirect* mechanism presumes that urea molecules act indirectly by altering the water structure and thereby the hydration of the protein getting enhanced [31-38]. Despite the extensive studies from both experiment and theory in the past several decades, the mechanisms by which urea-induced protein denaturation occurs are far from conclusive. For example, the studies on two peptides, chicken villin headpiece (HP-35) and its mutant, and a number of β-hairpin structures, Gao and co-workers proposed that urea induced denaturation of proteins involves both the *direct* and *indirect* mechanisms [38-40]. In an another study, it has been reported that both mechanisms are operative in urea-induced protein denaturation [37]. From the molecular dynamics (MD) simulation, Bennion and Daggett also suggest that both *direct* and *indirect* mechanism play an important role in the denaturation process of chymotrypsin inhibitor 2 (CI2) in 8 M urea [41]. Clearly, urea has strong direct and indirect effect on urea-induced protein denaturation and range of opinions are very broad. Therefore, it remains as an active field in protein science.

To adapt these harsh environmental conditions, organisms generally accumulate some other osmolytes that counteract protein perturbation. Based on the effects on both stability and function, these osmolytes are often classified either as 'compatible' or 'counteracting' [42, 43]. Compatible osmolytes increase protein stability against denaturation without affecting protein functional activity. Counteracting osmolytes, on the other hand are believed to cause changes in protein function. Some methylamines (trimethylamine-N-oxide [TMAO], betaine etc.) are considered counteracting osmolytes. And, certain amino

acids (e.g. proline and glycine) and polyols (e.g. trehalose, sucrose, and sorbitol) are considered compatible osmolytes that protect proteins from thermal and chemical denaturation. Among the compatible polyols, trehalose is a prevalent molecule used by nature to protect organisms against extreme conditions [44-46]. It is a non-reducing disaccharide and composed of two glucopyranosyl units linked together through an α, α -(1→1) glycosidic oxygen linkage between their anomeric carbon atoms. The chemical structure of trehalose is shown below.

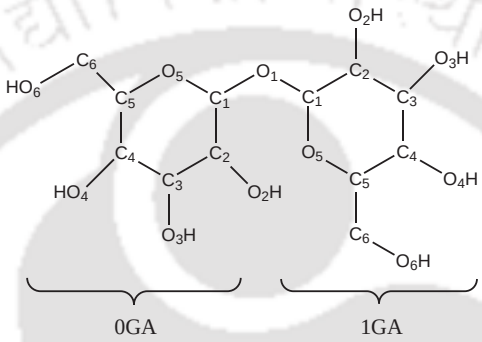

Trehalose molecule. All carbon, oxygen and hydroxyl hydrogen are labeled. The other hydrogen atoms are left off for clarity.

Certain organisms (for example yeast and nematodes), plants, and insects etc produce this sugar molecule to protect the biomolecules from the environmental stress and preserve the native activity of the protein [47, 48]. In addition, trehalose molecule is widely used as an additive for long term preservation of therapeutic proteins, foods and cosmetics in industries. Therefore, the use of trehalose molecules in the preservation of proteins becomes the active field of fundamental research for those industries [49-51]. Further, as reported recently, it also acts as a stabilizer to stabilize blood platelet cells [52].

The question of significant interest is then, how does trehalose cause protein stabilization and protect proteins from external stress? A large number of studies have been devoted in this direction, but the mechanism has remained somewhat elusive. On the basis of molecular properties, three hypothesis have been proposed to explain the action of trehalose on molecular level: (1) Mechanical entrapment hypothesis: According to this hypotheses trehalose molecules form a highly viscous glassy matrix that protects the biomolecule in its biological conformation (due to strong reduction in the protein dynamical fluctuations) like an insect trapped in amber [53, 54] *i.e.* concentrated trehalose solution is likely to

vitrify before the complete removal of water molecules. This glass formation by trehalose molecules can kinetically maintain the conformation of proteins and prevent the fusion of membranes. Again, Green and Angell [53] suggested that because of the higher glass transition temperature (T_g), trehalose is a better bioprotectant than maltose or sucrose. (2) Water replacement hypothesis: This hypothesis suggests that trehalose molecules replace water molecules from protein hydration shell (and form direct hydrogen bonds with the protein) thereby stabilizing the three-dimensional structure of protein during dehydration [55-57]. (3) Water entrapment hypothesis: According to this hypothesis trehalose molecules do not bind directly to biomolecules. Rather, they entrap the water molecules in the intermediate layer between them and the biomolecule, thus preserve the native solvation of the biomolecule [58]. This mechanism indirectly suggests the preferential exclusion of trehalose molecules from the protein surface [59, 60] and acts as preferential hydration hypothesis of the biomolecule. Many simulation studies of membrane/sugar/water systems [61-64] indicate that sugars, and especially trehalose, interact directly with membrane by forming hydrogen bonds between the several adjacent phospholipids. An IR spectra study of dry protein-sugar mixture shows that the protection of protein occurs due to formation of direct sugar-protein hydrogen bond [55]. On the other hand, Lines *et al.* [65] have studied trehalose-lysozyme interactions at a concentration of about 18 wt % and reported the trehalose induced retention of protein hydration layer. Similarly, Cotton *et al.* [66] have shown that trehalose is preferentially excluded from the protein surface at 50 and 89 wt %. Moreover, the destructuring effect of trehalose on water structure is also considered as another mechanism of trehalose bioprotection. According to Branca *et al.* [67, 68] trehalose destructure the tetrahedral hydrogen bond network of water and thereby obstruct the crystallization. So the damages caused by the formation of ice do not take place. In addition, several studies [69, 70] on the hydration of sugars said that trehalose strongly slow down the dynamics of the water molecules that are present in their vicinity. From the Terahertz spectroscopy measurement, Heyden *et al.* [69] observed that disaccharides slow down the dynamics of water at a distance of 6.5 Å from the solute molecules. Similarly, Magazu *et al.* [70] reported that trehalose induces a stronger retardation of water dynamics than other disaccharides (maltose and sucrose) from their Quasi Elastic Neutron Scattering experiment. Apparently, all the mechanisms that are proposed for trehalose is non-specific i.e any mechanism alone is not sufficient to answer this question.

Trehalose is produced by some anhydrobiotic organisms during the heat shock and thermo-tolerance. It has been found to protect the enzyme activity and protein ag-

gregation during heat shock [71], and also increase the thermal stability of proteins [72]. Trehalose increases the stability of proteins by raising the melting temperature of RNase A by 18 °C in 2M trehalose solution [72]. Thus trehalose makes them less prone to unfolding by heat, and helps them in retaining their structure and function. Thermal stabilization and retention of enzyme activity at 1.5 M trehalose solution is also observed by Sola-Penna *et al.* [73]. On the other hand, trehalose also preserve the cells from freezing damage by suppressing the ice formation [74]. Thus, trehalose not only protects biomolecules from heat, but also from freezing damage and that is why it is termed as cryoprotectant. Recent investigations carried out on Lysozyme [9, 75, 76], Beta-lactoglobulin [46] and bovine serum albumin [77] show that trehalose can protect the proteins from thermal denaturation. The detailed analysis of Raman scattering experiment [75, 76] and molecular dynamics simulation study [77] have shown that trehalose's thermostabilization effect on proteins is due to the two complementary effects. First, trehalose destructure the tetrahedral hydrogen bond network of water, which is in agreement with the analyses performed on water-sugar solutions [78, 79] and strengthening of the O-H interactions in the water hydrogen bond network. This strengthening of hydrogen bond network of bulk water surrounding the protein in presence of trehalose induces less flexibility to the tertiary structure of protein [75]. This is the main consequence of thermal stabilization of native structure from extended temperature range. Moreover, Lerbret *et al.* [77] suggested that the slowing down of dynamical properties of lysozyme and water in presence of trehalose causes stabilization of the globular proteins against thermal denaturation. Secondly, sugars are preferentially excluded form the protein hydration shell and preserve the native conformation, which is in line with preferential hydration hypothesis. Further, Dirama *et at.* [80] reported a strong coupling between lysozyme and trehalose molecules correlated with the dynamics of protein-sugar intermolecular hydrogen bonds. Most recently, it has been found that trehalose interact preferentially with the polar side chains of the protein and stabilizes the native conformation of protein from thermal denaturation [81].

Trehalose has also received a special attention as a protectant of structure and function of protein against chemical denaturation of urea. Recently, by means of differential scanning calorimetry and circular dichroism study, it has been reported that trehalose can offset the denaturation activity of urea on α-chymotrypsin. The results of this study demonstrated that 1:2 molar ratio of trehalose and urea is required in order to observe significant effectiveness of trehalose [82]. Contrary to this, very recent theoretical studies [83, 84] reported that 1:8 molar ratio of trehalose and urea is sufficient to fully offset the

deleterious effect of urea on protein. Zhang *et al.* [84] further argued (by citing previously reported comparative studies involving theoretical as well as experimental works [85-87]) that the molar ratio of structure protectant osmolyte and urea can be different for theory from the experiment and they may not necessarily always be the same. Nevertheless, in the context of urea-induced protein denaturation, these studies have directed towards the direct mechanism where urea molecules interact directly with the protein. They further suggested that in urea/trehalose mixed solution trehalose-induced protection of biomolecules comes from the enhancement in the water structure as well as preferential exclusion of trehalose molecules from the protein surface (along with this, expulsion of a few urea molecules due to trehalose-urea hydrogen bond interactions also observed). Apparently, the studies of the counteracting effect of trehalose on denaturing effect of urea on biomolecules are very limited.

Thus, how trehalose stabilizes proteins and counters the temperature induced and urea-conferred protein denaturation remains to be an important issue in protein science. In the current study, an effort has been made to address this issue by means of classical MD computer simulations. First, we extrapolate the results from binary trehalose solutions at different temperature. Secondly, we demonstrate the counteracting ability of trehalose against urea denaturation at ambient temperature condition. The simulation works and concluding remarks are presented in the subsequent four chapters. The next section of the present chapter deals with the basic techniques of MD simulation that is employed in our work. The details analyses of the applications of these techniques for specific systems are given in later chapters. This is followed by a brief description of the work presented in the current thesis.

■ METHODOLOGY

In this thesis, classical molecular dynamics (MD) simulation technique has been employed. It has been widely used to investigate the structure and dynamics of biomolecular systems, such as proteins, nucleic acids, and small molecules like amino acids and sugars. In MD simulation, the potential energy function (U) is described by all interactions between the atoms that are covalently bonded as well as non-bonded interactions between atoms and molecules in the condensed phase. The interactions between particles are governed by the so-called force field parameterization [88]. Note that, through out this thesis, specific AMBER10/12 force field parameter sets are used [89, 90].

The potential energy function is written as a sum of bonded and non-bonded

interaction terms

$$U = U_{bond} + U_{angle} + U_{dihedral} + U_{vdw} + U_{Coulomb} \tag{1.1}$$

The first three terms (U_{bond}, U_{angle}, $U_{dihedral}$) are the bonded terms, which describe the bond stretching, angle bending, and torsion rotation, and the last two terms are for the non-bonded potential. In bonded terms, the bond and angle contributions are described by harmonic potentials and all of the interactions between directly bonded atoms (1-2 interactions), angles (1-3 interactions, where two atoms bonded to a common atom), and torsion (interactions between pairs of 1-4 atoms) are defined as:

$$U_{bond} = \sum_{bonds} K_b(b_{ac} - b_{eq})^2 \tag{1.2}$$

$$U_{angle} = \sum_{angles} K_\theta(\theta_{ac} - \theta_{eq})^2 \tag{1.3}$$

$$U_{dihedral} = \sum_{dihedrals} \frac{V_n}{2}(1 + cos(n\phi - \delta)) \tag{1.4}$$

The letters b, θ, ϕ, and δ represent the bond length, bond angle, dihedral angle, and phase angle, respectively. The subscripts ac stands for actual and eq stands for equilibrium. The parameters K_b, K_θ, and V_n are the force constants for bond, bond angle, and dihedral angle, respectively.

The non-bonded potentials are calculated using two terms, the first one is the Lennard-Jones term (U_{vdw}) [91] describing the van der Waals interaction [92], and the second one is the Coulomb term ($U_{coulomb}$) [93] that deals with the electrostatic interactions between particles having partial charges on them. The non-bonding interaction terms are defined as:

$$U_{vdw} = \sum_i \sum_{i<j} 4\epsilon_{ij}\left[\left(\frac{\sigma_{ij}}{r_{ij}}\right)^{12} - \left(\frac{\sigma_{ij}}{r_{ij}}\right)^{6}\right] \tag{1.5}$$

$$U_{coulomb} = \sum_i \sum_{i<j} [\frac{q_i q_j}{4\pi\epsilon_o r_{ij}}] \tag{1.6}$$

where the overall sum is over all the atom pairs i and j. σ and ϵ are the Lennard-Jones separation at minimum (i.e. equilibrium distance) and well depth energy, respectively. r_{ij} is the inter-atomic distance. q_i and q_j are the partial charges on interaction sites i and j and ϵ_o is the electrical permittivity.

The aim of the MD simulation is to observe the evolution of atomic coordinates in time. We consider an N-particle system characterized by the following Hamiltonian

$$H = \sum_{i=1}^{N} \frac{p_i^2}{2m} + U(\mathbf{r}^N) \tag{1.7}$$

where m is the mass of each particle, p_i is the momentum of the i-th particle and $U(\mathbf{r}^N)$ is the total potential energy of the system which includes the all particle-particle interactions. The coordinates of the particles are denoted by $\mathbf{r}^N = \{\mathbf{r}_1, \cdots, \mathbf{r}_N\}$. The position and velocity of i-th particle is represented by $\mathbf{r}_i$ and $\mathbf{v}_i$, respectively. The method of molecular dynamics consists of solving the equation

$$a_i = \frac{\mathbf{F_i}}{m_i} \tag{1.8}$$

where $i = 1, 2, ...N$, m_i is the mass of i-th particle and $\mathbf{F}_i$ is the force acting on particle i. This equation is obtained easily from the Lagrangian

$$L = \frac{1}{2}\sum_{i=1}^{N} m_i \mathbf{v_i}.\mathbf{v_i} - \frac{1}{2}\sum_{i=1}^{N}\sum_{j\neq i}^{N} u(r_{ij}) \tag{1.9}$$

where the potential U has been assumed to be the sum of pair potentials u_{ij}. The Lagrangian equation of motion is

$$\frac{d}{dt}\left(\frac{\partial L}{\partial \dot{q}_i}\right) - \frac{\partial L}{\partial \dot{q}_i} = 0 \tag{1.10}$$

It is clear from Eq. 1.10 that the dynamics of particles is described by 3N number of second order differential equations.

It is also possible to write down the Hamiltonian (H) for the system and solve the the Hamiltonian equations of motion

$$\dot{\mathbf{q}}_k = \frac{\partial H}{\partial p_k} \tag{1.11}$$

$$\dot{\mathbf{p}}_k = -\frac{\partial H}{\partial q_k} \tag{1.12}$$

where $\mathbf{q}_k$ and $\mathbf{p}_k$ represent generalized coordinates and momenta. For a system with pairwise interaction potential, the Hamiltonian is

$$H = \frac{1}{2}\sum_{i=1}^{N} m_i \mathbf{v_i}.\mathbf{v_i} + \frac{1}{2}\sum_{i=1}^{N}\sum_{j\neq i}^{N} u(r_{ij}) \tag{1.13}$$

and Eqs. 1.11 and 1.12 yield

$$\frac{dr_i}{dt} = \frac{\mathbf{p_i}}{m_i} \tag{1.14}$$

$$-\dot{\mathbf{p}}_i = -\nabla \mathbf{u} = \mathbf{F_i} \tag{1.15}$$

where i=1,2,....N. There are now $6N$ first order differential equations to be solved.

The equation of motion is solved numerically to yield particle velocities and positions as a function of time. It is usually integrated by using finite difference approach. The Verlet algorithm is one of the most commonly used algorithm for this purpose [94]. The advantage of the use of Verlet algorithm is that its implementation is straightforward and storage requirements are modest. Although, it has the disadvantage of moderate precision during the calculation and velocity does not appear explicitly in the Verlet integration. As an improvement to the Verlet algorithm, the leap-frog algorithm [95] has been developed. But, it has a disadvantage that the positions and velocities are not synchronized. As an alternative of Verlet or the leapfrog algorithm, Velocity Verlet algorithm has been developed and the following relations are used to calculate new position and velocity at the same time:

$$r(t+dt) = r(t) + v(t)dt + \frac{1}{2}a(t)dt^2 \tag{1.16}$$

$$v(t+dt) = v(t) + \frac{1}{2}[a(t) + a(t+dt)]dt \tag{1.17}$$

To calculate the velocities at time t+dt, this method requires acceleration at time t and t+dt. In the present work, we have employed Velocity Verlet algorithm.

■ PRESENT WORK

Because of trehalose's well-documented counteracting effect against protein denaturation by high temperature or urea and its unresolved issues concerning the mechanism, we perform simulations for investigating the role of trehalose in stabilizing protein conformation both at ambient and high temperature and in presence of urea. Each of the chapters that describe our simulations (**Chapters 2-4**) is divided into two parts: Part A and Part B. Part A concentrates on role of trehalose on protein stabilization on thermal denaturation, whereas Part B focuses on the same in urea/trehalose mixture at ambient conditions. In **Chapters 2**, we deal with hydrophobicity of neopentane molecules with increasing trehalose concentration at different temperatures or urea-trehalose solution at ambient temperature. The small solute neopentane is computationally effective to understand hydrophobicity in aqueous environments and displays many of the characteristics that one expects to find only in very large hydrophobic objects. In Part A, we have examined the aggregation of non-polar solutes in pure water at five different temperature as well as in aqueous solutions of increasing trehalose concentrations. While, in Part B, hydrophobic aggregation is

investigated in pure water as well as binary and ternary solutions of urea and trehalose in relevance to protein denaturation and counteraction. An insight picture of the temperature- and osmolyte-induced modification of hydrophobic interaction is obtained by examining direct interactions of the solute with solution species. The neopentane-neopentane potential of mean force is investigated. Then, the preferential accumulation or depletion of solution species near the solute is examined by calculating time-averaged normalized ratio of water oxygen, urea carbon, and trehalose hydroxyl oxygens in different solutions. This is followed by investigation of solvation of osmolyte by water and its indirect effect on water structure is carried out. The usual water oxygen−oxygen radial distribution function (rdf) is used to describe water structuring. Finally, the hydrogen bond properties, cluster structure of trehalose and dynamics of solution species are studied to describe molecular behavior of trehalose on protein stabilization.

In **Chapter 3**, solvation characteristics of N-methylacetamide (NMA) are investigated thoroughly in presence and absence of urea and trehalose at different temperatures. The solute NMA is of interest mainly because it is the smallest amide that contains the peptide linkage, the important fraction determining the extent of protein (de)stabilization by osmolytes, as well as hydrophobic sites, and represents the typical solvent-exposed state of proteins. Part A of this chapter focuses on NMA solvation at five different temperatures with increasing trehalose concentration. The structural properties of NMA with the solution species together with the dynamical behavior of solution species are investigated. To shed light on the counteracting mechanism, we have also calculated here the number of hydrogen bonds of NMA with the water and trehalose molecules. In Part B, we have extended our examination of NMA hydration characteristics in pure water and binary and ternary solutions of urea and trehalose at ambient temperature. The solvation of NMA atomic sites is analyzed first in presence and absence of urea and trehalose. And then, preference of solution species near the solute is examined by calculating time-averaged normalized ratio of water oxygen, urea carbon, and trehalose hydroxyl oxygens in different solutions. This is followed by investigations of water structure in these different solution conditions are performed and water oxygen−oxygen rdf is used to describe water structuring. The hydrogen bond properties and dynamics of solution species are also examined.

Chapter 4 deals with counteracting behavior of trehalose with a more realistic 15-residue model peptide. Here, we have investigated the structural change of the peptide and interactions of peptide residues with solution species in pure water as well as in binary and ternary solutions of urea and trehalose at different temperatures. In Part A, we have

calculated the temperature dependent root mean square deviation (rmsd) of C_α atoms of the peptide to see the counteracting ability of trehalose against temperature denaturation. Further, site-site rdfs between the peptide and solution species are computed to observe the solution structure near the peptide in pure water and with increasing trehalose concentration at denaturing temperature. Thereafter, we have given a close look on the solution compositions near to the peptide. We also investigate the cluster structure of trehalose in different solutions. Finally, hydrogen bonding interactions between the peptide and solution species and dynamical properties are investigated to shed the molecular mechanism of trehalose on protein stabilization. In Part B, we address the counteracting effect of trehalose against the urea conferred protein denaturation. First, we analyze the role of urea on the urea-induced protein denaturation by analyzing structural and dynamical properties of binary urea solution. After that, we investigate, how does trehalose counteract the urea-induced protein denaturation? How does trehalose interact with the peptide residues, water and urea? What is the role of trehalose on the peptide solvation and water structure in ternary urea/trehalose solution? At the end, in **Chapter 5**, we present the summary of the results together with our view on trehalose's protein protecting action.

Chapter 2

Effect of Hydrophobic Interaction

"The hydrophobic effect – the tendency for oil and water to segregate – is important in diverse phenomena, from the cleaning of laundry, to the creation of micro-emulsions to make new materials, to the assembly of proteins into functional complexes. This effect is multifaceted depending on whether hydrophobic molecules are individually hydrated or driven to assemble into larger structures. Despite the basic principles underlying the hydrophobic effect being qualitatively well understood, only recently have theoretical developments begun to explain and quantify many features of this ubiquitous phenomenon."

– D. Chandler *Nature(London)* **437**, 640 (2005)

Hydrophobic interactions have been hypothesized as one of the driving force in biomolecular process [4, 96-99]. Most importantly, protein folding and unfolding depend on the collapse and aggregation of strongly hydrophobic amino acid residues in proteins. As in proteins, hydrophobic interaction plays an important role in other biological self-assembly processes such as micelle formation, lipid membrane formation, and molecular recognition. Because of its well-recognized importance in many physico-chemical and biomolecular phenomena, a large number of studies have been devoted to elucidate the molecular origin of the hydrophobic effect (hydrophobic hydration and the solvent-mediated attraction of nonpolar substances to aggregate in aqueous solution with respect to that which they would have in a nonpolar solvent). All facets of the hydrophobic effect are, however, not well understood even for the small hydrophobic solute, neopentane, and many of the issues concerning the hydrophobic effect in aqueous solutions are still going on.

In this chapter, we have presented a report on the hydrophobic interactions between neopentane molecules in aqueous solutions of trehalose with increasing temperature and in binary and ternary solutions of urea and trehalose. The chapter is divided into two parts. In Part A, we discuss the effects of trehalose on association and hydration of neopentane molecules in pure water and aqueous trehalose solutions with increasing temperature. On the other hand, in Part B, we explore the effects of trehalose on urea induced changes in hydrophobic interaction between solute neopentane molecules.

Part A:

Neopentane in Water and Aqueous Solutions of Trehalose at Different Temperatures

Overview: The influence of trehalose on temperature-induced changes of hydrophobic interactions is investigated by employing classical MD simulations. In this study, neopentane molecules are used to model typical nonpolar entities. For this, the systems of pure water and five different trehalose concentrations are used and for each system five different temperatures are considered. The calculations of potentials of mean force followed by estimation of the association constant values suggest that the trehalose induced reduction in the hydrophobic interactions observed at low temperature is getting reduced at higher temperature. This finding is further supported by the calculation of neopentane-water distribution functions. The calculations of the hydrogen bond properties reveal that in contrast to pure water system, the average number of water-water hydrogen bonds in a concentrated trehalose solution is insensitive to temperature change. Further, the analyses of trehalose cluster structures reveal the formation of higher order trehalose cluster on increasing trehalose concentration and the breaking of these higher order clusters as temperature increases. With increasing trehalose concentration, we also observe retardation of translational motion of all solution species and this slowing down of the translational dynamics is more pronounced for trehalose than that for water.

■ INTRODUCTION

The hydrophobic and hydrogen bond interactions within the secondary and tertiary structures contribute to the thermal stability of a protein. Hydrogen bonding and hydrophobic interactions are the two main driving forces of protein folding-unfolding process. Though a recent molecular dynamics simulation study argues about the role of hydrogen bond on protein conformation [100], other studies reveal that the contribution of hydrogen bonding interactions is 1.4 kcal/mol per hydrogen bond and for hydrophobic interactions it is 1.2 kcal/mol per CH_2 group [101, 102]. Nevertheless, these values suggest that the protein stability is sensitive to changes in environmental and chemical conditions such as temperature, pressure, presence of denaturants (e.g., urea and guanidium hydrochloride), salts etc. In proteins since the backbone atoms are identical, the main structural difference among proteins arises due to presence of different side chains [4, 99, 103]. These suggest that the hydrophobic interactions among different side chains play an important role in stabilizing the protein native state.

In view of the importance of side-chain hydrophobic interactions in the stability of proteins and to reduce complex interactions of protein residues with solution species, the temperature dependent hydrophobic interactions with the model systems such as methane, neopentane, and benzene etc in aqueous solution have been studied extensively [104-109]. For example, the studies of hydrophobic association and its parameter and temperature dependence by Pratt and Chandler [110-112] showed that the solvent separated minimum is energetically more favorable than the contact minimum and hydrophobic interaction decreases with increasing temperature. And, other simulation studies of methane like particles also have shown that the global minimum free energy of association appears at solvent separated distance [113-115]. In contradiction to this, several studies [116-118] have shown that the global minimum occurs at contact distance. Recently, it has been reported that the aggregation of methane particles in water increases with increasing temperature [105]. Similarly, Ludemann *et al.* [108, 109] has also shown the temperature dependent hydrophobic interaction between the two methane molecules. They reported the significant temperature dependence hydrophobic interactions and noted that the depth of the contact minimum of the methane-methane interaction increases with temperature. More recently, Angelika *et al.* [119] have shown from their potential of mean force calculation, that association of neopentane molecules increases with increasing temperature.

As discussed above, there have been many simulation studies that investigated the

hydrophobicity of nonpolar solutes in aqueous solution with increasing temperature. However, previous studies did not consider the behavior of neopentane in aqueous trehalose solution. In this part, we deal with the solvation characteristics and solvent-mediated attraction of neopentane molecules in pure water as well as aqueous trehalose solutions with increasing temperature. Note that, the choice of hydrophobic neopentane molecules as solutes over vastly used methane is due to fact that neopentane breaks hydrogen bond network of water whereas methane fits in to it. Moreover, the effective size of the nonpolar side chains in protein is larger than the size of a methane molecule. As mentioned in **Chapter 1**, since trehalose molecules act as a biomolecule stabilizer at high and low temperatures, here, we focus mainly on the role of trehalose on the neopentane hydrophobic interactions at various temperatures. For this, we have considered a wide range of temperatures (from 285 K to 345 K) and our goal is to see how temperature induced changes in the hydrophobic interactions are getting affected in presence of trehalose and thereby predict the role of trehalose on protein stability at different thermal conditions. We therefore, examine the solvation characteristics of hydrophobic neopentane solutes in aqueous trehalose solutions of varying concentrations. By calculating the potentials of mean force (PMFs) followed by the estimation of association constant value, we first examine whether trehalose has any significant effect on the temperature dependent changes in the neopentane aggregation in different solutions. An insight picture of effect of trehalose on neopentane aggregation is obtained by examining its effects on the water structure and also its direct interactions with the hydrophobic neopentane molecules. We use the familiar water oxygen-oxygen rdf to describe water structuring. Further, solute-solvent coordination number is used to calculate preferential binding with the solute. Furthermore, we investigate the trehalose and temperature induced changes in hydrogen bond properties and translational dynamics of different solution species.

In the next section, we have presented a description of the models and simulation method. Results are discussed thereafter, and this part is ended with a section whereof we have included our concluding remarks with a brief summary.

■ MODELS AND SIMULATION METHOD

Classical molecular dynamics simulations of neopentane-trehalose-water mixtures were carried out with six different trehalose concentrations and at five different temperatures. We have employed GLYCAM06 force field for trehalose [120] and SPC/E [121] force field for water. For neopentane, we have used OPLS/AA [122] force field because of the fact that

compared to single site united atom model the aggregation propensity of neopentane in water increases as branching increases [123]. Furthermore, the OPLS/AA neopentane model shows the characteristics that one would expect from a large hydrophobic surface [124]. We use AMBER10 program for all MD simulations [89]. We note that, a comparative study between different disaccharide force fields shows that the results of GLYCAM06 force field (which is mostly used for simulations of monosaccharides and oligosaccharides) are in well agreement with DFT and experimental values [125, 126]. A comparison of different water models reveals that the structural and dynamical properties of SPC/E water match well with the experimental results [127]. In this regard, we further note that a combination of GLYCAM06 force field (for trehalose and kojibose) and SPC/E water has recently been used elsewhere [128]. The systems considered here are summarized in Table 2A-1.

Table 2A-1. Overview of Systems[a]

System	N_{neo}	N_{tre}	N_{wat}	Volume (nm^3)					
				285 K	300 K	315 K	330 K	345 K	w_{tre}%
S0	20	0	1400	45.30	45.75	45.88	46.58	47.32	0
S1	20	10	1400	48.84	49.10	49.91	50.16	50.88	11
S2	20	20	1400	52.20	52.43	52.95	54.01	54.25	20
S3	20	50	1400	63.00	63.14	63.74	64.72	64.98	39
S4	20	75	1400	68.75	68.92	72.49	73.51	74.34	49
S5	20	100	1400	79.80	80.78	88.66	82.71	83.47	56

[a] N_{neo}, N_{tre}, N_{wat}, Volume and w_{tre} represent the number of neopentane, trehalose, water molecules, box volumes and weight percentage of trehalose respectively, for different systems.

The initial configurations of our systems were prepared using Packmol program [129]. All simulations were carried out in cubic box with temperature range of 285K to 345K. In order to obtain a reasonable initial structure, the systems were energy minimized for 5000 steps, where the first 2500 steps in steepest descent method and followed by the same number of steps in conjugate gradient method. After that each system was heated up slowly from 0K to the desired temperature for 100 ps in canonical ensemble (NVT) and then the systems were equilibrated in isothermal-isobaric (NPT) ensemble for 5 ns.

For calculating different structural and hydrogen bond properties, the production runs were performed for 35 ns in NPT ensemble and at 1 atm pressure. To maintain physical pressure, Berendsen thermostat with a pressure relaxation time of 2 ps was used [130] and the temperature was controlled by Langevin dynamics method with a collision frequency of 1 ps^{-1}. In all simulations, periodic boundary conditions were applied to remove the edge effects and a time step of 2 fs was used. A cutoff distance of 10 Å was considered for all non-bonding interactions and the long-range electrostatic interactions were treated using the particle mesh Ewald method. Bonds involving hydrogen were constrained by applying SHAKE algorithm [131]. For calculating the diffusion coefficients of different solution species, the simulations were, further, continued for another 15 ns in microcanonical (NVE) ensemble. Finally, the trajectories generated from production run were analyzed using the ptraj program of the AMBER10 toolkit and the Visual Molecular Dynamics (VMD) package [132] and the results are reported in the next section.

■ RESULTS AND DISCUSSION

Neopentane−Neopentane Pair Potentials of Mean Force: In order to get a picture about the hydrophobic interaction at pair level, we have calculated potentials of mean force of hydrophobic neopentane solutes from the solute-solute pair correlation function ($g_{ss}(r)$) using the relation

$$W(r) = -k_B T \ln g_{ss}(r) \tag{2.1}$$

where k_B is the Boltzmann constant, T is the absolute temperature and the pair correlations function ($g(r)$) is the ratio of probability of finding a pair of atomic sites at a distance r and the probability expected for a completely random distribution at the same density. Note that in order to calculate $W(r)$, we have considered neopentane-neopentane pair correlation function involving neopentane central carbon atoms. The PMF profiles of neopentane in aqueous solutions of varying trehalose concentrations at five different temperatures are shown in Figure 2A-1.

In each PMF curve, we observe two minima separated by a maximum. The first minimum at about 5.85 Å that arises from the direct contact of two neopentane molecules, is commonly known as contact minimum (CM) and the relatively weaker second minimum that appears at about 10.25 Å ascribes as solvent-separated minimum (SSM). The presence of these two minima reveals the existence of associated and solvent-separated states of neopentane. We note that, in the context of protein denaturation process, the CM and SSM loosely correspond to the folded and unfolded states of protein respectively. We have

used the term *loosely* here because of the fact that one of the energetic components that stabilizes the proteins in their native states is hydrophobic interaction. The maximum between the two minima that appears at about 8.5 Å is known as desolvation barrier (BARR).

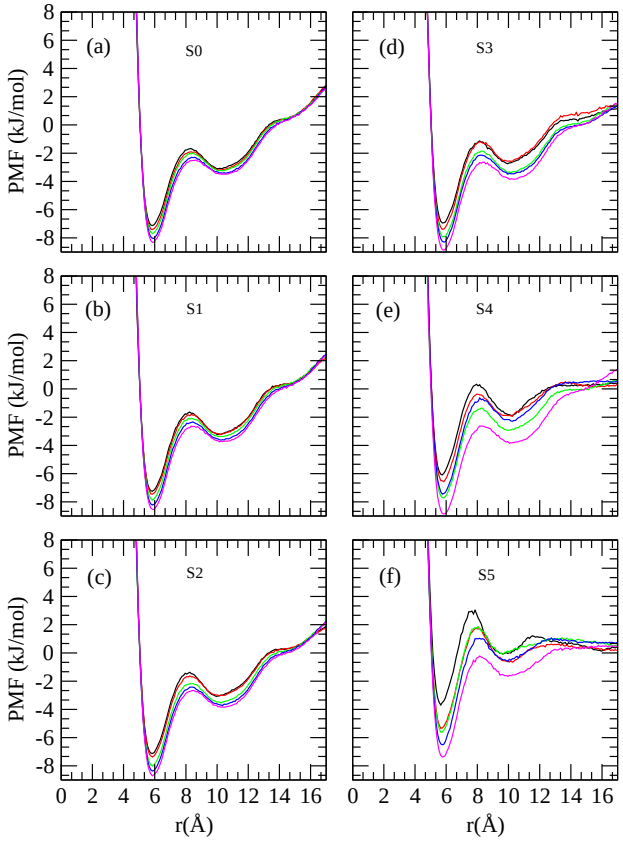

Figure 2A-1. *Neopentane-neopentane potential of mean forces for different systems. 285K (black), 300K (red), 315K (green), 330K (blue) and 345K (magenta).*

It is apparent from Figure 2A-1 that the well depth of CM is higher than that of SSM. Considering the system without trehalose (system S0) first, we find that the small system size of our simulation and the finite neopentane aggregates make the PMF profile to have a positive gradient that does not go to zero at large solute separations [133]. In regard to the increase of temperature on the PMF profiles, we observe: (a) a slightly outward movement of CM, SSM and BARR; (b) the enhancement in the well depth of both CM and SSM suggesting more pronounced free energy basins of both contact and solvent-separated states of neopentane; and (c) no change in the positive gradients that are observed at higher solute separation. At a fixed temperature, in regard to the influence

of trehalose concentration on the PMF of neopentane, two points are worth noting: (a) a reduction in the well depths of both CM and SSM with increasing trehalose concentrations and the effect is more pronounced at lower temperatures; and (b) a reduction in the slope of PMF curves at larger solute separation with increasing trehalose concentration. The PMF difference between SSM and CM, ($\Delta W_{f\to u}$) that indicates the association tendency of hydrophobic neopentane molecules, is related to the thermodynamic stability of neopentane associated state. For example, for system S0 at 285K, the value of $\Delta W_{f\to u}$ is +4.03 kJ/mol indicating that a neopentane molecule prefers to be in contact with other neopentane molecules rather than to be separated by solvent water molecules. Figure 2A-2 displays the variations in the $\Delta W_{f\to u}$ values with changing trehalose concentration at different temperatures. As can be seen that, in comparison to low temperature, trehalose helps in stabilizing the contact state at high temperatures when trehalose concentration is also high. Interestingly, high trehalose concentration diminishes the hydrophobic interactions between neopentane molecules at 285 K. These findings suggest that trehalose induced changes in the hydrophobic interactions between neopentane molecules are influenced dramatically with change in temperature.

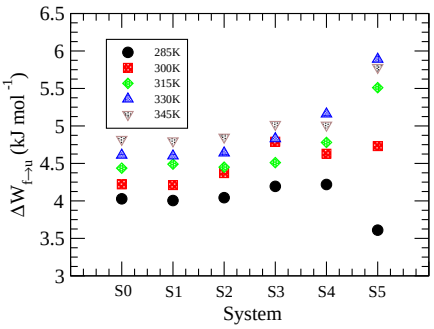

Figure 2A-2. *The free energy differences between SSM and CM for different systems.*

For a better understanding on the effect of increasing temperature on neopentane aggregation for various trehalose concentrations, we have calculated the neopentane-neopentane association constant, K_a, by integrating the PMF to the first maximum (the barrier), which defines the outer limit of the solute-solute contact configuration. The K_a is defined as [27, 134]

$$K_a = 4\pi \int_0^{r_a} r^2 e^{-W(r)/k_B T} dr \tag{2.2}$$

where r_a is the position of the barrier in the corresponding PMF curve. Note that, higher the value of K_a, greater will be the association tendency of the hydrophobic moieties in

aqueous system. Any perturbation that favors the associated state of solute will, therefore, increase the value of K_a. The values of K_a for different systems are presented in Table 2A-2.

Table 2A-2. Association Constant ($K_a(M^{-1})$) for Neopentane

System	S0	S1	S2	S3	S4	S5
285K	8.26	8.54	7.94	7.18	4.42	1.42
300K	8.34	8.31	7.80	7.40	5.12	2.83
315K	8.30	8.55	9.05	8.44	7.46	2.90
330K	8.41	8.54	9.17	8.57	5.98	3.75
345K	8.47	8.93	9.37	9.66	9.29	4.98

We have observed that for systems S0 and S1, the value of association constant is very large and with increasing temperature it remains practically unchanged. Interestingly, for other systems, the value of K_a increases with increasing temperature and this effect is more pronounced for systems of higher trehalose concentrations (i.e., systems S4 and S5). For example, for system S5, there is a three fold increase in the K_a value as temperature is increased from 285 K to 345 K. Furthermore, for a particular temperature, with increasing trehalose concentration the association constant value decreases. Though the decrease in its value is more pronounced at lower temperature, remarkably, at higher temperature the value of K_a changes noticeably only at higher trehalose concentrations. These observations suggest that the trehalose induced depletion in the neopentane-neopentane hydrophobic interaction observed at low temperature, is getting reduced at high temperature and trehalose molecules act as a stabilizing co-solute for hydrophobic interactions at high temperature. Here we note that, for system S0, where there is no trehalose molecules, the temperature has essentially no influence on the neopentane association constant value. This finding is in contradiction to the results of molecular dynamics simulation study of methane-like molecules in pure water reported by Lüdemann *et al.* [108]. They reported that as temperature increases, the equilibrium between contact pair and solvent-separated pair is shifted towards the former. In this regard, it is also worth noting that for system S0, the temperature induced changes in the $\Delta W_{f\to u}$ observed here (see Figure 2A-2) is due to the presence of temperature factor in the PMF expression.

Neopentane Cluster Structure Analysis: In order to quantify the clustering of hydrophobic neopentane molecules and the possible effects of trehalose and temperature on to it, we have estimated the average cluster size in all the systems simulated here. For this, we have adopted the method employed by Martinez *et al.* [135] for Lennard-Jones fluid. Our group in the simulation study of methane aggregation in aqueous osmolyte solutions successfully employed this method later [134]. Each neopentane molecule can be assigned low-, average-, or high-density clusters with the like molecules according to the following relations:

- low if $n < n_0 - \delta$
- high if $n > n_0 + \delta$
- average if $n_0 - \delta \leq n \leq n_0 + \delta$

Note that, in order to calculate the number of molecules in the solvation sphere (n) we have integrated the neopentane-neopentane pair correlation function up to the first minimum. And for calculating the average number of molecules (n_0), we have adopted the method proposed by Martinez *et al.* [135] We set the fluctuation, δ, at 20% of average number of molecules (n_0).

In Table 2A-3 we have shown the results of our cluster structure analyses for all systems. It can be seen that the difference between the values of $n - n_0$ is higher than the corresponding δ value for all systems considered here (except for system S5 at 285K temperature) indicating that the neopentane has some propensity to aggregate in pure water as well as in aqueous trehalose solutions. The much lower aggregation propensity of neopentane molecules for system S5 at 285 K acts as a corroborative evidence of what we observed in the free energy difference plot (Figure 2A-2). For a fixed temperature, the addition of trehalose molecules causes a drop in $n - n_0$ value and the drop is much sharper as one moves from system S3 to S5 through system S4. Moreover, the difference in the value of of $n - n_0$ and δ decreases as concentration increases. On the other hand, for a particular trehalose concentration, as temperature increases there is an increase in the $n - n_0$ value for all systems except for systems S0 and S1 in which $n - n_0$ values are essentially insensitive to temperature change. These findings are in consistent with our calculated association constant values for different systems discussed above. Here, we mention that for concentrated trehalose solutions, a substantial drop in the number of trehalose molecules and a sharp rise in the number of water molecules in the neopentane solvation shell is observed at lower temperature.

Table 2A-3. Neopentane Cluster Sizes for Different Systems[a]

System	Temperature (K)	n	n_0	δ	$n - n_0$	Remark
S0	285K	6.07	1.04	0.21	5.03	high
S0	300K	6.07	1.07	0.21	5.00	high
S0	315K	5.98	1.10	0.22	4.88	high
S0	330K	5.99	1.05	0.21	4.94	high
S0	345K	5.95	1.07	0.21	4.88	high
S1	285K	5.84	0.96	0.19	4.88	high
S1	300K	5.63	0.99	0.20	4.63	high
S1	315K	5.73	0.98	0.20	4.75	high
S1	330K	5.94	1.01	0.20	4.93	high
S1	345K	5.84	0.96	0.19	4.88	high
S2	285K	5.07	0.90	0.18	4.17	high
S2	300K	4.93	0.90	0.18	4.03	high
S2	315K	5.67	0.95	0.19	4.72	high
S2	330K	5.67	0.90	0.18	4.77	high
S2	345K	5.72	0.93	0.18	4.79	high
S3	285K	3.82	0.72	0.14	3.10	high
S3	300K	3.89	0.72	0.14	3.17	high
S3	315K	4.40	0.74	0.15	3.66	high
S3	330K	4.43	0.73	0.15	3.70	high
S3	345K	4.93	0.78	0.16	4.15	high
S4	285K	2.06	0.60	0.12	1.46	high
S4	300K	2.37	0.63	0.13	1.74	high
S4	315K	3.42	0.65	0.13	2.77	high
S4	330K	2.71	0.61	0.13	2.05	high
S4	345K	4.16	0.54	0.12	3.55	high
S5	285K	0.59	0.51	0.10	0.08	low
S5	300K	1.16	0.52	0.10	0.64	high
S5	315K	1.18	0.58	0.12	0.60	high
S5	330K	1.51	0.55	0.11	0.96	high
S5	345K	1.99	0.54	0.11	1.45	high

[a] n_0, n and δ are the average number of neopentane molecules, the number of neopentane molecules in the first coordination shell of a reference neopentane molecule and the fluctuation in n_0, respectively.

On the other hand, at higher temperature, we observe a much less exclusion of trehalose molecules from neopentane surface and less number of water molecule in the neopentane

solvation shell. These findings are discussed below.

Neopentane Hydration: The effects of trehalose and temperature change on the solvation of neopentane molecules have been investigated by computing site−site rdfs between neopentane and water. The rdfs involving neopentane central carbon atom and the oxygen atom of water (O_w) are shown in Figure 2A-3.

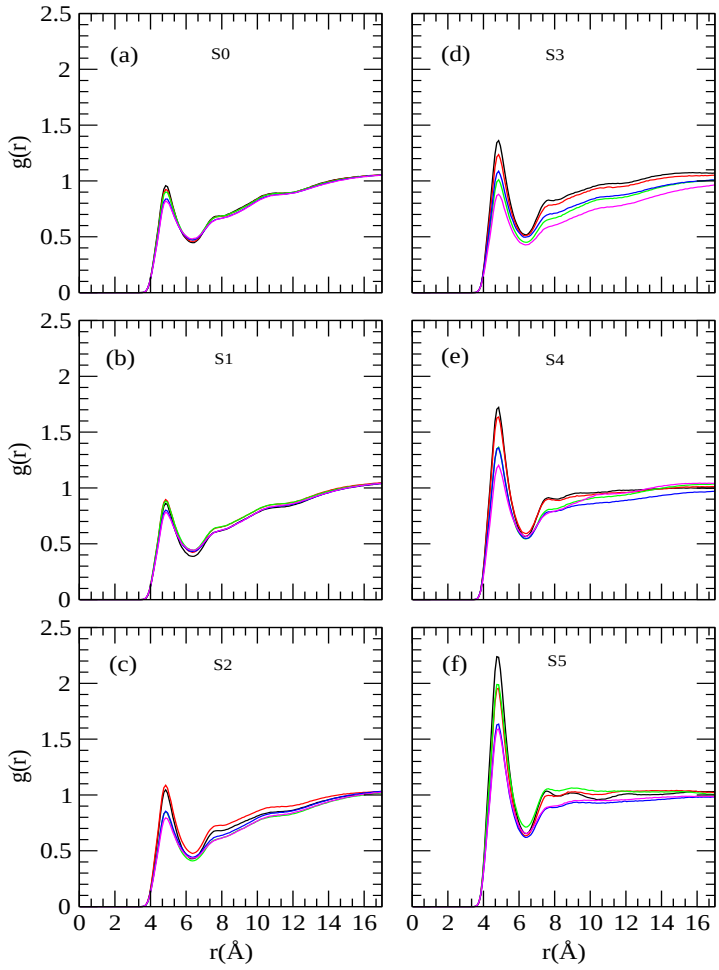

Figure 2A-3. *Site-Site distribution functions involving neopentane central carbon atom and water oxygen atom. 285K (black), 300K (red), 315K (green), 330K (blue) and 345K (magenta).*

Focusing on the hydration of neopentane at 285K in pure water (Figure 2A-3 (a)) first, we observed that the neopentane-water rdf starts to rise at 3.35 Å and it reaches to maximum at 4.85 Å. Hence, below 4.85 Å there is actually exclusion of water molecules from the solvation shell of neopentane. The first minimum, appears at 6.35 Å indicates the outer limit of the first hydration shell of neopentane. In pure water, we find that water density is low in the first hydration shell of neopentane and is only 0.96 times to the bulk water

density. Further, it can be seen that the height of the first peak decreases monotonically, without affecting very much to the position of the first minimum when temperature increases from 285K to 345K. This low water density around neopentane compares well with that of the already reported results [133]. The effects of trehalose on the neopentane-water rdf at different temperatures are shown in Figure 2A-3 (b)-(f). Considering the influence of temperature on hydration of neopentane in presence of trehalose, we find that for all the systems considered here, the first peak height decreases gradually in neopentane-water rdfs with increasing temperature without changing the first peak position and this effect is more prominent for systems S3, S4 and S5. Further, for a particular temperature, as trehalose concentration is increased, we find a sharp increase in the first peak height of neopentane-water rdf and this effect is less pronounced at high temperatures. These findings suggest that the solvation of neopentane molecules by water is reduced in concentrated trehalose solution when the temperature is high.

The solvation of Neopentane is further analyzed by calculating first shell coordination number (CN) of the water or trehalose molecules around the solute neopentane molecule. The CN is calculated using the following relation:

$$CN = 4\pi\rho_\beta \int_0^{r_c} r^2 g_{\alpha\beta}(r) dr \tag{2.3}$$

where ρ_β and r_c represent the number density of species β and the position of the first minimum in the corresponding distribution function respectively.

The number of water and trehalose molecules that are present in the first coordination shell of a neopentane is calculated using equation 2.3 and the same are presented in Tables 2A-4 and 2A-5, respectively. Note that, in order to calculate CNs for water, we have considered the rdfs involving neopentane central carbon atom and water oxygen atom and the same for trehalose the neopentane central carbon and glycosidic oxygen (O1) rdfs are used. For a fixed temperature with increasing trehalose concentration though the first peak height in the corresponding neopentane-water rdfs increases (see Figure 2A-3) but, from Table 2A-4 it can be seen that the number of first shell water molecules around a neopentane does not follow any particular trend. For 285K temperature, the aggregation of neopentane causes a depletion in the value of CN as we moves from system S0 to S1, then it (CN) starts increasing with increasing trehalose concentration. These observations are in accordance with the association constant value presented Table 2A-2. We trace this anomaly is due to decrease in water number density as trehalose is added. Since, trehalose molecules were added without replacing water molecules, the box volume increases with

increasing trehalose concentration leading to a decrease in the water number density. To consider this reduced water number density effect, we have calculated the coordination numbers assuming that the only change with added trehalose molecules comes through the number density of water and these values are shown in the parentheses of Table 2A-4. From this table it is apparent that for a particular temperature, the difference between the calculated and "expected" coordination number is small for low trehalose concentrations and this difference increases with further addition of trehalose molecules. Moreover, for systems S4 and S5, the difference between these two coordination number values decreases (mainly due to a sharp decrease in the calculated coordination number value) as temperature is increased. For example, for system S5, the difference between estimated and "expected" coordination number value is 8.57 at 285 K and the value for the same at 345 K is 6.35. From these observations it appears that the trehalose-induced enhancement of hydrophobic solvation (by water) for systems S5 and S4 that occurs at low temperature is reduced as temperature increases.

Table 2A-4. Number of water molecules in the first solvation shell of a neopentane molecule[a]

System	285K	300K	315K	330K	345K
S0	16.51	15.46	15.36	14.54	14.27
S1	13.57 (15.31)	13.78 (14.41)	13.69 (14.12)	12.67 (13.50)	13.10 (13.27)
S2	13.63 (14.33)	15.14 (13.49)	12.13 (13.31)	12.43 (12.54)	12.30 (12.45)
S3	15.05 (11.87)	13.96 (11.20)	12.18 (11.06)	12.56 (10.46)	10.37 (10.39)
S4	15.93 (10.53)	15.57 (10.26)	13.32 (9.72)	13.78 (9.21)	12.80 (9.08)
S5	17.92 (9.37)	15.96 (8.76)	15.72 (8.63)	13.95 (8.19)	14.44 (8.09)

[a]For a fixed temperature, the numbers given in parentheses represent the first shell water molecules if the only change with added trehalose came through the water number density change.

The data in Table 2A-5 show that for all temperatures, the number of trehalose molecules in neopentane's first solvation shell decreases on addition of trehalose suggesting exclusion of trehalose molecules from neopentane solvation shell. In the same Table, we also present the "expected" number of trehalose around solute neopentane by considering the trehalose number densities for different systems. As can be seen from the difference between actual and "expected" trehalose coordination number values that there is a sharp decrease in its value for system S4 and S5 as temperature increases from 285 K to 345 K and this effect is less prominent for other systems. Thus, for concentrated solutions, the

exclusion of trehalose molecules from the neopentane first solvation shell is more at lower temperature compared to that at higher temperature.

Table 2A-5. Number of trehalose molecules in the first solvation shell of a neopentane molecule[a]

System	285K	300K	315K	330K	345K
S1	1.19	0.87	0.83	0.87	0.81
S2	0.63 (2.23)	0.55 (1.63)	0.76 (1.56)	0.57 (1.74)	0.68 (1.52)
S3	0.38 (4.61)	0.49 (3.38)	0.46 (3.25)	0.42 (3.37)	0.50 (3.18)
S4	0.47 (6.14)	0.43 (4.65)	0.42 (4.29)	0.47 (4.45)	0.31 (4.15)
S5	0.44 (7.28)	0.46 (5.29)	0.39 (5.07)	0.43 (5.28)	0.41 (4.94)

[a]For a fixed temperature, the numbers given in parentheses represent the first shell trehalose molecules if the only change with added trehalose came through the water number density change.

Trehalose's Interaction with Neopentane: Further, the role of trehalose molecules on neopentane aggregation is also investigated by calculating selected site-site rdfs of central carbon of neopentane and trehalose O6 and O5 oxygen atoms with varying trehalose concentration and temperature and the same are presented in Figures 2A-4 and 2A-5. Keeping temperature fixed, considering neopentane central atom-O6 rdf first (see Figure 2A-4) we observe: (a) a depletion in the first peak height with increasing trehalose concentration; (b) the second peak that was observed for system S1, starts disappearing on increasing trehalose concentration. By examining neopentane central atom-O5 rdf in Figure 2A-5, we find that the disappearance of the first peak that appeared at about 4.8 Å and appearance of a second peak at 7 Å as trehalose concentration is increased. These results reveal that the propensity of neopentane-trehalose interaction decreases as more and more trehalose is added. From these figures, it can also be seen that with increasing temperature the first peak height of these rdfs decreases substantially for systems S1 and S2 and for other systems there is essentially no strong qualitative temperature dependence is evident. In regard to the effects of trehalose concentration on neopentane-O5 rdf, we observe a drop in the first peak height of these rdfs as trehalose is added though except for systems S1 and S2, these functions are not strong functions of trehalose concentrations. These results suggest the exclusion of trehalose molecules from neopentane surface as temperature and trehalose concentration increases.

Trehalose's Solvation and Its Effect on Water Structure: An explicit picture of

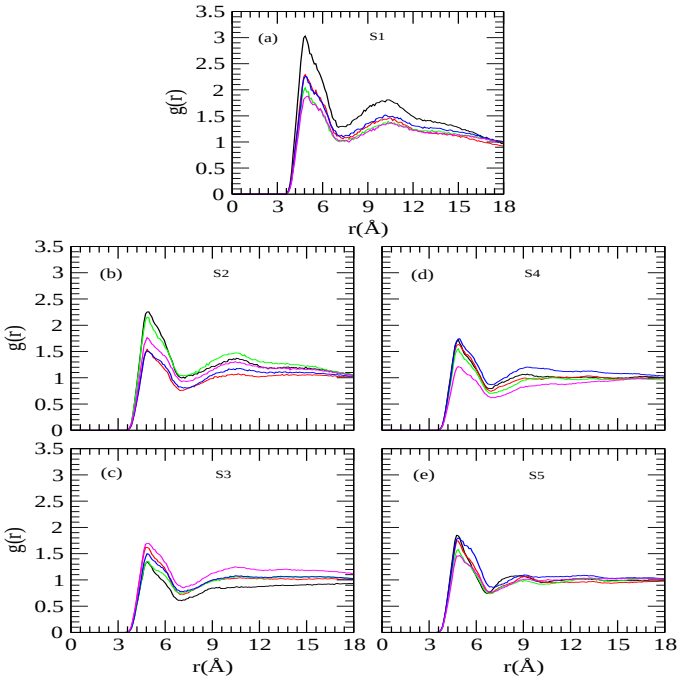

Figure 2A-4. *Site-Site distribution functions involving neopentane central carbon and hydroxylic oxygen (O6) of trehalose. 285K (black), 300K (red), 315K (green), 330K (blue) and 345K (magenta).*

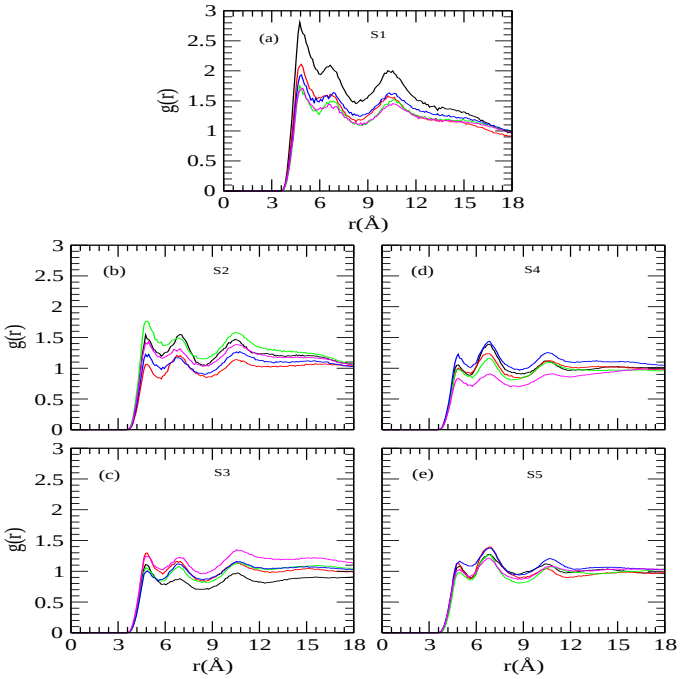

Figure 2A-5. *Site-Site distribution functions involving neopentane central carbon and hydroxylic oxygen (O5) of trehalose. 285K (black), 300K (red), 315K (green), 330K (blue) and 345K (magenta).*

interactions between water and trehalose molecules, which in turn influences the solvation of neopentane molecules is obtained by examining the selected site-site rdfs involving water and trehalose molecules. In Figure 2A-6 we have shown the typical rdfs involving one of the hydroxylic oxygens (O6) of trehalose and water oxygen. The distribution functions involving glycosidic oxygen (O1) and acetalic ring oxygen (O5) atoms of trehalose with respect to water oxygen for different systems are also presented in Figures 2A-7 and 2A-8.

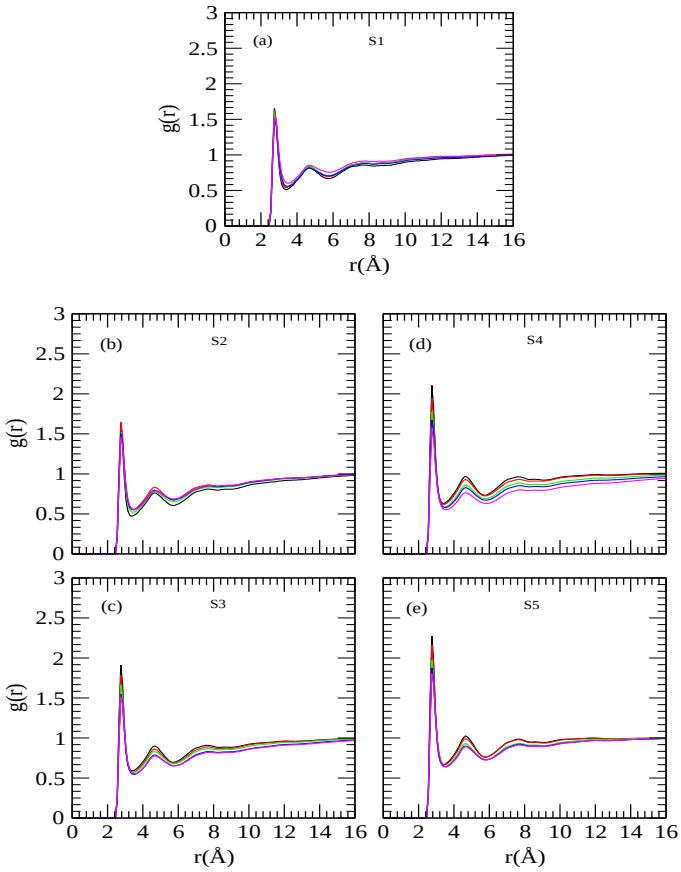

Figure 2A-6. *Site-Site distribution functions involving trehalose hydroxylic oxygen (O6) and water oxygen. 285K (black), 300K (red), 315K (green), 330K (blue) and 345K (magenta).*

Note that, the rdfs involving other hydroxylic trehalose oxygen atoms (O2, O3 and O4) and water oxygen behave in similar fashion as that of O6-water oxygen rdf except for the fact that the second shell of *O*4-water oxygen rdf is slightly less pronounced when compared to other hydroxyl oxygen-water oxygen distribution functions. In consistent with the previously reported results, [136-139] the observed characteristics of our calculated rdfs also suggest water mediated solvation of trehalose hydroxyl groups with well-defined nearest

neighbor peaks in the corresponding trehalose O6 oxygen and water oxygen rdfs (see Figure 2A-6). The presence of a sharp peak in this rdf at 2.75 Å suggests that water molecules are hydrogen bonded to trehalose hydroxyl groups. On the other hand, glycosidic oxygen (O1) atom (as well as O5 oxygen atom) of trehalose does not possess such a well defined first solvation peak (see Figures 2A-7 and 2A-8) implying that, due to geometric constraint, the probability of finding water molecules in the vicinity of the glycosidic oxygen of (1-1)-linked disaccharide is very small [138, 140]. Considering first, the effect of temperature at a fixed trehalose concentration we find that the first and second peak in O6-water oxygen rdfs are essentially unchanged for systems S1 and S2 barring the fact that the first peak becomes slightly broaden as temperature increases.

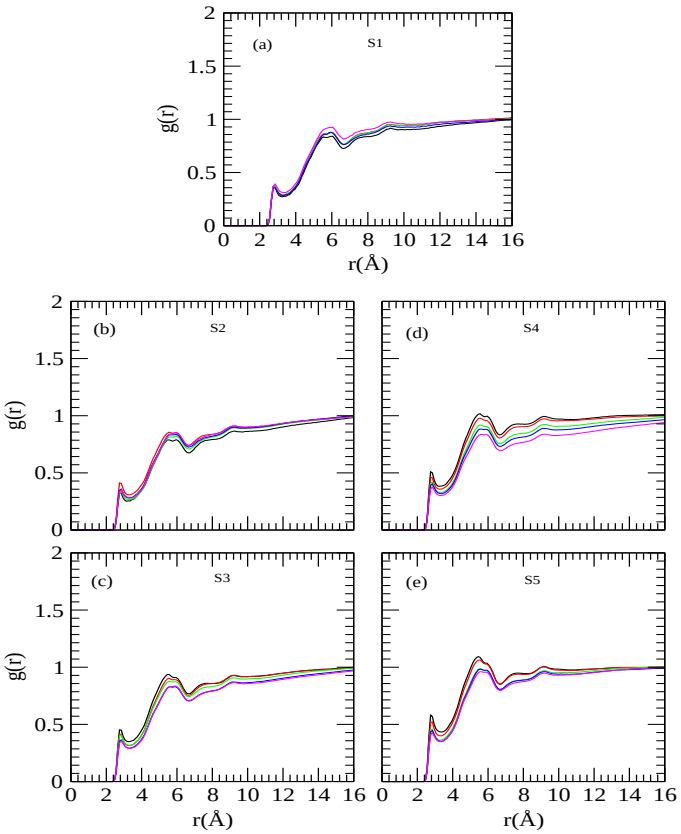

Figure 2A-7. *Site-Site distribution functions involving trehalose acetalic ring oxygen (O5) and water oxygen. 285K (black), 300K (red), 315K (green), 330K (blue) and 345K (magenta).*

On the other hand, for other systems, with increasing temperature, the height of both these peaks decreases and the position of the first peak remains essentially unaltered. Since, hydroxylic O6 atom can potentially form hydrogen bond with water molecules, above findings

indicate that the temperature has a little influence on the hydrogen bonding interactions between water and trehalose molecules for systems S1 and S2 (discussed below).

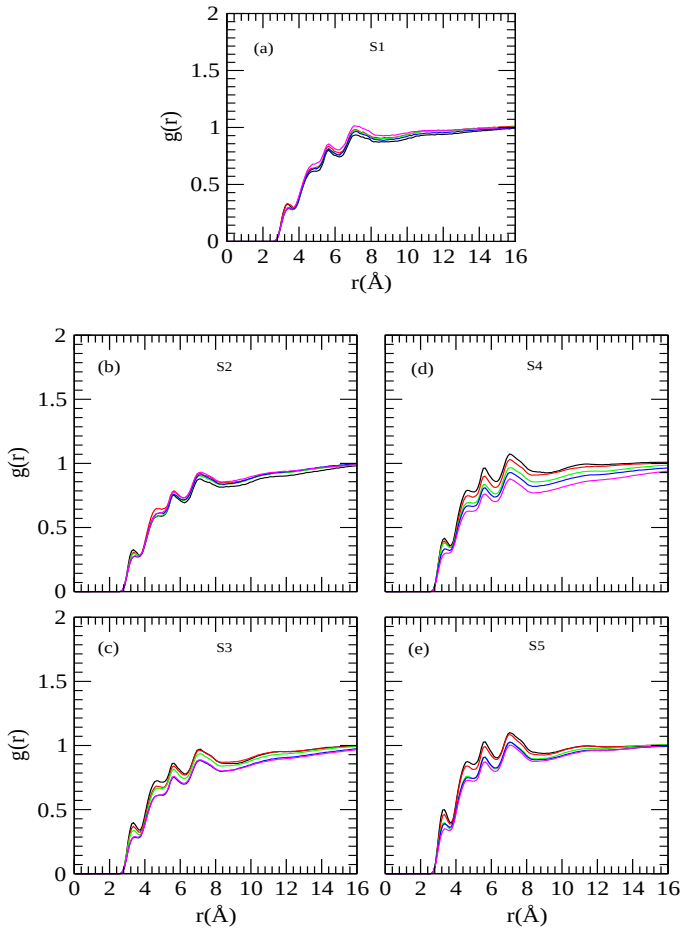

Figure 2A-8. *Site-Site distribution functions involving trehalose glycosidic oxygen (O1) and water oxygen. 285K (black), 300K (red), 315K (green), 330K (blue) and 345K (magenta).*

Further, the temperature dependent changes in the height and width of the first peak is reflected in the calculated number of first shell water molecules around a trehalose molecule presented in Table 2A-6. From this table it can be seen that for systems S1 and S2, the number of water molecules in the first solvation shell of trehalose increases as temperature is increased whereas it decreases for other systems. For a particular temperature, addition of trehalose causes a small enhancement in first peak height and a shallower first valley. Though we observe an increase in the first peak height of the rdfs but the number of first shell water molecules around trehalose decreases as trehalose concentration is increased. We attribute this is due to changes in the water number density as we move from

system S1 to S5. The shallower first valley that appears at higher trehalose concentrations indicates a breaking in the water-trehalose hydrogen bond network. This is further confirmed by our calculations of average number of water-trehalose hydrogen bonds discussed below. We note, further, that at lower temperatures, the number of water molecules in the trehalose first solvation shell presented here matches well with the already reported values considering the fact that we have used different temperatures and different trehalose concentrations [136, 141] and we have employed a different method in calculating first shell coordination number when compared to other studies [142].

Table 2A-6. Number of water molecules in the first solvation shell of a trehalose molecule[a]

System	285K	300K	315K	330K	345K
S1	22.78	23.59	23.75	24.11	25.62
S2	20.73	21.68	21.45	21.45	22.30
S3	19.77	19.63	19.26	18.55	18.96
S4	19.93	18.86	18.24	18.14	16.81
S5	19.51	18.52	17.78	18.02	17.44

The influence of trehalose molecules and the effect of temperature change on water structure, which indirectly provides the details of hydrophobic solvation of neopentane molecules by water molecules, are reflected in the water oxygen-water oxygen ($O_w - O_w$) rdfs shown in Figure 2A-9. The first and second peaks that appear at 2.75 Å and 4.45 Å characterize the H-bonded first neighbor and tetrahedrally located second neighbor respectively. The locations of these peaks in $O_w - O_w$ rdf are similar to those already reported in the literature [38, 123, 133, 143]. We find trehalose-induced enhancement in the first peak height of $O_w - O_w$ distribution function as we move from low to high trehalose concentration. Considering the effect of temperature at a fixed trehalose concentration, we observe that the locations of first and second peak remain unaffected with increasing temperature. However, the height of the first and second peak decreases and the first valley becomes shallower as temperature is increased. In this regard, we note that the temperature induced changes in the water-water correlation functions observed here are in accordance with the previous simulation studies of water-methane system [105]. These findings suggest that temperature and trehalose has two opposite effects in regard to changes in the water structure. In specific, the water in the solutions becomes less structured as temperature is increased which in turn makes the water molecules more mobile. On the other

hand, addition of trehalose molecules makes the water molecules more structured and they become less mobile (see diffusion coefficient values discussed later).

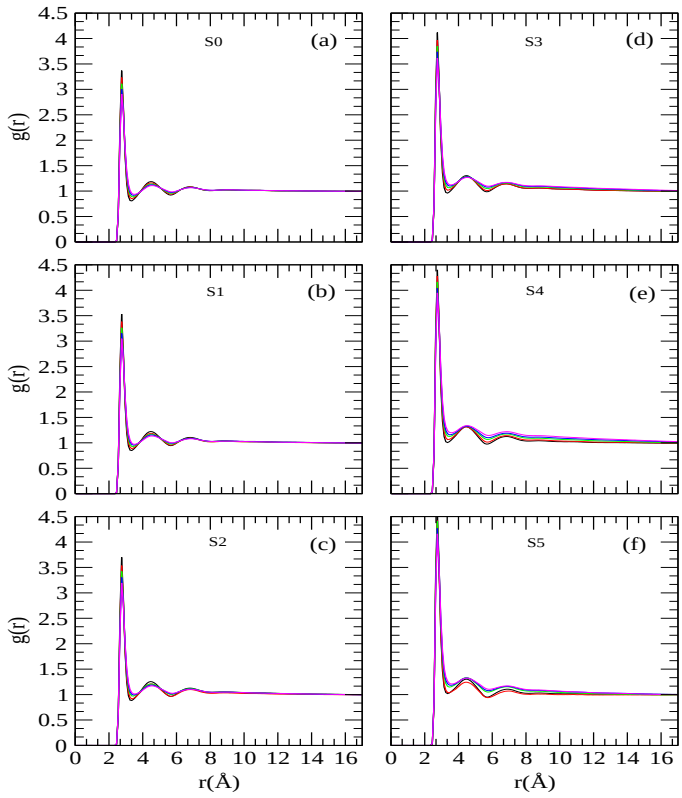

Figure 2A-9. *Site-Site distribution functions involving oxygens atoms of water molecules. 285K (black), 300K (red), 315K (green), 330K (blue) and 345K (magenta).*

Affinity of Neopentane for Solution Species: The increase in trehalose concentration and rise in temperature causes exclusion of trehalose molecules from neopentane solvation shell and more and more water molecules are preferred by neopentane molecule in its solvation shell. It directed us to examine the difference between the local environment of a neopentane molecule to that of the bulk solution and this difference can be estimated by measuring the preferential binding parameter ($\tau_{w/t}(r)$) as a function of distance. Following previous works, [144] $\tau_{w/t}(r)$ can be defined as:

$$\tau_{w/t}(r) = n_w(r)/n_{tre}(r) - N_w/N_{tre} \tag{2.4}$$

where $n_w(r)$ and $n_{tre}(r)$ are the number of water and trehalose molecules, respectively, at a distance r from the neopentane central carbon atom. N corresponds to the total number of molecules in the system with subscripts w and tre standing for water and trehalose

molecules, respectively. So, $\tau_{w/t}(r)$, that represents the local ratio of number of water to trehalose molecules minus their bulk ratio, is the measure of binding parameter and it gives the information about the deviation from an ideal solvation model. A negative value of $\tau_{w/t}$ indicates preferential interaction of trehalose with neopentane molecule over water and its positive value implies preferential hydration or preferential exclusion of trehalose in that region. Here we note that, though the transfer chemical potentials depend on the global thermodynamic preferential interaction parameters (as reported by the solvation experts Timasheff, Schellman and Parsegian [59, 145-147]) in this work our goal is not to correlate our estimated $\tau_{w/t}(r)$ values with the transfer chemical potentials. Thus, our calculation of $\tau_{w/t}(r)$ gives only a qualitative idea of preferential accumulation or exclusion of a solution species (over the second one) around a solute molecule at a distance r.

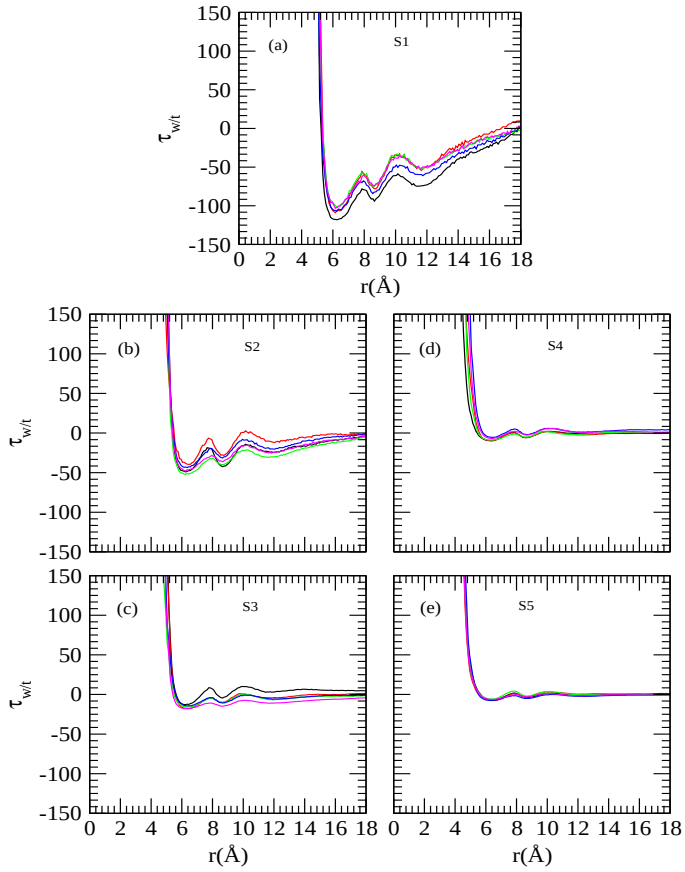

Figure 2A-10. *Preferential interaction parameters around the neopentane molecule as a function of temperature and concentration. 285K (black), 300K (red), 315K (green), 330K (blue) and 345K (magenta).*

Figure 2A-10 shows the changes in the $\tau_{w/t}$ for neopentane central atom as a func-

tion of distance. The initial positive numerical value of $\tau_{w/t}$ at shorter distance is directly related to the relatively larger exclusion radius of trehalose molecules. Considering system S1 at 285 K temperature first, we observe the local ratio becomes equal to the bulk ratio at about 5.25 Å and then $\tau_{w/t}$ value starts decreasing with distance and reaches a minimum at 6.2 Å where it becomes negative. We further notice that, for this system, with increasing temperature $\tau_{w/t}$ increases slightly. On considering the effect of trehalose it can be seen that as trehalose concentration increases, the value of $\tau_{w/t}$ becomes more positive than system S1 suggesting exclusion of trehalose molecules (and preference of water molecules) from neopentane surface. Moreover, for systems S3, S4 and S5 the value of $\tau_{w/t}$ is close to zero indicating both water and trehalose molecules are equally preferred by neopentane and the relative distribution of water to trehalose is more ideal like. Further, for these three systems, temperature has essentially no influence on $\tau_{w/t}$ value.

Hydrogen Bond Properties: As observed in the water-trehalose rdfs, due to presence of hydroxyl groups, in aqueous solution a trehalose molecule possesses a high affinity to form hydrogen bonds with water and also with other trehalose molecules. The water structure and trehalose-trehalose interactions are greatly affected by the formation of hydrogen bonds between water and trehalose molecules and subsequently, this may have an impact on the role of trehalose molecule (as a protective cosolute) to biomacromolecules [148, 149]. We have calculated the hydrogen bond number, by adopting a geometric criteria [150-153] where two molecules are considered to be hydrogen bonded if the distance between the donor and acceptor is less than (or equal) to 3.4 and simultaneously, the donor-hydrogen$\cdots$ acceptor angle is greater than or equal to 120^o. For all systems, the average number of hydrogen bonds between trehalose-trehalose, water-water and water-trehalose (per trehalose) are shown in Table 2A-7. We note that, for system S1 at 300 K, the estimated number of water-trehalose hydrogen bond per trehalose presented in this study matches well with the results of Dinnamaria *et al.* [137]. On the other hand, by using the same hydrogen bonding criteria, Liu *et al.* [153] reported that the average trehalose-water (per trehalose) hydrogen bond number is 22.4 for TIP3P water model. This anomaly in hydrogen bond number can be attributed due the fact of the use of different water model in their study and the presence of solute neopentane molecules and higher trehalose concentration used in our study. Further, with increasing temperature, as expected, Gulliot *et al.* [154] observed a decrease in the average number water-water hydrogen bonds.

In the present study, our results (see Table 2A-7) also show that the average number of water-water hydrogen bond decreases monotonously for low trehalose concentrations

when temperature is increased. Surprisingly, when trehalose concentration is very high (e.g., for systems S4 and S5), the average number of water-water hydrogen bonds is insensitive to temperature change.

Table 2A-7. Average number of water-water (per water), water-trehalose (per trehalose) and trehalose-trehalose (per trehalose) hydrogen bonds for different systems

Systems	285K	300K	315K	330K	345K
		$HB_{water-water}$			
S0	3.51	3.48	3.45	3.40	3.36
S1	3.43	3.38	3.35	3.32	3.28
S2	3.33	3.31	3.26	3.26	3.20
S3	3.07	3.07	3.11	3.04	2.98
S4	2.86	2.83	2.85	2.84	2.89
S5	2.61	2.68	2.67	2.67	2.68
		$HB_{water-trehalose}$			
S1	11.87	13.17	12.23	11.86	12.56
S2	11.61	11.44	11.72	10.56	11.09
S3	11.39	10.99	10.23	9.53	9.98
S4	11.08	10.64	9.91	9.63	8.64
S5	10.94	10.27	9.70	9.58	9.03
		$HB_{trehalose-trehalose}$			
S1	0.68	0.84	0.78	0.75	.66
S2	1.51	1.38	1.52	1.22	1.23
S3	1.89	1.84	1.73	2.02	2.16
S4	2.01	2.25	2.43	2.48	2.34
S5	2.28	2.27	2.64	2.47	2.48

Considering, water-trehalose (per trehalose) hydrogen bond number for low trehalose concentrations we find that these hydrogen bonds are not a strong function of temperature. On the other hand, for systems S4 and S5, the average number of water-trehalose (per trehalose) hydrogen bonds decreases with increasing temperature. From these findings we make the following conclusions: (a) When trehalose concentration is low, the temperature induced breaking of water-water hydrogen bond enhances the hydrophobic solvation of a neopentane molecule (by water). (b) For higher trehalose concentrations, the temperature induced breaking of water-trehalose hydrogen bonds causes release of some water and trehalose molecules. Some of these free water molecules form water-water hydrogen bonds

and as a result the average number of water-water hydrogen remains constant that would otherwise decrease as temperature is increased. These observations, indirectly, imply that for systems S4 and S5, the trehalose induced enhancement of the hydrophobic solvation of a neopentane molecule (by water) observed at low temperature, is being reduced as temperature increases. It, further, acts as a corroborative evidence of what we observe in neopentane-water rdfs (discussed above). (c) For systems S4 and S5, some of the trehalose molecules that were released due to temperature induced breaking of water-trehalose hydrogen bonds form hydrogen bonds with like molecules. As a result we observe an enhancement in the trehalose-trehalose hydrogen bonds for these systems as temperature is increased. In regard to trehalose-trehalose hydrogen bonds, we find that for a fixed temperature addition of trehalose molecules increases the average number of trehalose-trehalose hydrogen bonds.

Trehalose Cluster: As observed above, for a fixed temperature, the increase in the trehalose concentration causes an enhancement in the average number of trehalose-trehalose hydrogen bonds. As a result the association of trehalose molecules takes place [149, 155]. Moreover, Molinero *et al.* [156] reported that the dynamical properties of the solution species is greatly affected due to the formation of extended sugar-sugar hydrogen bond network. Thus, in order to examine the effect of trehalose concentration on its self-aggregation and the possible influence of temperature on to it, it is important to estimate the mean trehalose cluster size. We consider a trehalose cluster is an assembly of like molecules that are connected to each other with at least one hydrogen bond. The mean trehalose cluster size, ($< n_{tre} >$), can be defined as follows:

$$< n_{tre} >= \sum n_{tre} P_{tre} \tag{2.5}$$

where n_{tre} and P_{tre} are the number of trehalose molecules in a given cluster and its probability of formation, respectively.

The normalized mean trehalose cluster size, $< n_{tre} > / N_{tre}$, (where N_{tre} is the number of trehalose molecules in a system) for systems S1 and S5 at different temperatures are shown in Figure 2A-11 (a). Notwithstanding the error bars, it can be seen that the value of $< n_{tre} > / N_{tre}$ for system S5 is much higher than that of system S1 for all temperatures suggesting that on addition of trehalose, the average trehalose cluster size increases. Furthermore, for system S5 the value of $< n_{tre} > / N_{tre}$ reaches to 0.68 at 285 K implying that even for the highest trehalose concentration (and lowest temperature) considered in this study, the percolation of trehalose hydrogen bond network is yet to be achieved. In this

context we note that, Lerbret *et al.* [155] reported the percolation of trehalose hydrogen bond network (in water-trehalose system) at 66% trehalose concentration. This anomaly is attributed to the fact of the use of large number of neopentane molecules in our study. From this figure, we further notice that the value of $< n_{tre} > /N_{tre}$ for both systems decreases with increasing temperature indicating the formation of more number of smaller clusters from the breaking of higher order trehalose cluster.

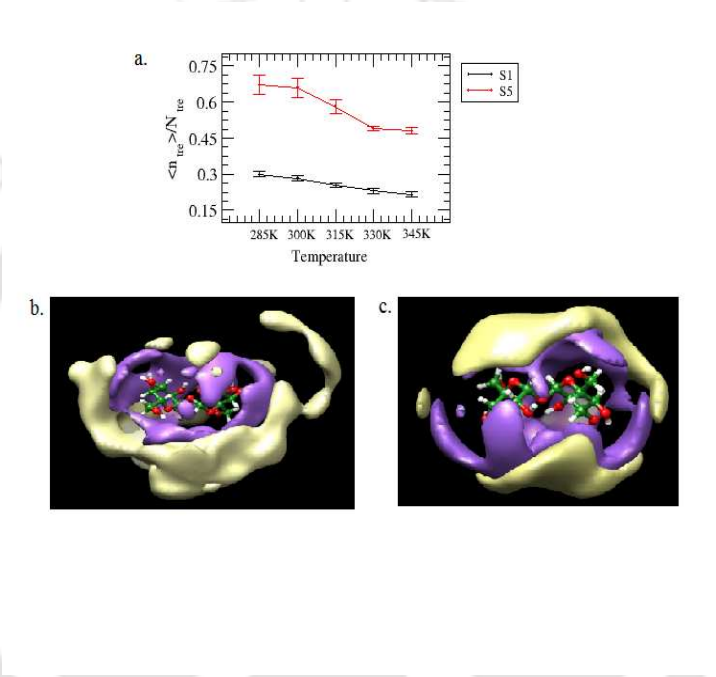

Figure 2A-11. *(a) The normalized mean trehalose cluster size, $< n_{tre} > /N_{tre}$ for systems S1 and S5 at different temperatures. The standard errors are calculated using block average over 1 ns. (b) and (c) represent a projection of spatial distribution function of trehalose-trehalose interaction for system S5 at temperatures 285 K and 345 K, respectively. The isosurface in blue represents the higher probability density of direct hydrogen bonding interactions with the central reference trehalose molecule and isosurface in yellow corresponds to the high density region of up to 10 Å, from the reference trehalose molecule.*

In Figure 2A-11 (b) and (c), considering C1-O1-C1 as reference coordinate system, we have shown the projection of spatial distribution function of trehalose-trehalose interaction around a reference trehalose molecule for system S5 for the highest and lowest temperatures considered here. We observe that there is an overlap between the high probability density region for directly hydrogen bonded trehalose molecules and the high density region up to 10 Å and the effect is much more prominent for lower temperature when compared to higher

temperature. This fact confirms the observations of cluster structure analyses discussed above and it further reveals the formation of hydrogen bond mediated trehalose clusters present in the system.

Diffusion Coefficients: It has already been observed that trehalose has profound effect on the dynamical properties of different solution species present in aqueous trehalose solution. This is due to the fact that the concentrated aqueous trehalose solution has a very high glass transition temperature and it forms a highly viscous glassy matrix that helps in protecting the biomolecule in its biological conformation like an insect trapped in amber [53]. In view of this, we have estimated the translation diffusion coefficients of different solution species for different systems by using the widely used Einstein's relation:

$$D = \frac{\lim_{t\to\infty} < |r(t) - r(0)|^2 >}{6t} \tag{2.6}$$

Using the above Eq. 2.6, the diffusion coefficients (D) can be calculated from the long time slope of mean square displacement (MSD). The results obtained for water, trehalose together with the available experimental diffusion coefficient values [157] at three temperatures are shown in Figure 2A-12. The diffusion coefficient values of neopentane for different systems are presented in Table 2A-8.

Table 2A-8. Diffusion coefficients of neopentane (D_{np})

Systems	285K	300K	315K	330K	345K
		D_{np} $(10^{-5}cm^2s^{-1})$			
S0	0.08	0.08	0.37	0.34	0.52
S1	0.04	0.17	0.38	0.25	0.43
S2	0.06	0.06	0.06	0.11	0.27
S3	0.03	0.02	0.03	0.04	0.08
S4	0.04	0.04	0.04	0.03	0.08
S5	0.03	0.03	0.13	0.07	0.09

For a fixed temperature the addition of trehalose reduces the diffusion coefficients of both water (D_w) and trehalose (D_{tre}). However, the drop in the diffusion coefficient value is more pronounced for trehalose. For example, at 285 K temperature, $D_w \times 10^5$ is reduced from 1.58 to 0.24 (approximately 6.5 times drop) as one moves from system S1 to S5 whereas the same for trehalose molecules we observe 20 times drop in the D_{tre} value (from 0.06 of system S1 to 0.003 for system S5). Moreover, in accordance with the previously reported results of NMR experiments, [157] for all temperatures considered here,

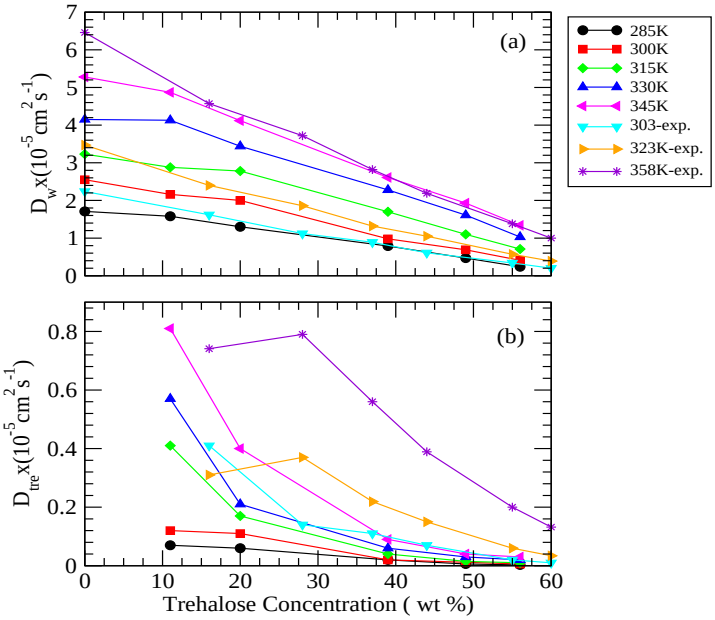

Figure 2A-12. *Diffusion coefficient of (a) water and (b) trehalose for different systems at 285 K, 300K, 315 K, 330 K and 345 K temperatures. The experimental diffusion coefficient values are taken from Reference 157. .*

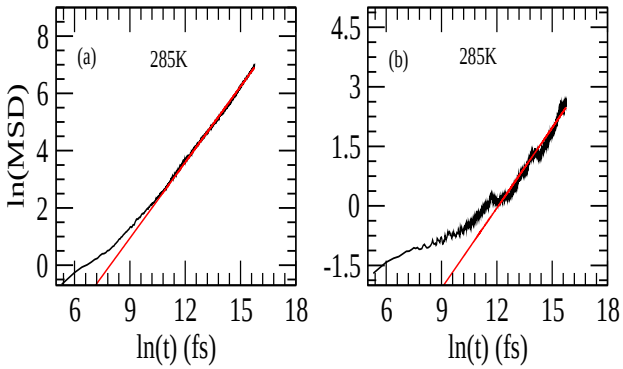

Figure 2A-13. *Black line represents log-log plot of mean-squared displacement (MSD) vs. time for (a) water and (b) trehalose for system S5 at temperature 285 K. The slope of the curve becomes unity once the molecules reach the diffusive regime. The red line has unit slope.*

we also find a drop in the value of D_{tre}:D_w as trehalose concentration increases. We note that the sharp drop in the D_{tre} values, particularly at higher trehalose concentrations, is

in well agreement with the sharp increase in the viscosity value reported earlier [158]. In this regard it is worth noting that formation of stable water-trehalose hydrogen bonds and trehalose induced significant decrease in the diffusion coefficient of water molecules that are present near 5.5 Å of a solute molecule has already been reported elsewhere [159]. Further, the results of a recent Terahertz absorption measurement study [69] also suggest trehalose-induced retardation of translational and rotational motion of water molecules. In regard to the effect of temperature, we find that for a particular trehalose concentration, as expected, the value of both D_w and D_{tre} increases with increasing temperature. We note, our estimated diffusion coefficient values for water and trehalose compare reasonably well with the experimental findings. In this context we note that the results of photo correlation spectroscopy and viscosity measurements study of aqueous trehalose solution also show a similar trend of diffusion coefficient change with respect to temperature change [160-162]. The diffusion coefficient of neopentane (D_{np}) decreases with increasing trehalose concentration and it increases as temperature is increased, however, we note that the change in its value is not a strong function of either trehalose concentration or temperature. Furthermore, the non appearance of the so-called "*boson*" peak in the log-log plot of mean square displacement of trehalose (see Figure 2A-13) even for highest trehalose concentration and lowest temperature considered here suggests that the most concentrated trehalose solution in our study is still above the glass transition temperature.

■ SUMMARY AND CONCLUSIONS

We have discussed the hydrophobic interaction of neopentane in pure water and binary solutions of trehalose. For this, we have considered one pure water system and five different trehalose concentrations and for each of the systems five different temperatures were used. From the neopentane-neopentane potentials of mean force, we found trehalose induced destabilization of neopentane contact pair at low temperature. Interestingly, concentrated trehalose solution helps in stabilizing the contact pair state of neopentane at high temperature. Thus, at high concentration trehalose molecules acts as a stabilizing cosolute when temperature is also very high. These observations are further supported by the estimated association constant values and cluster structure analyses for different systems.

To provide molecular level understanding of the influence of trehalose and temperature change, the calculated neopentane-water rdf at ambient conditions, showed a decreased structure in the more concentrated trehalose solutions suggesting efficient hydration of neopentane by water. On the other hand, the first peak height of neopentane-water

rdf is reduced gradually on increasing temperature and this effect is very prominent for concentrated trehalose solution. These observations imply that trehalose induced solvation of neopentane (by water) in concentrated solution that was observed at lower temperatures is getting reduced as temperature is increased. This fact is further confirmed by calculated number of water molecules present in the first solvation shell of a neopentane. In regard to neopentane-trehalose interactions, we found that addition of more trehalose molecules causes exclusion of trehalose molecules from neopentane surface supporting preferential hydration hypothesis [58]. In this context it is worth noting that exclusion of trehalose from the protein domain has already been reported earlier [59].

Investigation of hydrogen bond properties reveal that with increasing temperature, though the average number of water-water hydrogen bonds decreases for systems with low trehalose concentrations remarkably, for concentrated trehalose solution temperature has no influence on the average number of water-water hydrogen bonds. In regard to water-trehalose hydrogen bonds, we found that for concentrated trehalose solution, the average number of this type of hydrogen bond decreases with increasing temperature. By examining the effect of trehalose concentration and temperature change on the trehalose clusters we observed a breaking (or formation) of higher order trehalose clusters as temperature (or trehalose concentration) is increased. The value of the normalized mean cluster size indicates that the percolation of trehalose hydrogen bond network has not been achieved even for highest concentration and lowest temperature considered in this study. The calculation of diffusion coefficients of different solution species showed trehalose induced slowing down of translational motion of all solution species and the effect is much more pronounced for trehalose than that of water (or neopentane). For a fixed trehalose concentration, as expected, we observed an enhancement in the diffusion coefficient values as temperature increases. In consistent with the NMR experiment [157], we also found that for a fixed temperature, the ratio of diffusion coefficient values of water and trehalose increases with increasing trehalose concentration. Further, our calculated log-log plot of mean-squared displacement vs. time does not show the appearance of *boson* peak as reported previously suggesting that the most concentrated trehalose solution considered in our study is still above the glass transition temperature [139].

In the context of proteins, the present study shows significant effects of trehalose and temperature on association of small hydrophobic groups to explain their role as protein stabilizer or destabilizer. Their effect on the protein backbone will be treated in **Chapter 3**.

Part B:

Neopentane in Water and Aqueous Solutions of Urea and Trehalose

Overview: Classical MD simulations are performed to explore the effects of urea and/or trehalose on the assembly of hydrophobic solute neopentane in aqueous solutions. The potential of mean force calculation followed by association constant estimation suggest urea induced reduction of neopentane-neopentane association in aqueous urea solution and this neopentane-neopentane association is slightly enhanced in ternary urea and trehalose solution. The preferential interaction calculation suggests that neopentane has preference for water over urea and trehalose in ternary urea and trehalose solution. On the other hand, in binary aqueous trehalose solution, neopentane prefers to interact more with trehalose than water. We also observe the second shell collapse of water structure in aqueous urea solution and urea-trehalose mixture and strengthening of the first peak of water-water rdf in ternary urea and trehalose solution. Again, we find the decrease of translational motion of solution species in presence of osmolytes and effect is more pronounced for trehalose than for water.

■ INTRODUCTION

In order to understand the hydrophobic interactions that are responsible for protein folding and unfolding, solvation of neopentane in aqueous urea solution have also been investigated. It is generally believed that in concentrated urea solution, the hydrophobic contacts are dissolved and thereby contributing to the denaturating process of globular proteins [21, 29, 31, 163-165]. In accordance with it, Trzesniak *et al.* [166] reported the hydrocarbon transfer free energies from water to the urea solution. Their results predict that, except for methane, aliphatic hydrocarbons such as ethane, propane, *n*-butane, isobutane, and neopentane are more soluble in 6.9 M urea than in water.

Recently, Lee and Van der Vegt [27] investigated the influence of urea on the pair interaction of hydrophobic moieties using different models of neopentane, water, and urea molecules. From the analyses of equilibrium constant values of solvent-separated configuration relative to contact pair, they reported that the equilibrium shifts significantly in favor of the solvent-separated configuration in comparison to the equilibrium in pure water. Further, the analyses of the number density of water and urea molecules for the neopentane contact and solvent-separated pair show that urea preferentially interact with the nonpolar solutes. Their observation agrees with previous simulation studies on hydrophobic solvation of aliphatic [166] and aromatic hydrocarbons [28] in urea solution. It was argued that the urea-separated pair is stabilized because of the interstitial urea molecules interact through dispersion forces with two neopentane molecules at the same time [27].

In regard to the importance of hydrophobic interaction in protein science, the counteraction of the hydrophobic interaction by counteracting osmolytes like TMAO against urea denaturation have been studied extensively [26, 123, 167-169]. The results of PMFs for pairs of neopentane molecules in binary and ternary solutions of urea and TMAO shows the TMAO-induced reduction of the hydrophobic attraction both in water−TMAO and water−urea−TMAO solutions [168, 169]. Athawale *et al.* [167] investigated the effects of TMAO on the thermodynamics of hydrophobic hydration and interaction of small solutes as well as on the folding-unfolding conformational equilibrium of a hydrophobic polymer in water. The major conclusion of their study is that TMAO has a negligible effect either on the thermodynamic stability of contact and solvent-separated conformations relative to pure water.

As discussed above, the effects of urea and TMAO on hydrophobic interaction between neopentane pair have been studied previously. However, to the best of our knowl-

edge, there is no prior study that investigates the influences of urea and trehalose on the assembly of neopentane molecules in aqueous solutions. This issue is addressed in this part. We describe here the solvation characteristics of neopentane in binary and ternary solutions of urea and trehalose using 20 neopentane solute molecules. We first examine the effect of urea or trehalose on the hydrophobic interaction by calculating the solute−solute PMF followed by estimation of the association constant. To get deeper insight into how this aggregation is affected by these two, we investigate their effects on the water structure and also its direct interactions with the hydrophobic solute. The familiar water oxygen-oxygen rdf is used to describe water structuring. We also investigate the preferential accumulation of osmolytes around the neopentane molecule. Finally, hydrogen-bonding interaction and translational dynamics of different solution species are examined.

The models and simulation details are briefly described in the next section. This is followed by a section whereof we discuss our results, and our conclusions with brief summary is presented in last section.

■ MODELS AND SIMULATION METHOD

We have carried out classical molecular dynamics simulations in pure water as well as binary and ternary solutions of urea and trehalose to study its effects on neopentane aggregation. The four different systems are summarized in Table 2B-1. The initial configuration of our systems are prepared by using Packmol program [129]. For trehalose, the GLYCAM06 force field [120] is used. The SPC/E potential is used for water model [121] and smith model is used for urea [170]. For neopentane, we have used OPLS/AA [122] force field to describe the model. All the MD simulations are carried out using AMBER10 [89] suite programs at 300 K in a cubic box. The choice of different force field and simulation protocols are identical to those discussed in Part A of this chapter.

Table 2B-1. N_{neo}**,** N_{tre}**,** N_{ure} **and** M_{wat} **are the number of neopentane, trehalose, urea and water molecules and molar concentration of the trehalose respectively for all the systems**

System	N_{neo}	N_{tre}	N_{ure}	N_{wat}	volume(nm^3)	M_{tre}	M_{ure}
NW	20	0	0	1400	45.69	0.00	0.00
NTW	20	20	0	1400	52.43	0.70	0.00
NUW	20	0	250	950	49.71	0.00	8.35
NUTW	20	35	250	800	57.47	1.01	7.23

■ RESULTS AND DISCUSSION

Neopentane−Neopentane Pair Potentials of Mean Force: The neopentane−neopentane PMFs for all the systems are calculated using Eq. 2.1 and are shown in in Figure 2B-1.

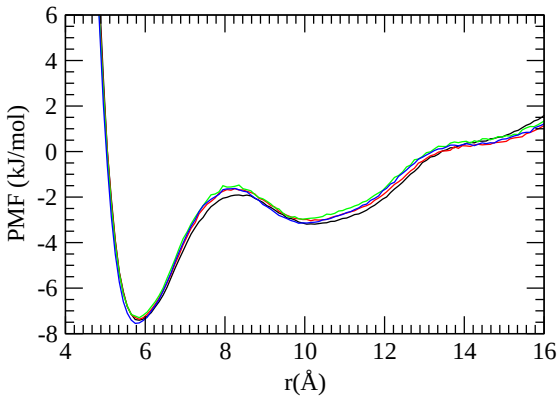

Figure 2B-1. *Neopentane−Neopentane PMFs for all the systems. NW (black), NTW (red), NUW (green), NUTW (blue).*

Focusing on the system without trehalose and urea (NW), we find the values of PMFs at CM and SSM are -7.41 kJ/mol and -3.19 kJ/mol respectively and their corresponding position of appearances are 5.85 and 10.25 Å . For this system, we observe that the well depth of CM is significantly deeper (more negative) than that of SSM. The PMF difference between SSM and CM ($\Delta W_{f\rightarrow u}$), which is related to the thermodynamic stability of the associated state, or in other words, to the association propensity of neopentane molecules in water, is positive (+4.22 kJ mol^{-1}). The positive value of $\Delta W_{f\rightarrow u}$ suggests that, a neopentane molecule prefers to be in contact with other neopentane molecules rather than to be separated by solvent molecules. The high association propensity of neopentane molecules in pure water is also reflected in the positive gradient of PMF plot at large solute separation. Now considering the trehalose solution alone (system NTW), the CM is insensitive with respect to the pure water system and the position of the SSM and BARR are slightly shifted to the shorter-r distance as compared to the pure water. On the other hand, in binary urea solution (system NUW), the CM is slightly more positive as compared to the pure water and binary trehalose solution and the position of the SSM and BARR are also shifted slightly to the shorter-r distance. These findings reveal that in binary trehalose solution, the association of neopentane molecules is reduced slightly as compared to the pure water system and also indicate slightly more reduction of hydrophobic interactions between

the neopentane molecules in binary urea solution as compared to the binary trehalose system. Now considering the mixture of urea and trehalose solution (system NUTW), we find that CM becomes slightly more deeper (more negative) than the pure water and binary solutions and SSM remains similar to the binary solutions. It suggests that hydrophobic interactions between the neopentane molecules increases in ternary solution than the binary solutions. Thus, this finding suggests that the addition of trehalose to urea solution enhances slightly the hydrophobic interaction between the neopentane molecules.

In order to understand the behavior of neopentane assembly more closely, we have computed the association constant, K_a (using Eq. 2.2) and the values of K_a for different systems are presented in Table 2B-2. We find that the value of K_a decreases in binary urea and trehalose solution as compared to the pure water, and the reduction is slightly more for binary urea solution. Note that, the decrease of association constant values with the increasing trehalose concentration is discussed in Part A of **Chapter 2**. The reduction of hydrophobic interaction in presence of urea has also been observed elsewhere [123]. So, urea helps to enhance the hydrophobic hydration. Now, considering the effect of trehalose on urea induced hydrophobic association, we observe that the association constant value increases in ternary solution compared to the both binary solutions. It indicates that urea induced lowering of hydrophobic interaction is reduced by trehalose molecules. These findings support the osmolyte induced changes in the PMF curves.

Table 2B-2. Association Constant (K_a) for Neopentane

System	$K_a(M^{-1})$
NW	8.34
NTW	7.80
NUW	7.56
NUTW	8.11

Site−Site Radial Distribution Functions: In order to obtain the molecular details of neopentane solvation in pure water and binary and ternary solutions of urea and trehalose, the site-site rdfs between the neopentane and solution species (water, urea and trehalose) are computed. And, we have also calculated the number of solution species around the neopentane solute using Eq. 2.3.

Figure 2B-2 displays the rdfs of water oxygen atom around the neopentane central carbon atom.

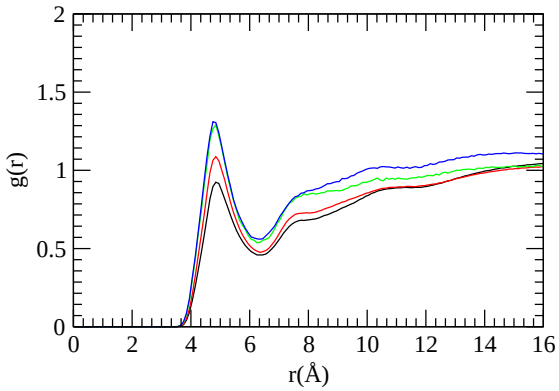

Figure 2B-2. *Site-Site distribution functions involving neopentane central carbon atom and water oxygen. NW (black), NTW (red), NUW (green), NUTW (blue).*

Focusing on the hydration of neopentane in pure water, we notice that the neopentane-water rdf starts to rise at 3.35 Å and reaches the maximum at 4.85 Å of g(r)= 0.92. Hence, below 4.85 Å , water molecules are excluded from the solvation shell of neopentane. The first minimum which appears at 6.35 Å indicates the outer limit of the first hydration shell of neopentane. We also find that the first peak water density is only 0.92 times to the bulk water density. This low water density around the neopentane molecules compares well with the already reported results [133]. Again, this significantly small water density around the neopentane indicates the high aggregation propensity of neopentane molecules in pure water. Further, we observe that with the addition of osmolytes the first peak height increases monotonically. The first peak height for binary urea solution is higher than the binary trehalose solution, suggesting lower hydration of neopentane molecules in trehalose solution than urea solution. These results are in accordance with the observed association constant values. On the other hand, in ternary urea/trehalose solution, the first peak height remains similar to the binary urea solution, although, we have observed higher hydrophobic interaction in ternary mixture than the binary solutions. This can be considered as due to the large exclusion of trehalose molecules form the neopentane surface (discussed below).

We have calculated the first shell coordination number to understand the extent of hydrophobic solvation of neopentane molecules in pure water and binary and ternary solutions and these are presented in Table 2B-3. We have observed that first shell water coordination number decreases in both binary and ternary solutions of urea and trehalose though the first peak height and first minimum increases in the corresponding neopentane-

water rdfs. We trace this anomaly is due to the presence of osmolytes and also due to the reduced number density of water. To exclude the effect of reduced number density of water in osmolytes solutions, we have calculated the coordination numbers assuming that the only change with added osmolyte comes through the reduced number of water and these values are given in the parentheses of Table 2B-3. From these normalized coordination numbers, we noticed that in both binary and ternary solutions, there is an increment in number of water molecules in the first hydration shell of neopentane. This observation suggest the dispersion of neopentane molecules in the osmolytes solutions. However, this increment is slightly lower for ternary urea/trehalose solution than the binary urea solution. Moreover, we find that the ratio of first shell water molecules in pure water and aqueous osmolytes solutions is lower as compared to the respective ratio of water molecules in those systems. For example, the ratio of water molecules in pure water and in binary urea solution is 1.29:1, which is lower than the ratio of total number of water molecules in those systems (1.47:1). These observations also indicate the urea induced hydration of neopentane molecules.

Table 2B-3. First shell coordination number (CN) for water (O_w), urea (C_u) and trehalose (O1) around a neopentane molecule[a]

System	CN_{Ow}	CN_{Cu}	CN_{O1}
NW	15.46	-	-
NTW	15.14 (13.49)	-	0.55
NUW	11.95 (9.65)	4.39	-
NUTW	9.29 (7.03)	3.67 (3.79)	0.58 (0.87)

[a]The numbers given in parentheses represent the first shell trehalose molecules if the only change added osmolytes came through the water number density change.

To understand the role of trehalose and urea on neopentane aggregation, we have calculated the selected site-site rdfs of trehalose and urea around neopentane molecule and the same are shown in Figure 2B-3.

The rdfs of trehalose hydroxyl oxygen (O6), acetalic ring oxygen (O5) and glycosidic oxygen (O1) around the neopentane central carbon atom are shown in (a)-(c) of Figure 2B-3. In the neopentane central carbon atom-trehalose hydroxyl O6 rdf (Figure 2B-3 (a)), the first peak appears at about 4.85 Å with a peak height 1.53 in binary trehalose solution. It indicates the considerable interaction of trehalose with neopentane in binary trehalose solution. But, in urea/trehalose mixture, we find that first peak height and first

minimum decreases significantly for this rdf. The other two trehalose oxygen O5 and O1 (Figure 2B-3 (b) and (c)) also show decreased interaction with the neopentane in ternary solution. It suggests the exclusion of trehalose molecules from the neopentane surface.

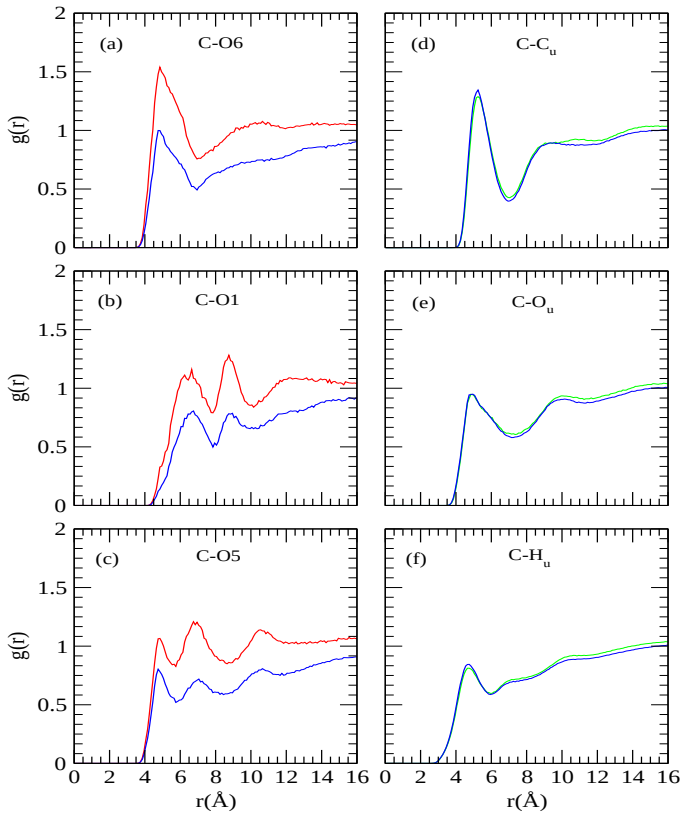

Figure 2B-3. *(a), (b) and (c) represent the neopentane-trehalose site-site distribution functions and (d), (e) and (f) represents the neopentane-urea site-site distribution functions. NTW (red), NUW (green), NUTW (blue).*

Furthermore, we have calculated the first shell coordination number of trehalose glycosidic oxygen (O1) around the neopentane central carbon atom and are presented in Table 2B-3. We find that the coordination number for both the systems are similar though the ternary system has higher trehalose concentration. However, the expected value that is calculated by considering reduced number density of trehalose, is much larger than the first shell coordination number. These features also indicate the exclusion of trehalose molecules from the neopentane surface in ternary solution. Considering the interaction of urea with the neopentane, in Figure 2B-3 (d)-(f), we have shown the rdfs of neopentane central carbon atom and urea carbon, oxygen and hydrogen atom. For neopentane carbon and urea carbon

rdf in binary urea solution (see Figure 2B-3 (d)), the first peak appears at 5.25 Å with a peak density of 1.25 and first minimum appear at 7.05 Å . It is interesting to note that, the urea density around the neopentane is higher compared to the water density in binary solution, which indicate the direct interaction of urea molecules with the neopentane. Further, we find that the neopentane-urea interaction does not show much awareness of the presence of trehalose molecules in ternary solution. Since the neopentane-urea interaction does not change significantly and neopentane-trehalose interaction weaken in ternary solution, these results support the rise of neopentane-water rdfs in ternary solution. Again, we noticed that urea's density around the neopentane is much higher than trehalose in ternary urea/trehalose solution, which suggests more preference for urea as compared to trehalose in urea/trehalose mixture. These observations indicate the exclusion of trehalose molecules from the neopentane surface, which is further supported by the preferential interaction parameter calculations (discussed below).

To evaluate the influence of urea and trehalose on water structure, which indirectly provides the details of the hydrophobic hydration of neopentane molecules by water molecules, we have shown the water oxygen-water oxygen (g_{Ow-Ow} (r)) distribution functions (Figure 2B-4). In pure water system, the first peak, which characterizes the first H-bonded neighbor and the second peak that represents the tetrahedrally located neighbor in $O_w - O_w$ rdf appear at about 2.75 Å and 4.45 Å, respectively. The locations of these peaks are consistent with those already reported elsewhere [38, 123, 133]. Considering the effect of trehalose on $O_w - O_w$ rdf (system NTW), we observe that the magnitude of both first peak height and second peak height increase slightly keeping their locations unchanged. But, in binary urea solution, the first peak height becomes even more stronger and urea make the first valley shallower and as a consequence the second peak becomes less pronounced. This suggests a modest second shell collapse of water structure in urea solution. This change of water structure in urea solution is consistent with the previously reported results [38]. On the other hand, in ternary urea/trehalose solution, the first peak height increases further and the second shell becomes more shallower.

In Figure 2B-5, we have shown the typical site-site rdfs involving trehalose hydroxyl oxygen (O6), glycosidic oxygen (O1) and acetalic ring oxygen (O5) atoms with respect to the water oxygen. As discussed in part A of this chapter, we notice the presence of sharp peak at about 2.75 Å of peak intensity 1.64 in the trehalose hydroxyl oxygen (O6) and water oxygen rdf, which indicates the hydrogen bonding interaction between water and trehalose (see Figure 2B-5 (a)).

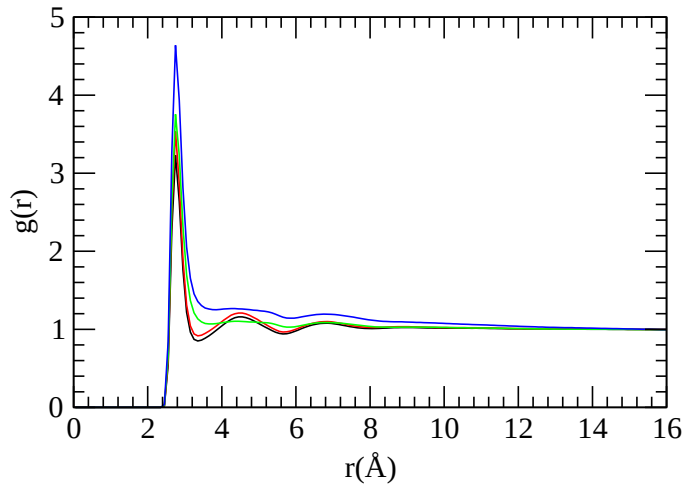

Figure 2B-4. *Site-site distribution functions involving water oxygen and water oxygen. NW (black), NTW (red), NUW (green), NUTW (blue).*

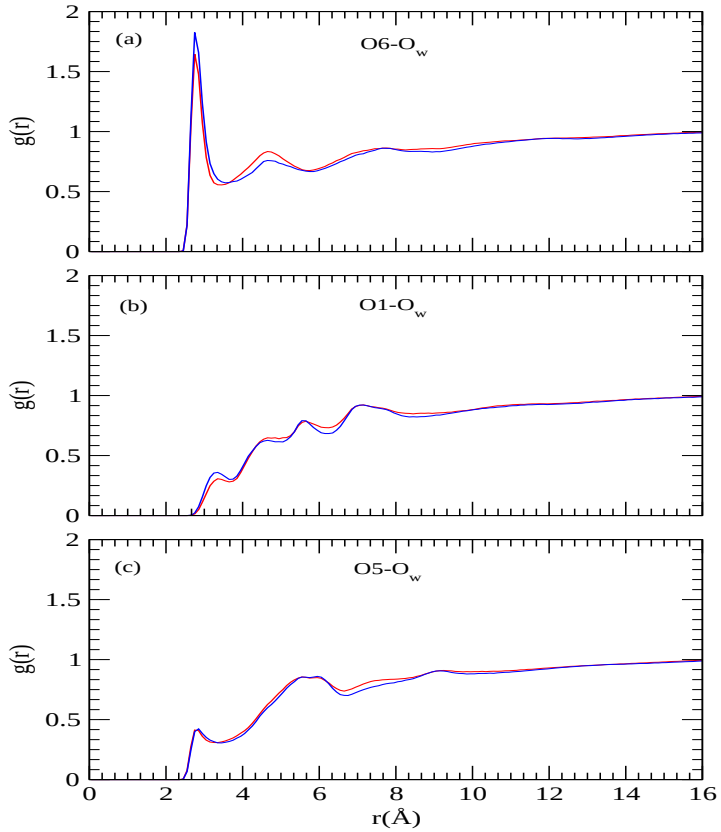

Figure 2B-5. *Site-site distribution functions between trehalose and water. NW (black), NTW (red), NUW (green), NUTW (blue).*

Since, the other hydroxyl oxygen atoms (O2, O3 and O4) show similar hydration behavior as that of hydroxyl O6 atom, we show only the O6-O_w rdf. Unlike hydroxyl oxygen of trehalose, the O1-O_w and O5-O_w rdfs (Figure 2B-5 (b) and (c)) do not show such well defined solvation peaks, therefore these oxygens are not well hydrated. Thus, the hydroxyl oxygens of trehalose only participate in hydrogen bonding interactions with the water molecules. We note that these typical behavior of trehalose oxygens and water oxygen are reported in literature and our results match well with those results [136-140]. Furthermore, in ternary solution, we find that the height of the first peak of these rdfs are getting enhanced. This enhancement in trehalose-water rdf act as a corroborative evidence what we have observed in neopentane-trehalose rdf. Though the peak height increases, the first shell water molecules around the trehalose decreases from 21.68 (in system NTW) to 14.28 (in system NUTW). This decrease of coordination number can be attributed to the effect of reduced water number density for system NUTW. As a result, water-trehalose hydrogen bond number decreases from binary trehalose system to ternary urea/trehalose solution (see below).

The interaction of trehalose hydroxyl oxygen O6, glycosidic oxygen (O1) and acetalic ring oxygen with urea (oxygen and hydrogen) by considering selected site-site rdfs are shown in Figure 2B-6. From the magnitude of the first peak height of these distribution functions (Figure 2B-6 (a)), it confirms that the trehalose hydroxyl oxygen (O6) involves sufficiently in the trehalose-urea hydrogen bonding interaction. The hydrogen bonding interaction between urea and trehalose molecules is also quite evident from oxygen O6 and hydrogen (H_u) of urea rdfs (Figure 2B-6 (b)). By comparing the first peak heights of O_u-O6 and H_u-O6 rdfs, we find that in the hydrogen bonding interaction between trehalose and urea, the later preferably acts as an acceptor.

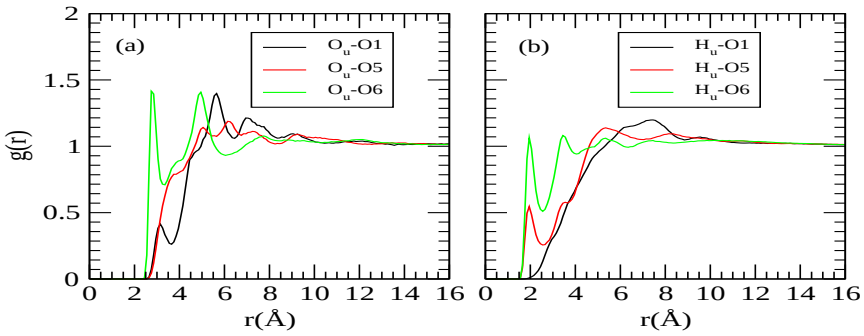

Figure 2B-6. *Site-site distribution functions between urea and trehalose for NUTW system.*

The distribution of water molecules around different atomic sites of urea are displayed in Figure 2B-7. For binary urea solution, we observe the first contact peaks at about 2.85 Å and 1.85 Å in urea oxygen-water oxygen ($O_u - O_w$) and urea oxygen-water hydrogen ($O_u - H_w$) rdf profiles, respectively, which reflect the formation of urea-water hydrogen bond. Note that the first peak in $O_u - H_w$ rdf is much stronger than the $H_u - O_w$ rdf. Thus in water-urea hydrogen bonding urea prefers to be a hydrogen bond acceptor rather than a donor. This hydrogen bonding interaction between urea and water increases moderately in ternary urea and trehalose system.

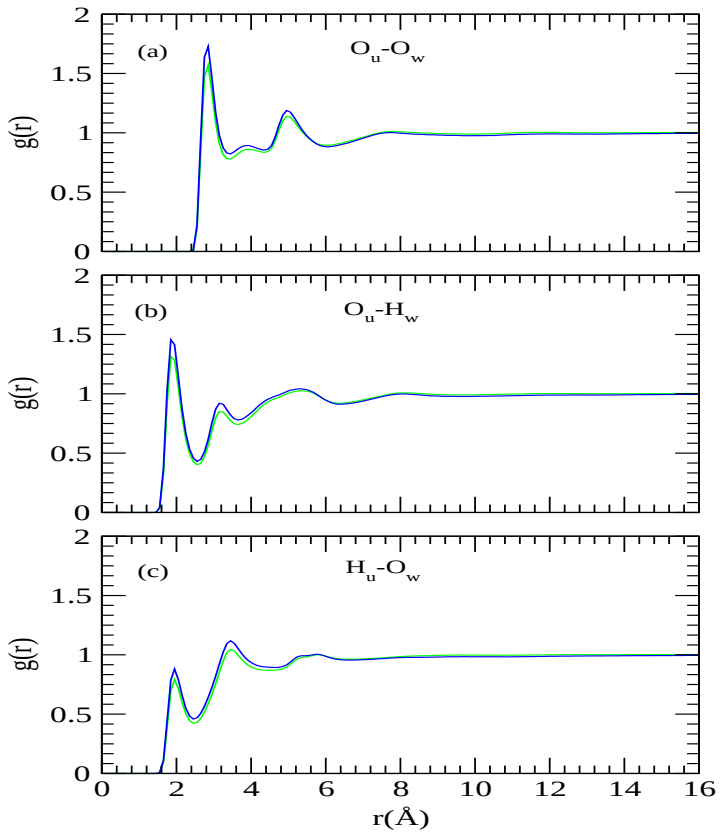

Figure 2B-7. *Site-site distribution functions between urea and water for NUW (green) and NUTW (blue) system.*

Preferential Interaction: To understand the neopentane solvation in different binary and ternary solutions more closely, we have also examined the local environment of neopentane in different solutions and compared it with that of the bulk solution. Thus, following earlier works [84, 171] the time-averaged normalized ratio of water ($g_{ow}(r)$), trehalose ($g_{ot}(r)$) and urea ($g_{cu}(r)$) are calculated. These parameters provide the information about the relative

local distribution of these solution species at a distance r from neopentane molecule and are defined as

$$g_{ow}(r) = \frac{n_{ow}(r) \times (N_{ow} + N_{ot} + N_{cu})}{N_{ow} \times (n_{ow}(r) + n_{ot}(r) + n_{cu}(r))} \tag{2.7}$$

$$g_{ot}(r) = \frac{n_{ot}(r) \times (N_{ow} + N_{ot} + N_{cu})}{N_{ot} \times (n_{ow}(r) + n_{ot}(r) + n_{cu}(r))} \tag{2.8}$$

$$g_{cu}(r) = \frac{n_{cu}(r) \times (N_{ow} + N_{ot} + N_{cu})}{N_{cu} \times (n_{ow}(r) + n_{ot}(r) + n_{cu}(r))} \tag{2.9}$$

where $n_{ow}(r)$, $n_{cu}(r)$ and $n_{ot}(r)$ are the number of water oxygen, urea carbon and trehalose hydroxyl oxygens, respectively, in the local domain of radius r from the neopentane center of mass and N_{ow}, N_{cu} and N_{ot} represent the total numbers of water oxygen atoms, urea carbon atoms and trehalose hydroxyl oxygen atoms in the simulation box, respectively. In the close proximity of neopentane, if the ratio g_{ow}(r) is greater than one, the neopentane is preferentially hydrated by water molecules, conversely, water is preferentially excluded from neopentane surface, if the value of g_{ow}(r) is lower than one. We have shown the normalized ratio of water oxygen, urea carbon and trehalose hydroxyl oxygens as function of distance from neopentane center carbon atom in Figure 2B-8.

Considering the changes of the ratio $g_{ow}(r)$ with the distance, we observe that the value of $g_{ow}(r)$ is greater than 1 in the close proximity of neopentane surface for all the binary and ternary solutions. For binary trehalose solution, the value of $g_{ow}(r)$ is almost equal to one. But, for binary urea solution, this value is slightly above one. These results suggest the modest preference for water molecules near to the neopentane in binary osmolytes systems. On the other hand, in mixed urea/trehalose ternary system, the value of $g_{ow}(r)$ is greater than one and this ratio remains higher than the binary osmolyte systems. It indicates that in ternary solution, neopentane molecules prefer to be hydrated by water molecules. This observation acts as an corroborative evidence of what we have observed in neopentane water-rdfs. Further, the ratio of $g_{ot}(r)$ for binary trehalose solution suggests the higher preference for trehalose over water and this can be considered as the reason of reduction of hydrophobic interaction in binary urea solution. But, the magnitude of $g_{ot}(r)$ for mixed urea/trehalose solution reveals that neopentane's preference for trehalose decreases moderately compared to the binary trehalose solution.

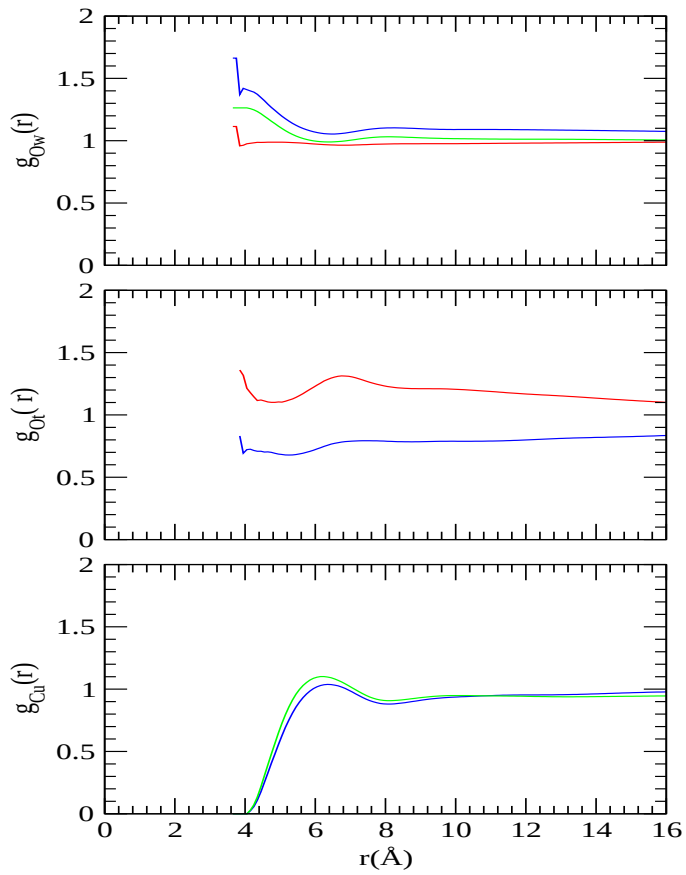

Figure 2B-8. *Time-averaged normalized fraction of water, urea and trehalose as a function of the distance from the neopentane center of mass. NTW (red), NUW (green), NUTW (blue).*

In binary urea solution, the value of $g_{cu}(r)$ is slightly higher than one in the close proximity of neopentane and remains close to one at larger-r distance. Now, comparing the value of $g_{ow}(r)$ and $g_{cu}(r)$ in binary urea solution, we find that in the close proximity of neopentane, water is more preferred than the urea. On the other hand, the preferential interaction parameter, $g_{cu}(r)$, decreases slightly in the close proximity of the neopentane for mixed urea/trehalose system as compared to the binary urea solution. Therefore, in ternary mixed osmolytes system, the trehalose molecules are expelled largely from the neopentane solvation layer along with urea molecules and neopentane interacts preferentially with water. This preferential exclusion of trehalose and urea from the neopentane surface can be attributed to the trehalose's bioprotection ability.

Hydrogen Bonding: As observed in trehalose-water rdfs, in aqueous solution, trehalose has high propensity to form hydrogen bonds with water molecules because of the presence

of hydrophilic hydroxyl group in it. Due to this, trehalose also forms hydrogen bonds with urea and other trehalose molecules effectively. The formation of these hydrogen bonds has great effect on the water structure and trehalose aggregation, which subsequently may impact on trehalose's role as a protective co-solute to biomolecules [148, 149]. The average number of hydrogen bonds between water-water, water-trehalose, water-urea, urea-urea, trehalose-trehalose and urea-trehalose are shown in Table 2B-4 (see Part A for methods).

Table 2B-4. HB_{W-W}, HB_{U-W}, HB_{U-U}, HB_{T-W}, HB_{T-T} **and** HB_{U-T} **represents the average number of water-water, urea-water (per urea), urea-urea, water-trehalose (per trehalose), trehalose-trehalose, and urea-trehalose (per urea) hydrogen bonds, respectively**

System	NW	NT	NU	NUT
HB_{W-W}	3.48	3.31	2.68	2.34
HB_{U-W}	–	–	3.37	2.70
HB_{U-U}	–	–	1.20	1.12
HB_{T-W}	–	11.44	–	7.20
HB_{T-T}	–	–	1.38	1.56
HB_{U-T}	–	–	–	0.88

The water-trehalose hydrogen bonds per trehalose for binary trehalose system is 11.44, which is in agreement with the earlier works [137, 172]. However, considering the same hydrogen bonding criterion, Liu *et. al.* reported that the average water-trehalose hydrogen bond number is 22.4 for TIP3P water model [153]. This difference in the hydrogen bond number is due to the presence of neopentane molecules and higher trehalose concentration. We observe that on addition of osmolytes, the average number of water-water hydrogen bond number (per water) decreases. This decrease is due to the formation of hydrogen bonds between water and osmolytes (urea and trehalose). In comparison to binary urea solution, we find that urea-urea hydrogen bond number decreases in ternary urea/trehalose mixture. Further, the presence of trehalose molecules in ternary solution causes a reduction in the urea-water hydrogen bond number and about 0.67 number of urea-water hydrogen bond is lost by per urea molecule as one moves from binary urea solution to ternary urea/trehalose mixture. We also observe the reduction of 0.08 urea-urea hydrogen bond number for ternary system. These loss of hydrogen bonds by urea molecules is well compensated by the urea-trehalose hydrogen bonds.

Trehalose Clusters and Diffusion Coefficients: To obtain further insights in to the

effect of trehalose on trehalose cluster and dynamical properties more closely, we have calculated the mean cluster size $< n_{tre} >$ (using Eq. 2.5) as well as diffusion coefficients (using Eq. 2.6) of all solution species. The average trehalose cluster size together with the diffusion coefficient values of water (D_w), trehalose (D_T), urea (D_U) and neopentane (D_N) for different systems are presented in Table 2B-5.

Table 2B-5. D_w**,** D_T**,** D_U**,** D_N **and** $< n_{tre} > /N_{tre}$ **correspond to diffusion coefficient of water, trehalose, urea, neopentane and normalized mean cluster size, respectively**[a]

System	D_w	D_T	D_U	D_N	$< n_{tre} > /N_{tre}$
NW	2.55	–	–	0.08	–
NTW	2.00	0.11	–	0.06	0.31 ($\pm$0.02)
NUW	2.49	–	1.18	0.11	–
NUTW	1.28	.03	0.40	0.03	0.33 ($\pm$0.02)

[a] Diffusion coefficient are the time $10^{-5} cm^2 sec^{-1}$. The standard errors for normalized mean cluster size is given in parenthesis, which calculated using the block average over 1 ns.

The values of $< n_{tre} > /N_{tre}$ for binary trehalose and ternary urea/trehalose system are 0.31 and 0.33, respectively. Though the trehalose concentration is slightly higher for the ternary system than the binary trehalose system, the observed mean cluster size for both the systems are almost similar. This behavior of cluster size in ternary solution is due the formation significant trehalose-urea hydrogen bonds. Moreover, for both the trehalose solutions, the percolation of trehalose hydrogen bond network is yet to be achieved, which is due to the lower trehalose concentration and the presence of neopentane and urea molecules in the systems. In this context, Lerbret *et al.* [155] reported that in water-trehalose system, the percolation of trehalose hydrogen bond network occurs at 66 wt% of trehalose. Note that, the the change in $< n_{tre} > /N_{tre}$ values are in accordance with trehalose-trehalose (per trehalose) hydrogen bond formation for these systems discussed above (see Table 2B-4).

Now, by observing the dynamical properties of solution species, we find that diffusion coefficient values of all solution species decreases with the addition of osmolytes. In pure water, the diffusion coefficient of water is $2.55 \times 10^{-5} cm^2 sec^{-1}$, which compares reasonably well with the experimental finding of diffusion coefficient value [157]. A more insights in to the diffusion coefficients values of water reveal that the reduction of water dynamics in binary trehalose solution is more than the binary urea solution. This is because of the formation of strong trehalose-water hydrogen bonds in binary trehalose solution. The presence of both osmolytes (urea and trehalose) in ternary solution, decreases the

diffusion coefficient of water further. Here, we note that Terahertz absorption measurement also shows the slowing down of translational and rotational motion of surrounding water molecules by trehalose molecules [69]. In this context, it is hypothesized that the bioprotection ability of trehalose comes because of the retardation of the surrounding water molecules due to presence of trehalose molecules [70, 173]. Again, the dynamics of urea molecules also decreases due to the urea-trehalose hydrogen bond in ternary solution, which is 2.95 times lower than the binary urea solution. The diffusion coefficient of trehalose decreases from $0.11 \times 10^{-5} cm^2 sec^{-1}$ in binary trehalose system to $0.03 \times 10^{-5} cm^2 sec^{-1}$ in ternary urea/trehalose system (almost 3.66 times lower). This rapid decrease of D_{tre} value is because of the sharp increase in its viscosity value [158]. We also observe the decrease of neopentane diffusion coefficient values in presence of osmolytes, but the change is more prominent for ternary urea/trehalose system.

■ SUMMARY AND CONCLUSIONS

In this part, we discuss the hydrophobic interactions of neopentane molecules and also the structure of solution in presence of two naturally occurring osmolytes urea and trehalose. The potential of mean force calculations and followed by association constant values suggest that relative to pure water, the binary trehalose solution destabilize the hydrophobic interactions between the neopentane molecules slightly and thereby trehalose favors the hydration of neopentane molecules. Further, to find the origin of increased solubility of neopentane in binary trehalose solution compared to pure water, we have studied the interaction preference of neopentane with water and trehalose and the role of trehalose molecules on the water structure. We have observed that neopentane molecules interact preferably with trehalose molecules over water molecules. On the other hand, the destabilizing effect of binary urea solution on neopentane aggregation is slightly higher than the binary trehalose solution. Note that, urea induced decrease of hydrophobic interaction of neopentane molecules is in agreement with the increased solubility of neopentane in aqueous urea solution [166]. Again, the analysis of rdfs of urea and water around neopentane indicates that urea is preferred in the solvation shell of neopentane. This clearly suggests that urea-induced reduction of hydrophobic interaction is due to the direct interaction of urea with the nonpolar molecules. The PMF and association constant analyses suggest that in ternary urea/trehalose solution, the hydrophobic interaction increases slightly than the binary urea and trehalose solutions. This indicates the slight counteracting effect of trehalose on urea induced hydrophobic interaction. Moreover, the hydration of neopentane

and exclusion of trehalose and urea molecules are also observed in urea/trehalose mixture.

The hydrogen bond analyses show that water-water hydrogen bond network is disrupted by urea and trehalose molecules. The breaking of water-water hydrogen bond (per water) is more in binary urea solution than binary trehalose solution and it breaks further in urea/trehalose mixture. We also observed decrease of water-trehalose (per trehalose) and water-urea (per urea) hydrogen bond numbers. And strong hydrogen bonding interaction between urea and trehalose. The solvation of trehalose by urea and water along with trehalose induced strengthening of water-water first peak could be an important factor in preventing water and urea molecules to solvate the protein and consequently prevent the protein denaturation. Further, translational diffusion coefficient calculations show the trehalose induced slowing down of translational motion of all solution species and the effect is more pronounced for trehalose molecules than that for water. The calculation of diffusion coefficient for water and trehalose molecules are compared reasonably well with the available experimental values.

Combining the results of Part A and Part B, it is reasonable to conclude the exclusion of trehalose molecules from the hydrophobic side-chains of proteins both at low and high temperature and also in presence of urea, which significantly affects the hydrophobic interaction. In all likelihood, trehalose also exerts its protein stabilizing effect via the protein backbone. In the next chapter, we shall treat the trehalose's effect on protein backbone.

Chapter 3

Solvation of Protein Backbone

"The major factor which opposes and overrides the side chain preference for denaturation and results in the stabilization of proteins observed in osmolytes is the highly unfavorable exposure of polypeptide backbone on unfolding. ....The prevalence of the unfavorable transfer free energy of the peptide backbone, and the fact that the peptide backbone unit is the most numerous group in a protein, makes it an extremely important factor in influencing the character of protein conformations existing in both stabilizing and destabilizing solvents."

– Y. Liu and D. W. Bolen *Biochemistry* **34**, 12884 (1995)

The previous chapter of this thesis dealt with hydrophobicity of hydrocarbon neopentane (**Chapter 2**). However, protein stability is governed not only by hydrophobic interactions, but also by the backbone hydrogen bonding interactions. A substantial works on free energy change that accompany the solvation of amino acid side chains and peptide backbone units from water to other solvent have been carried out to understand the protein folding process [174-177]. Therefore, the measurement of hydrophobicity, hydrogen bonding, and aqueous solvation of proteins are key to understand the protein structure and stability [99, 178]. Moreover, the protein backbone is found to play a dominant role in determining the extent of protein (de)stabilization by osmolytes, with the side-chains playing only a minor role, and consequently, it was concluded that the osmolytes exert their effect on protein stability predominantly via the protein backbone [176, 177, 179, 180]. So there is a natural choice of investigation of backbone solvation in aqueous osmolytes solutions.

In response to the backbone solvation in aqueous osmolytes solutions, in this chapter, we use N-methylacetamide (NMA) as model of protein backbone. The solute NMA is the smallest amide that contains a peptide linkage ($O = C - N - H$) terminated by hydrophobic (methyl) groups on the carbonyl carbon and on the amide nitrogen. Hence it holds the special status as a minimal model of the protein backbone with the advantage of being small enough to be accessible by both current experimental and computational techniques. In the work described in this chapter, we have considered the dilute NMA solutions in order to provide sufficient number of NMA solvation sites for solution species avoiding NMA-NMA hydrogen bonds as much as possible. In other words, the systems considered here, therefore, have negligible NMA-NMA hydrogen bonds and they represent the typical solvent exposed states of protein in which protein backbone atoms are free to interact with the solution species.

As before, the chapter is organized into two parts. The temperature dependence solvation of NMA in aqueous trehalose solutions are explored in Part A, and we discuss solvation of NMA in aqueous solutions of urea and trehalose in Part B.

Part A:

Amide Solvation in Water and Aqueous Trehalose Solutions at Different Temperatures

Overview: To investigate the solvation of protein backbone, we report MD simulation results of aqueous solution of NMA both in presence and absence of trehalose at five different temperatures ranging from 285 K to 345 K at 1 atm pressure. For each temperature, we consider six different trehalose concentrations ranging from 0% to 66%. For a given temperature, we find the accumulation of more than *expected* water molecules in the first solvation shell of hydrophobic methyl group of NMA when trehalose concentration is very high. Further, our calculations of hydrogen bond properties reveal the formation of more and more trehalose-NMA hydrogen bonds and the breaking of water-NMA hydrogen bonds as trehalose concentration is increased. Though we observe temperature induced breaking of water-trehalose hydrogen bonds, interestingly, water-water and water-trehalose hydrogen bonds tend to off set the effect of temperature when trehalose concentration is high. The calculated site-site distribution functions involving NMA and water molecules show that NMA prefers to act as acceptor and not to be a donor when it forms hydrogen bonds with water. In regard to water structures in different systems, we find that trehalose and temperature has two opposing effects. To be specific, increased temperature causes breaking in water structure on the other hand water in the solutions becomes more structured as trehalose concentration is increased. The translational motions of different solution species are also calculated and we observe trehalose induced retardation in the diffusion coefficient values for different solution species with more pronounced effect for trehalose and NMA. We also observed: (a) Enhancement in the trehalose-trehalose hydrogen bond network as trehalose concentration increases and (b) involvement of NMA molecules in the trehalose cluster.

■ INTRODUCTION

Amides are important in biochemistry, because it provides the simplest model for studying the structural and conformational characteristics of protein or peptide backbone. The solvation of amides has widespread biological importance and therefore, the molecule NMA has been the subject of extensive experimental and theoretical investigations to understand the chemical and biological processes. Interestingly, water molecules can form hydrogen bonds with the main chain through $C = O$ and $N - H$ group of peptide and plays an important role in the structural properties of proteins. Many theoretical work have been performed to investigate the hydrogen bonding interaction in solvated NMA and provide information of protein hydration at molecular level [181-183]. In aqueous solution, NMA can act both as donor and acceptor, as revealed by UV Raman studies [184-187] and normal coordinates analysis [188]. Water hydrogen bonding to the carbonyl oxygen has been reported to be stronger than that of amide hydrogen [184-190]. Moreover, combining FT-IR spectroscopy with density functional theory (DFT) calculations for various solute concentrations of NMA in a water saturated solution of carbon tetrachloride, K*ö*ddermann and Ludwig [189] showed that the peptide−peptide interactions are stronger than the peptide−water interactions. On the other hand, approximately isoenergetic amide−amide and amide−water interactions were indicated in a separate study [191].

The majority of works are focused on the hydration of NMA in NMA-water mixtures and providing the useful information about backbone hydration. In 2011, Kaminsk*ý* *et al.* [192] reported the temperature dependence amide I vibration as well as water structure around the carbonyl carbon and amide hydrogen from the DFT and MD calculations. Their result showed that temperature weaken the interaction of water with the carbonyl oxygen and amide hydrogen. Moreover, they found that the hydration of $N - H$ group is weaker as compared to the CO group in NMA-water solution.

As discussed above, a much less number of work has been done to understand the effects of osmolyte and temperature on NMA hydration and NMA-osmolyte direct interaction. Moreover, the details analysis of solvation of NMA in presence of trehalose has not been done previously, to provide the the molecular mechanism of the bioprotecting ability of trehalose. Therefore, to get better idea of backbone solvation, we investigate herein the solvation characteristics of NMA in binary solution of trehalose at different temperature. Various structural, and dynamical properties that describe NMA solvation are examined first. We then study the solvation of trehalose by water with an attempt to

dissect the molecular mechanism.

What follows in this part are brief description of the models and simulation method, discussion of the results obtained, and finally, our concluding remarks and brief summary.

■ MODELS AND SIMULATION METHOD

We carried out classical MD simulation of NMA-trehalose-water solutions at five different temperatures ranging from 285 K to 345 K and at 1 atm pressure. Keeping in mind that trehalose protects the biomolecules at extreme environmental conditions (as discussed in the **Chapter 1**), the temperatures of our study were chosen in such a manner that the effect of trehalose can be examined at low to moderate to high temperature regions. For each temperature, we consider six different systems with a regime of trehalose concentrations and these are presented in Table 3A-1.

Table 3A-1. Overview of Simulations[a]

System	N_{NMA}	N_{tre}	N_{wat}	Volume (nm^3)					
				285 K	300 K	315 K	330 K	345 K	w_{tre}%
S0	20	0	1000	31.96	32.15	32.60	33.19	33.68	0
S1	20	10	1000	35.28	35.29	36.04	36.49	36.95	16
S2	20	20	1000	38.97	39.30	39.75	40.05	40.47	28
S3	20	50	1000	49.63	49.83	50.37	50.95	51.59	49
S4	20	75	1000	58.44	58.86	59.46	59.80	60.49	59
S5	20	100	1000	67.36	67.97	68.51	69.16	69.47	66

[a] N_{NMA}, N_{tre}, N_{wat}, volume and w_{tre} represent the number of NMA, trehalose, water molecules, box volumes and weight percentage of trehalose respectively, for different systems.

The starting configuration of our systems are prepared using Packmol program [129]. For trehalose molecule we employ GLYCAM06 force field [120] that is widely used for the simulations of monosaccharides and oligosaccharides. In our study we use the popular SPC/E [121] model for water. For NMA, all atom force field is employed in which the hydrogens of methyl groups are considered explicitly [193]. For each system, the solution properties are investigated by performing MD simulations on AMBER12 [90] suite of programs.

For the details of choice of different force field and simulation protocols, one can go through **Chapter 2**. In brief, MD simulations were performed in a cubic box at five different temperature, initially, energy minimization was carried out for 5000 steps and then heat up the system slowly from 0 K to the desired temperature for 100 ps in NVT ensemble. After that, systems were equilibrated in NPT ensemble for 2 ns and production run were further carried out for another 40 ns in NPT ensemble. After that, we continued for another 15 ns NVE ensemble simulation for calculating diffusion coefficients of different solution species.

■ RESULTS AND DISCUSSION

Interaction of NMA with Solution Species: A selection of site-site rdfs that illustrate the interactions between NMA with the solution species are presented in Figures 3A-2−3A-5. Since NMA molecules contain hydrophobic methyl groups, in this section our goal is to explore the effect of trehalose and temperature on the hydrophobic hydration of these methyl groups. In order to have a more detailed solvation picture of NMA we also examine the first-shell coordination number of water molecules around the methyl groups of NMA. Furthermore, hydrophilic carbonyl oxygen and amide hydrogen of NMA also participate in hydrogen bonding interaction with water and trehalose molecules. So, we have calculated number of the hydrogen bonds between NMA and solution species as function of temperature and trehalose concentration using a geometric criteria (see Part A of **Chapter 2** for method). However, in support of the hydrogen bond criteria that used in this section for defining hydrogen bonds between solution components, we have presented the probability contour plots as a function of Donor-Hydrogen-Acceptor angle and Acceptor-Hydrogen distance for system S5 at 300K in Figure 3A-1. It can be seen that the hydrogen bond criteria used in this section fall in the region of high probability of formation of strong hydrogen bonds.

The site-site NMA-water rdfs that provide information about hydrophobic hydration of hydrophobic methyl group of NMA and different hydrogen bonding interactions between water and NMA molecules are plotted in Figures 3A-2−3A-6. In this thesis, the methyl carbon attached to carbonyl carbon of NMA is termed as Me_1 and the other methyl carbon that attached to nitrogen atom of NMA is termed as Me_2. The Me_1-water oxygen and Me_2-water oxygen distribution functions are are shown in Figures 3A-2−3A-3.

Considering the rdfs between different hydrophobic atomic sites of NMA and water molecules first (see Figure 3A-2−3A-3), we notice that both the methyl groups of NMA

show the typical behavior of hydrophobic hydration [123, 134].

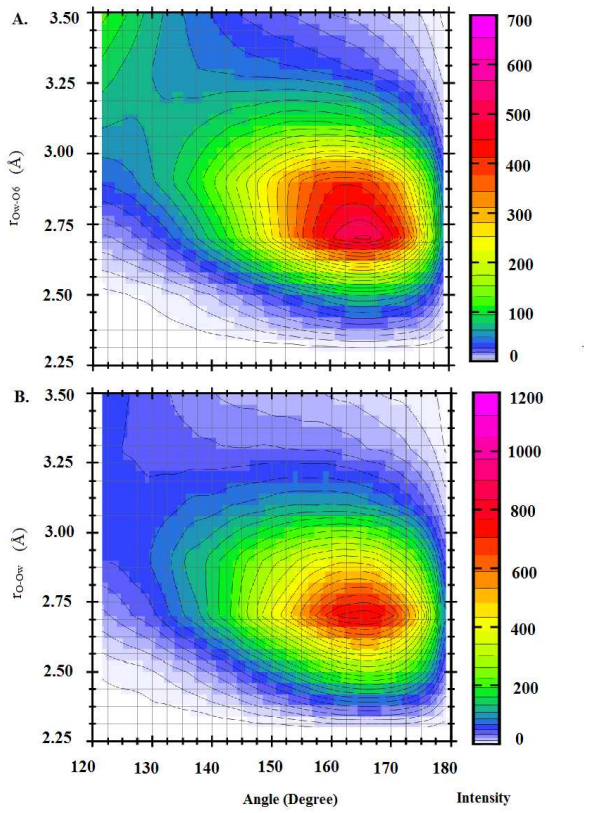

Figure 3A-1. *Probability distribution contour plots as function of hydrogen bond angle (Donor-Hydrogen-Acceptor) and Acceptor-Hydrogen distance for system S5 at 300K. (A) is for water oxygen-trehalose hydroxyl oxygen (O6) (B) is for NMA oxygen-water oxygen.*

In specific, for pure water system the rdf of Me_1 and water oxygen (and hydrogen), O_w (and H_w), (Figure 3A-2 (a)), we find that $Me_1 - O_w$ rdf starts to rise at 2.75 Å and reaches the bulk density at 3.65 Å for which g(r)=1. Thus, below 3.65 Å water molecules are actually excluded from the solvation shell of methyl group. The first minimum of this rdf, which appears at 5.45 Å is considered as the outer limit of the first hydration shell of the Me_1 group. We also find that $Me_2 - O_w$ rdf (Figure 3A-3 (a)) shows similar hydration characteristics as that of $Me_1 - O_w$ rdf. But, the water distribution around the former is slightly better defined as compared to that of the later as revealed by an enhancement in the first peak height and the inward movement of the first minimum in $Me_2 - O_w$ distribution function. We note that for these two methyl groups, the water distribution is less narrower when compared to that of methane [134].

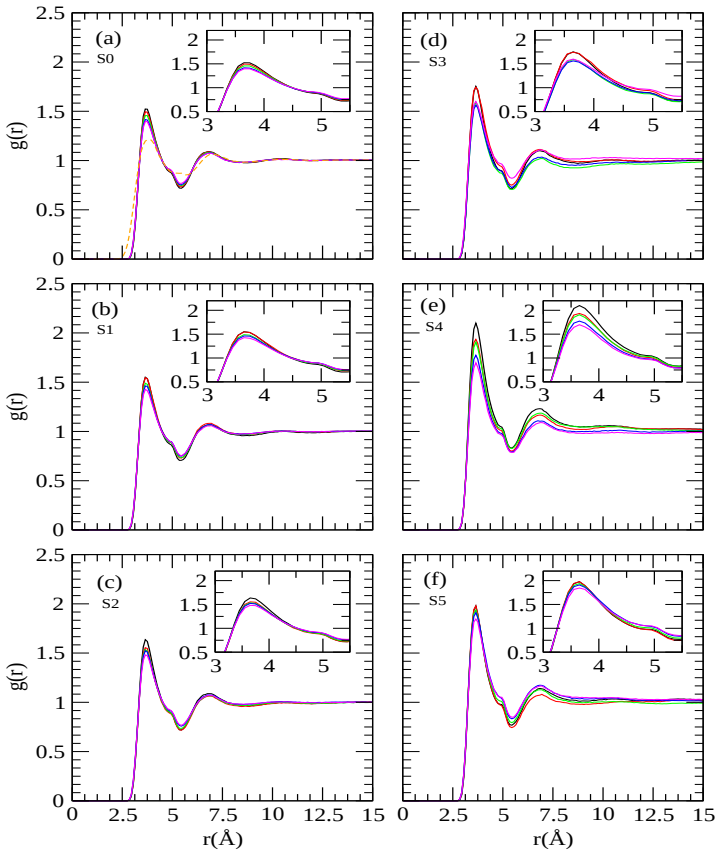

Figure 3A-2. *Site-site distribution functions involving NMA methyl (Me_1) group and water oxygen atom. The inset shows the temperature dependence changes in the first peak heights of the corresponding rdfs. The broken line in (a) represents Me_1-water hydrogen rdf. 285K (black), 300K (red), 315K (green), 330K (blue) and 345K (magenta).*

Furthermore, it is also observed that the water structure around these hydrophobic regions is perturbed due to the presence of other groups [166, 194]. For example, it has been reported by Pratt and Chandler that the solvent distribution around a methyl group in ethane is somewhat less structured than that of methane [194]. Similarly, the study of Trzesniak *et. al.* also revealed that the water peaks are narrower and sharper for spherical molecules (e.,g., methane, neopentane etc.) than those of non-spherical molecules [166]. In addition, the appearance of first peak at similar locations in Me_1 (and Me_2)-water oxygen and Me_1 (and Me_2)-water hydrogen rdf implies the surface parallel orientation of water molecules near the hydrophobic methyl groups and the appearance of the tail at shorter distance for water hydrogen reflects a closer approach of it toward these methyl groups. As shown in Figure 3A-2 and 3A-3, Keeping temperature fixed, we observe an enhancement in

the first peak height and this effect becomes more prominent for systems of concentrated trehalose solutions. With respect to the effect of temperature on a particular system it can be seen that temperature has negligible influence on the height of the first peak of Me_1-water oxygen (as seen in the insets of Figure 3A-2) except for the system S4 where a modest change in the first peak height is observed.

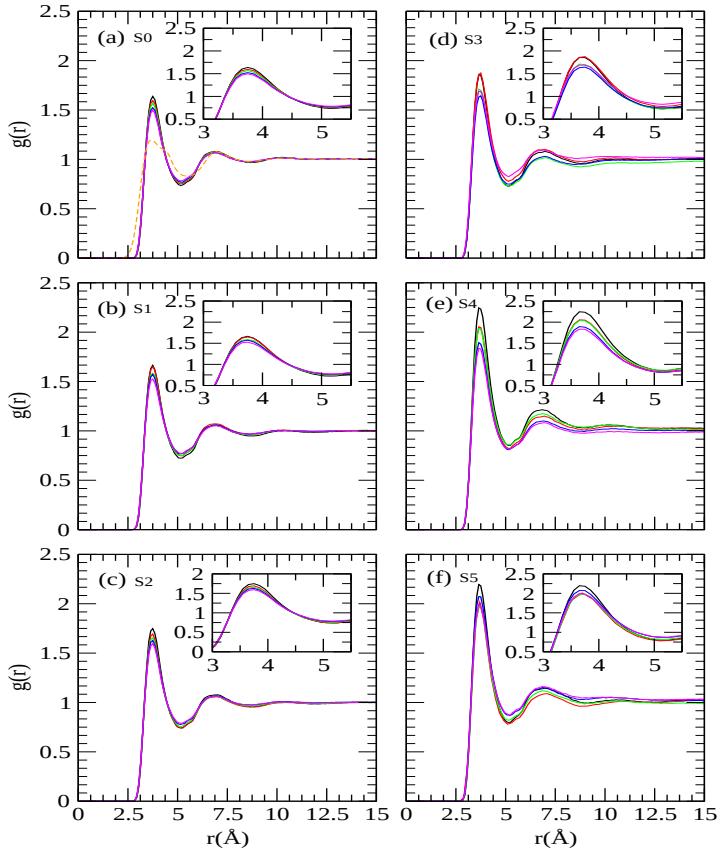

Figure 3A-3. *Site-site distribution functions involving NMA methyl (Me_2) group and water oxygen atom. The inset shows the temperature dependence changes in the first peak heights of the corresponding rdfs. The broken line in (a) represents Me_2-water hydrogen rdf. 285K (black), 300K (red), 315K (green), 330K (blue) and 345K (magenta).*

In order to have more insight in to the hydration of NMA methyl group by water molecules, we further calculate the number of first shell water molecules around Me_1 of NMA by integrating Eq. 2.3 to the first minimum of Me_1-water oxygen rdf and the results are presented in Table 3A-2. For a particular temperature, though the height of the first peak of NMA methyl-water oxygen increases as trehalose is added, our calculations of the first shell coordination number show a decrease in the coordination number values. We

trace this anomaly is due to reduced water number density. To nullify the effect of reduced water density and to see the effect of trehalose exclusively, we have further estimated the *expected* coordination numbers and these values are also shown in the parentheses of Table 3A-2. As can be seen that for a fixed temperature, the difference between the estimation and *expected* values is small when trehalose concentration is low and this difference is more prominent for concentrated trehalose solutions e.g., systems S4 and S5. These findings indicate the presence of excess water molecules near the methyl group of NMA.

Table 3A-2. The number of water molecules in the first solvation shell of the methyl group (Me_1) of NMA molecule[a]

Systems	285K	300K	315K	330K	345K
		$Me_1 - O_w$			
S0	17.72	17.59	17.39	17.07	16.91
S1	15.93 (16.05)	16.10 (16.03)	15.72 (15.73)	15.61 (15.52)	15.32 (15.41)
S2	15.06 (14.53)	14.70 (14.52)	14.53 (14.26)	14.56 (14.15)	14.36 (14.07)
S3	12.19 (11.41)	12.47 (11.45)	11.39 (11.25)	11.43 (11.12)	11.98 (10.97)
S4	12.22 (9.69)	11.50 (9.62)	11.45 (9.53)	10.77 (9.47)	10.41 (9.42)
S5	9.85 (8.40)	9.77 (8.40)	9.86 (8.27)	10.01 (8.19)	9.83 (8.19)

[a] The numbers given in parentheses represent the first shell water molecules if the only change with added trehalose came through the water number density change.

A broad insight into the nature of hydrogen bonding interactions between NMA and water can be obtained by considering site-site distribution functions involving their oxygen and hydrogen atoms (see Figures 3A-4–3A-6). The first peaks in NMA oxygen-water oxygen ($O - O_w$) and NMA oxygen-water hydrogen ($O - H_w$) distribution functions (see Figure 3A-4 and 3A-5) appear at 2.75 Å and 1.75 Å respectively. The positions of the appearance of these peaks indicate the presence of hydrogen bonding interactions between NMA and water molecules where the former acts as an acceptor. Further, the presence of amide hydrogen in NMA makes it a potential hydrogen bond donor. In NMA hydrogen-water oxygen rdf ($H - O_w$), the appearance of the first peak at 2.05 Å implies the presence of NMA-water hydrogen bond where NMA molecules act as donor (Figure 3A-6). Comparing the first peak heights of $O - H_w$ and $H - O_w$ rdfs, we note that the former is more stronger than the latter indicating that water prefers to be a hydrogen bond donor in NMA-water hydrogen bonds as already reported elsewhere [195]. From these rdfs it can, further, be seen that for a particular trehalose concentration the effect of change in temperature is not dramatic. In specific, we observe that with increasing temperature, the

height of the first peak decreases slightly suggesting the breaking of NMA-water hydrogen bonds at higher temperature. Our in detailed calculations of hydrogen bond properties act as a supportive evidence of this observation (see Table 3A-3). From this table it is apparent that the average number of water-NMA bond decreases slightly as temperature increases. Though, at a given temperature, addition of trehalose causes an enhancement in the first peak height of these rdfs (and the effect is more pronounced for systems S4 and S5) but Table 3A-3 shows a decrease in the average number of NMA-water hydrogen bonds with increasing trehalose concentration. This is not surprising considering the fact that addition of trehalose makes water density lower and since trehalose can potentially form hydrogen bonds with both NMA and water molecules (see below), some of the NMA-water hydrogen bonds are replaced by water-trehalose and NMA-trehalose hydrogen bonds.

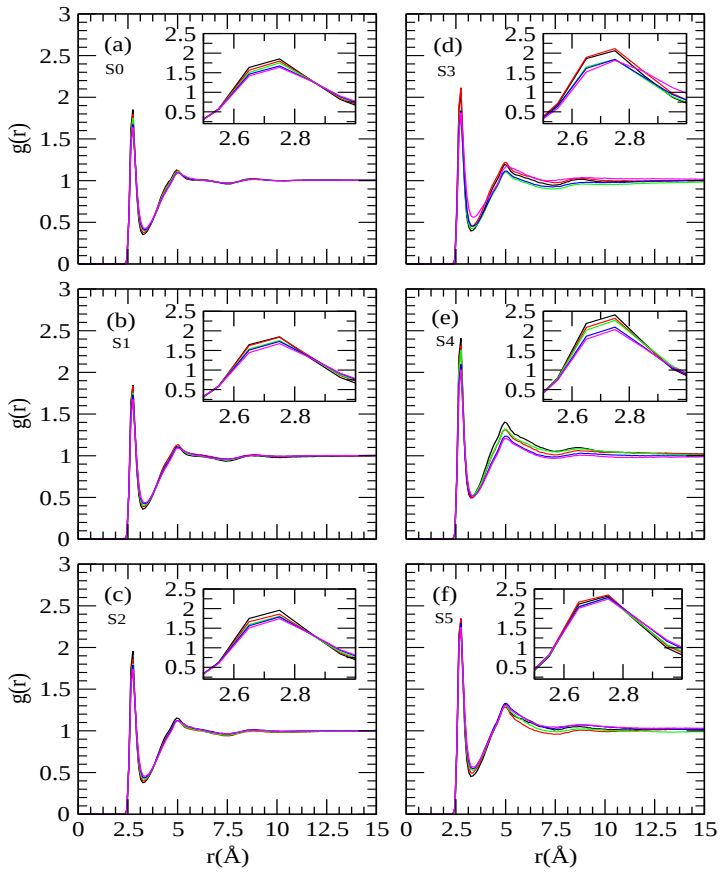

Figure 3A-4. *Site-site distribution functions involving NMA oxygen and water oxygen. The inset shows the temperature dependence changes in the first peak heights of the corresponding rdfs. 285K (black), 300K (red), 315K (green), 330K (blue) and 345K (magenta).*

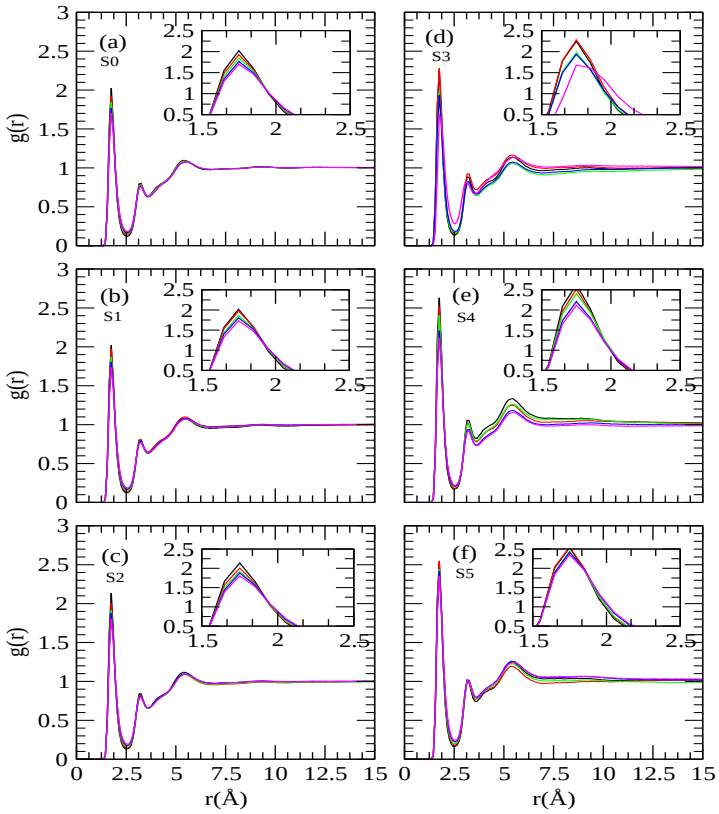

Figure 3A-5. *Site-site distribution functions involving NMA oxygen and water hydrogen. The inset shows the temperature dependence changes in the first peak heights of the corresponding rdfs. 285K (black), 300K (red), 315K (green), 330K (blue) and 345K (magenta).*

Table 3A-3. Average number of NMA-water and NMA-trehalose per NMA molecule hydrogen bonds for different systems

Systems	285K	300K	315K	330K	345K
		$HB_{NMA-water}$			
S0	2.32	2.30	2.26	2.24	2.19
S1	2.14	2.13	2.08	2.07	2.00
S2	2.04	1.97	1.97	1.96	1.93
S3	1.70	1.75	1.56	1.58	1.65
S4	1.60	1.58	1.59	1.54	1.52
S5	1.41	1.49	1.37	1.38	1.32
		$HB_{NMA-trehalose}$			
S1	0.20	0.16	0.18	0.15	0.15
S2	0.26	0.30	0.29	0.28	0.24
S3	0.57	0.50	0.67	0.60	0.52
S4	0.60	0.57	0.60	0.68	0.64
S5	0.67	0.78	0.72	0.71	0.68

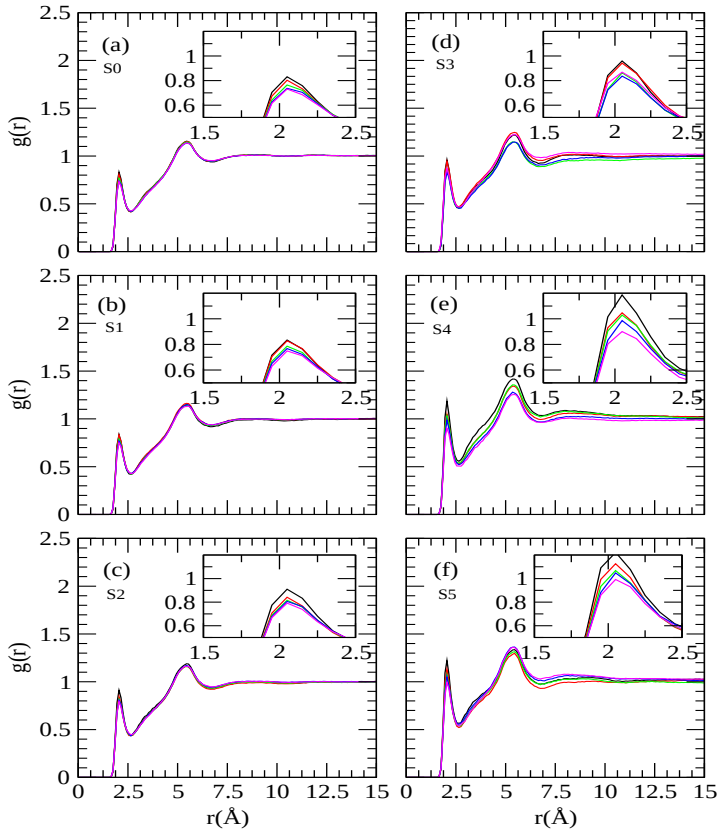

Figure 3A-6. *Site-site distribution functions involving NMA amide hydrogen and water oxygen. The inset shows the temperature dependence changes in the first peak heights of the corresponding rdfs. 285K (black), 300K (red), 315K (green), 330K (blue) and 345K (magenta).*

The presence of hydroxyl oxygen and hydrogen atoms in trehalose help it in forming hydrogen bonds with NMA (and water) molecules. The hydrogen bonding interactions between NMA and trehalose are shown by considering the distribution functions involving oxygen and hydrogen present in the amide group of NMA and O6, O5 and O1 atoms of trehalose for systems S1, S3 and S5 (see Figures 3A-7−3A-9). In this context we note that, since the rdfs involving other hydroxyl oxygens (O2, O3 and O4) and NMA oxygen are very similar to that of trehalose O6-NMA oxygen rdf those rdfs are not included here. From the peak heights of the rdfs it is clear that the hydrogen bonding interactions between hydroxyl oxygen (O6) and NMA is much more stronger than ring oxygen (O5) and glycosidic oxygen (O1)-NMA interactions. Further, from the distribution functions it can be seen that the effect of temperature on the height of the first peak is not very prominent except for system S3 where we observe a modest drop in the peak height of trehalose O6-NMA oxygen rdf.

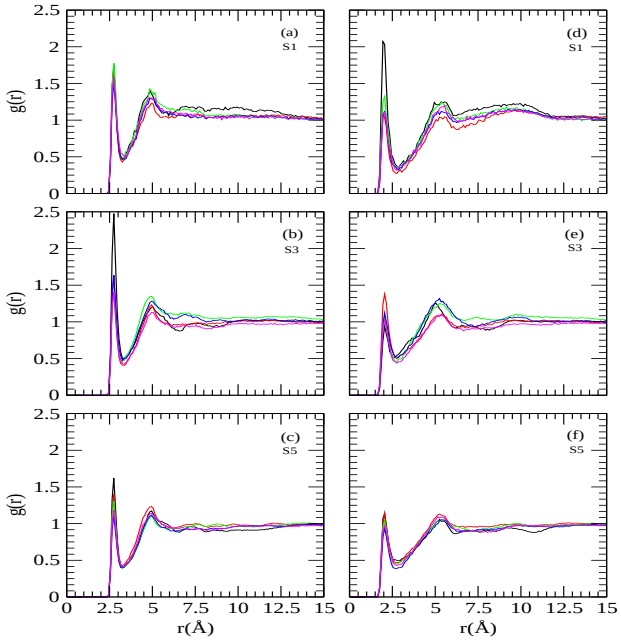

Figure 3A-7. *Site-site distribution functions between trehalose oxygen (O6) and amide oxygen (left panel) and hydrogen (right panel) of NMA for systems S1, S3 and S5. 285K (black), 300K (red), 315K (green), 330K (blue) and 345K (magenta).*

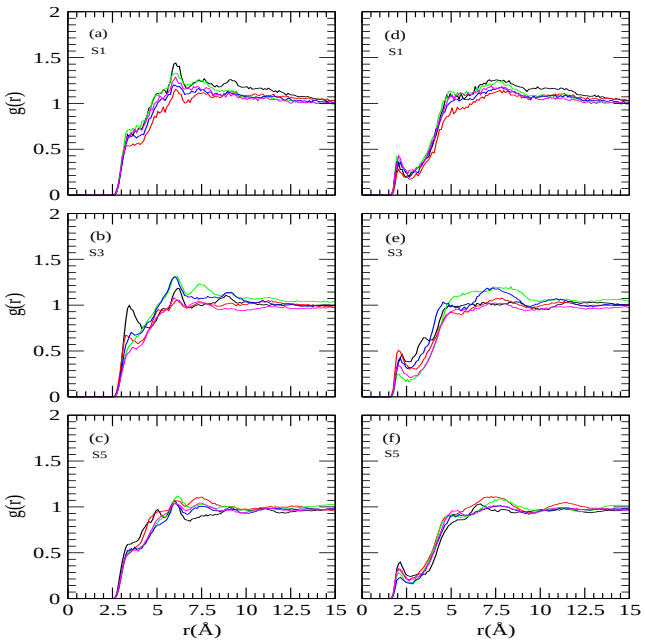

Figure 3A-8. *Site-site distribution functions between trehalose oxygen (O5) and amide oxygen (left panel) and hydrogen (right panel) of NMA for systems S1, S3 and S5. 285K (black), 300K (red), 315K (green), 330K (blue) and 345K (magenta).*

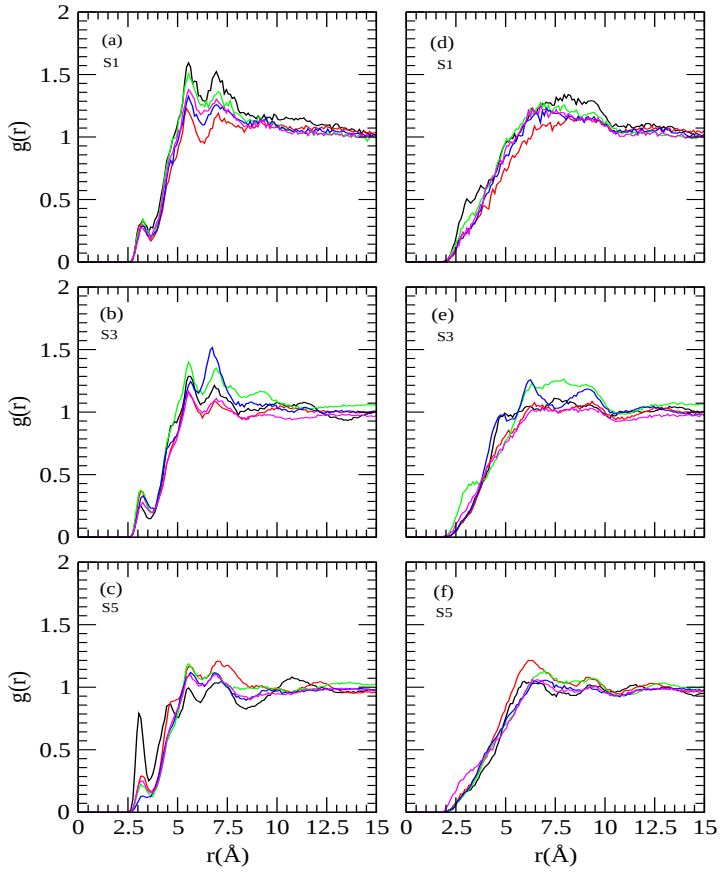

Figure 3A-9. *Site-site distribution functions between trehalose oxygen (O1) and amide oxygen (left panel) and hydrogen (right panel) of NMA for systems S1, S3 and S5. 285K (black), 300K (red), 315K (green), 330K (blue) and 345K (magenta).*

The details of NMA-trehalose hydrogen bond properties are also shown in Table 3A-3. From this table, we observe that the average number of NMA-trehalose hydrogen bonds is not a strong function of temperature and the temperature has negligible effect on to its value. Further, for a given temperature, on addition of trehalose the average number of hydrogen bond increases. What is more that for a given temperature the average hydrogen bond number formed by single NMA molecules with the solution components viz. water and trehalose remains nearly unchanged. For example, at 330 K temperature, the total number of hydrogen bonds formed by one NMA molecule with other molecules is 2.22 for system S1 and the same for system S5 is 2.09. These suggest that addition of trehalose causes replacement of NMA-water hydrogen bonds by nearly same amount of NMA-trehalose hydrogen bonds. In support of the above observations, in Figure 3A-10, we have shown the atomic mass density map of water and trehalose molecules for system S3

at 300 K at different time intervals (i.e., 20, 30 and 40 ns). The density maps of water and trehalose molecules are calculated with a cell side of 0.5 Å within 5 Å of NMA. From this contour diagram, it can be clearly seen that as simulation progresses, some of the water molecules are replaced by trehalose molecules.

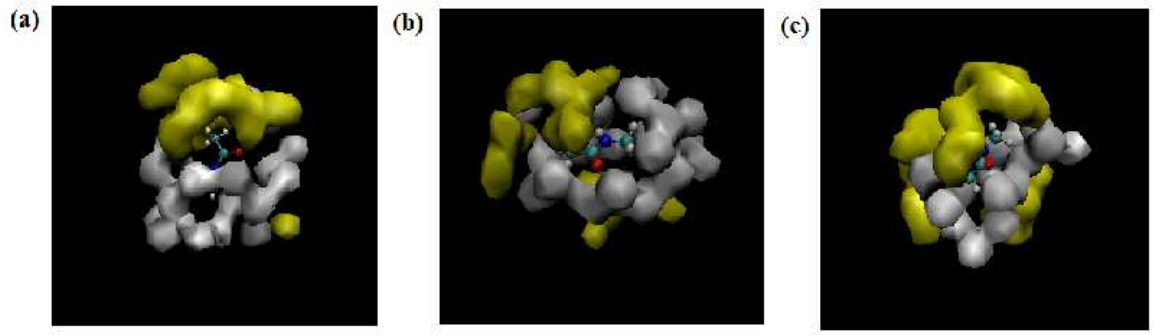

Figure 3A-10. *Contours of trehalose and water density within 5 Å around the NMA for system S5 at 300K. (a) is for 20 ns (b) is for 30 ns and (c) is for 40 ns. The colors grey and yellow correspond to water and trehalose molecules respectively.*

Interaction Between Solution Species: Selected site-site rdfs that show the influence of temperature on the water-trehalose distribution functions are shown in Figures 3A-11−3A-13. Results are shown for rdfs involving trehalose O6, O5 and O1 atoms and water oxygen. We find that $O5 - O_w$ and $O1 - O_w$ rdfs are nearly insensitive to change of either temperature or trehalose concentration. For $O6 - O_w$ distribution function, on the other hand, an enhancement in the first peak height is observed as trehalose concentration is increased. With respect to the effect of temperature change on the $O6 - O_w$ rdf, we observed a drop in the first peak height as temperature increases (see inset of Figure 3A-11). Further, the effects of change of temperature and trehalose concentration are more noticeable for systems S4 and S5. The average number of trehalose-water hydrogen bonds per water is shown in Table 3A-4 for all systems considered here. It is worth noting that for system S1 at 300 K temperature, the number of water-trehalose hydrogen bonds presented here are in accordance with that reported elsewhere [137]. We find that, for a given temperature, the number of water-trehalose hydrogen bond increases as trehalose is added. Further, with increasing temperature, the average number of water-trehalose hydrogen bond decreases when trehalose concentration is high. Interestingly, for a particular trehalose concentration, the average number of water-trehalose hydrogen bonds is insensitive to change in temperature when trehalose concentration is low. These findings suggest that temperature

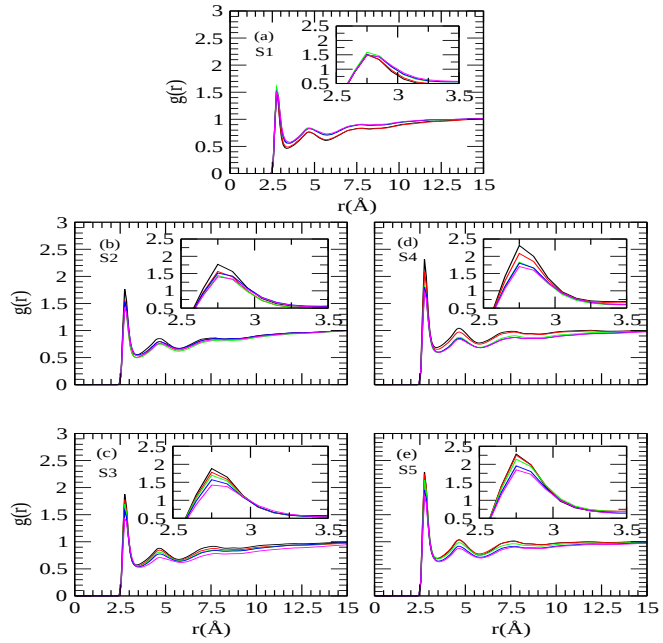

Figure 3A-11. *Site-site distribution functions involving trehalose oxygen (O6) and water oxygen. The inset shows the temperature dependence changes in the first peak heights of the corresponding rdfs. 285K (black), 300K (red), 315K (green), 330K (blue) and 345K (magenta).*

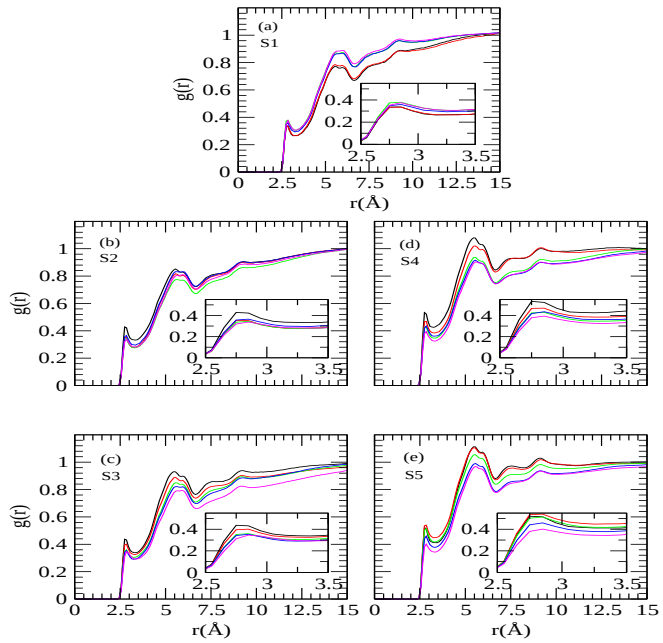

Figure 3A-12. *Site-site distribution functions involving trehalose oxygen (O5) and water oxygen. The inset shows the temperature dependence changes in the first peak heights of the corresponding rdfs. 285K (black), 300K (red), 315K (green), 330K (blue) and 345K (magenta).*

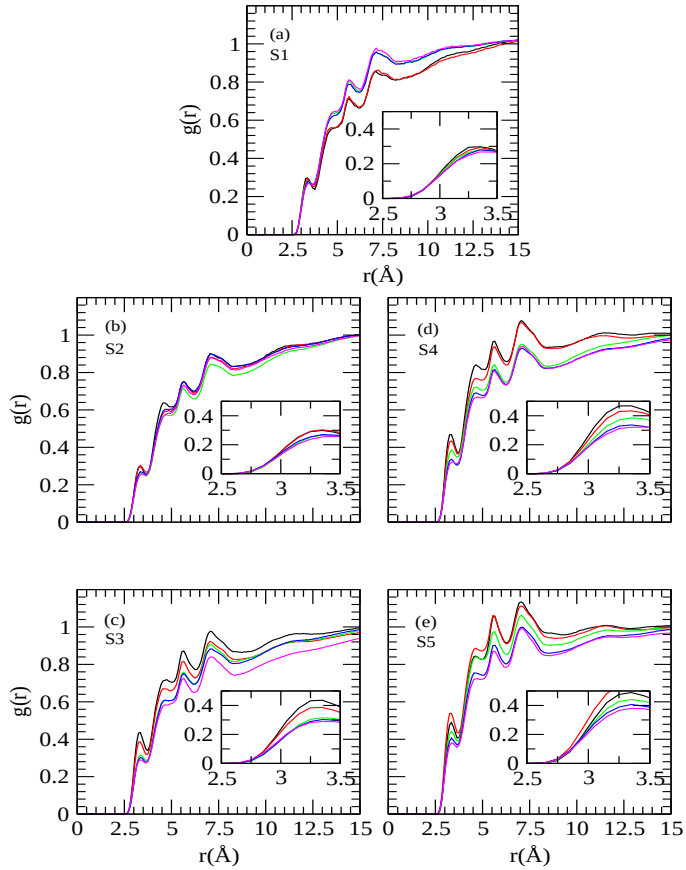

Figure 3A-13. *Site-site distribution functions involving trehalose oxygen (O1) and water oxygen. The inset shows the temperature dependence changes in the first peak heights of the corresponding rdfs. 285K (black), 300K (red), 315K (green), 330K (blue) and 345K (magenta).*

induced breaking in the water-trehalose hydrogen bonds that we observe for higher trehalose concentration causes release of some water and trehalose molecules. Some of these free water and trehalose molecules form hydrogen bonds with the like molecules and as a result the average number of water-water and trehalose-trehalose hydrogen bonds do not show any temperature-induced depletion in their values for those systems (see below).

In order to understand the possible effects of temperature change and the change of trehalose concentration on water structure, which can be expected to provide information about hydration pattern of NMA, we have also examined distribution functions involving water oxygen atoms ($O_w - O_w$) for different systems considered here. These rdfs are shown in Figure 3A-14. The first and second peaks (at 2.75 Å and 4.45 Å respectively) in $O_w - O_w$ rdf characterize the H-bonded first neighbor and tetrahedrally located second neighbor

respectively. As suggested in previous chapter, we note that the positions of these peaks are in consistent with those already reported in the literature [38, 123, 143].

Table 3A-4. Average number of trehalose-water (per water), water-water and trehalose-trehalose hydrogen bonds for different systems

Systems	285K	300K		315K	330K	345K
			$HB_{trehalose-water}$			
S1	0.11	0.11		0.11	0.12	0.12
S2	0.23	0.22		0.21	0.20	0.19
S3	0.54	0.49		0.47	0.43	0.44
S4	0.78	0.72		0.65	0.64	0.61
S5	0.95	0.91		0.87	0.83	0.78
			$HB_{water-water}$			
S0	3.34	3.31		3.27	3.23	3.18
S1	3.22	3.17		3.16	3.11	3.07
S2	3.07	3.08		3.03	3.04	3.01
S3	2.76	2.79		2.75	2.81	2.65
S4	2.46	2.53		2.57	2.54	2.57
S5	2.32	2.33		2.32	2.31	2.32
			$HB_{trehalose-trehalose}$			
S1	1.42	1.76		0.86	1.03	1.00
S2	1.98	1.70		2.19	1.43	1.61
S3	2.35	2.50		2.66	2.46	2.70
S4	2.56	2.48		2.93	2.97	2.81
S5	2.82	2.76		2.94	3.17	3.21

For a given trehalose concentration, as expected, we observe a decrease in the first and second peak height and shallower first minimum as temperature is increased. With respect to the influence of trehalose on the water-water rdfs we find that for a fixed temperature, the addition of trehalose does nothing to decrease solvent structural perturbation induced by temperature, rather it appears to be enhanced by the trehalose, with the rdfs peaks further increasing in height. From these findings it is safe to imply that trehalose and temperature has two opposite effects with respect to change in water structure. In brief, as temperature increases the water in the solution becomes less structured which in turn makes the water molecules more mobile. Contrary to this, the water becomes more structured as trehalose concentration increases and as a result the diffusion coefficient of water decreases (see diffusion coefficient calculations discussed below). Further, the estimated water-water average number of hydrogen bonds (shown in Table 3A-4) indicates that the temperature induced breaking of hydrogen bonds that was observed for low trehalose concentration is getting prevented when the concentration of trehalose is high.

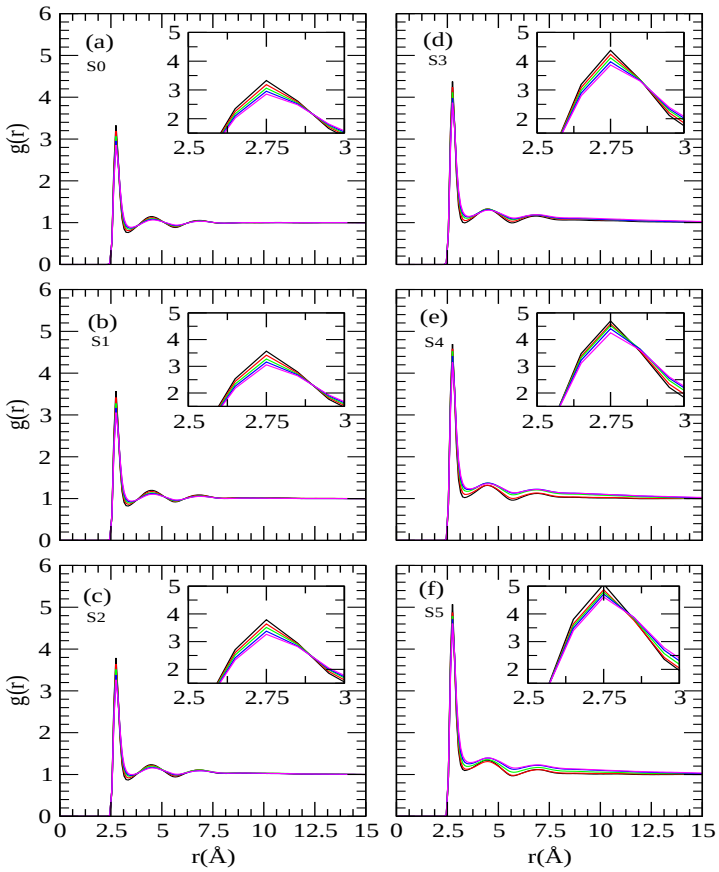

Figure 3A-14. *Site-site distribution functions between water oxygen and water oxygen. The inset shows the temperature dependence changes in the first peak heights of the corresponding rdfs. 285K (black), 300K (red), 315K (green), 330K (blue) and 345K (magenta).*

Trehalose-Trehalose Hydrogen Bond Properties and Cluster Structure Analysis: As discussed in **Chapter 2**, trehalose can form extended sugar-sugar hydrogen bond network and which leads to the formation of trehalose clusters of different sizes. In view of this, we have also calculated trehalose hydrogen bonding interactions with like molecules (see Table 3A-4) as well as trehalose clusters structure analysis for different systems. Considering the average number of trehalose-trehalose hydrogen bonds first, we see that for low trehalose concentration, as per the expectation, there is a drop in the average hydrogen bond number as temperature increases. Interestingly, for concentrated trehalose solutions increasing temperature results a modest enhancement in the hydrogen bond number. The influence of temperature and trehalose concentration on the self-aggregation of trehalose molecules can be obtained by estimating average trehalose cluster sizes for different systems using Eq. 2.5. For systems S1 and S5, the change in $< n_{tre} > /N_{tre}$ (where N_{tre} is the

number of trehalose molecules in a system) values for different temperatures are shown in Figure 3A-15 (a).

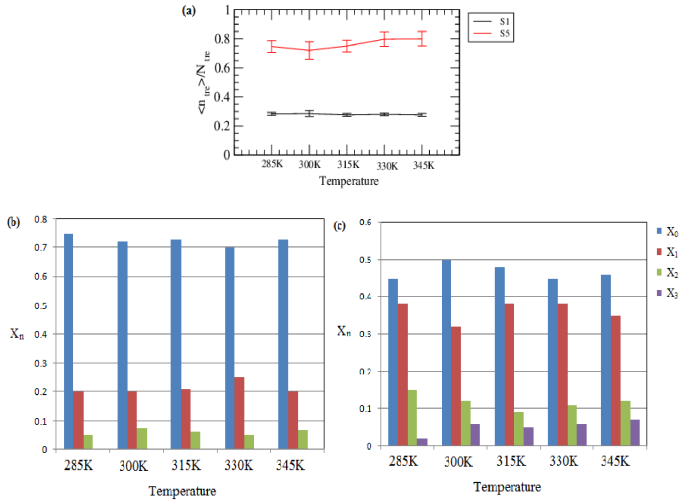

Figure 3A-15. *(a) The normalized mean trehalose cluster size,* $< n_{tre} > /N_{tre}$ *for system S1 and S5 at different temperature. The standard errors are calculated using block average over 2ns. (b) and (c) Correspond to the fraction of NMA molecules* (X_n) *that form n number of hydrogen bonds with trehalose molecules that are present in trehalose cluster of size* $n_{tre} > 1$ *for systems S1 and S5 respectively.*

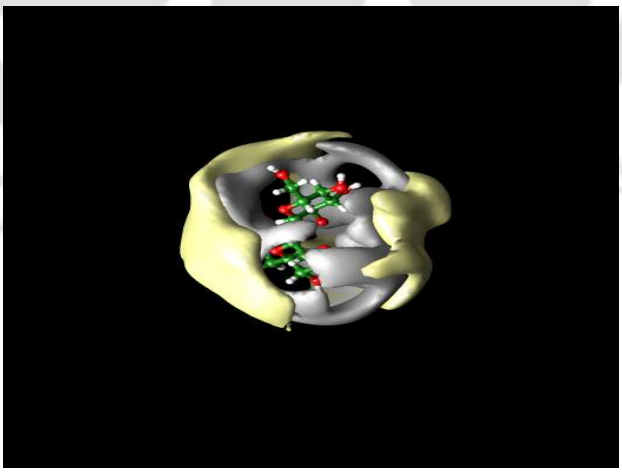

Figure 3A-16. *A projection of spatial distribution function of trehalose-trehalose interaction for system S5 at 345 K temperature. The isosurface in grey corresponds to the higher probability density of direct hydrogen bonding interactions with the central reference trehalose molecule and isosurface in yellow corresponds to the high density region of up to 10 Å, from the reference molecule.*

The growth of trehalose cluster, as trehalose concentration increases, is quite evident from this figure. At a given temperature, the value of $< n_{tre} > /N_{tre}$ increases as concentration is increased and this is in accordance with the average number of trehalose-trehalose hydrogen bonds (see Table 3A-4). Notwithstanding the error bars, we observe that for the highest concentration considered here, the value of $< n_{tre} > /N_{tre}$ reaches to 0.8 implying that the percolation of trehalose hydrogen bond network yet to be achieved. In this regard, we note that, the percolation of sugar hydrogen bond network has been reported earlier at 66 wt % trehalose concentration of trehalose-water binary system [155]. This anomaly is due to the presence of NMA molecules in our systems that participate in large number of hydrogen bonds with the trehalose molecules. The formation of hydrogen bond mediated trehalose cluster is also evident from the projection of the spatial density distribution presented in Figure 3A-16.

From this figure we observe an overlap between the regions of high probability density region for directly hydrogen bonded trehalose molecules and the density region up to 10 Å around a reference trehalose molecule. In order to have a "gross" picture of the involvement of NMA molecules in trehalose cluster we, further, estimated the fraction of NMA molecules that participate in the n number of hydrogen bonds with trehalose molecules in a cluster of size $n_{tre} > 1$ and the same is shown in Figure 3A-15 (b) and (c) for systems S1 and S5. In this process we divide last 10 ns of our simulations in to 5 equal blocks and considered the average solution structure for each block. From this figure it is apparent that as concentration increases, in a trehalose cluster more and more NMA molecules participate in hydrogen bonding interactions with trehalose. We further observe that with increasing trehalose concentration, the fraction of NMA molecules that engage in more than one hydrogen bond formation with trehalose increase. With respect to the effect of temperature, we find that this distribution is not a strong function of temperature. This is not unexpected given the fact that there is some arbitrariness in the calculation of fraction of NMA molecules present in a trehalose cluster for different systems.

Diffusion Coefficient: As evidenced from previous study [53] that concentrated aqueous trehalose solution has very high glass transition temperature and it forms a highly viscous glassy matrix that helps to keep the biomolecules fixed. Formation of this glassy matrix protects the conformation of the biological molecules. Trehalose induced retardation of the translation motion of water molecules that are present near to a solute molecule has also been reported earlier [159]. And the retardation in the dynamics of water molecules in presence of trehalose helps in protecting biological molecules in aqueous trehalose solution

[70, 173]. Since protein-water dynamics are coupled, the protein dynamics are greatly influenced by the surrounding "slow" water molecules in presence of trehalose. Significant slowing down of rotational and translational motion of water molecules has also been observed in a recent Terahertz absorption measurement study [69]. In view of this, we have calculated the translational diffusion coefficients (D) for different solution species using Eq. 2.6. The diffusion coefficients of NMA (D_N) for different systems are presented in Table 3A-5 and the same for water (D_w) and trehalose (D_{tre}) together with the available experimental diffusion coefficient values (for binary trehalose-water systems in absence of NMA) are shown in Figure 3A-17.

Table 3A-5. Diffusion coefficient of NMA (D_N)

Systems	285K	300K	315K	330K	345K
		D_N $(10^{-5}cm^2sec^{-1})$			
S0	0.92	1.24	1.41	1.88	2.48
S1	0.40	0.72	0.89	1.28	2.23
S2	0.34	0.32	0.71	0.95	1.07
S3	0.15	0.19	0.24	0.54	0.74
S4	0.06	0.09	0.13	0.23	0.36
S5	0.02	0.03	0.06	0.11	0.19

We find that the calculated diffusion coefficients of water and trehalose in our model solutions are in qualitative agreement with the experimental values considering the fact that we have NMA molecules in our systems [157]. We note that, for a given temperature, due to formation of trehalose-water hydrogen bonded complex, trehalose decreases the diffusion coefficient of water and water decreases the diffusion coefficient of trehalose such that the smallest diffusion coefficients for both the species are found for system S5, where the total trehalose concentration is the highest. A further insight in to the different diffusion coefficient values reveals that for a given temperature, the decrease in diffusion coefficient values are more pronounced for trehalose and NMA when compared to that of water. For example, at 285K, on changing trehalose concentration from 16% to 66% (from system S1 to S5), the diffusion coefficient of water is reduced from $1.17 \times 10^{-5}cm^2sec^{-1}$ to $0.13 \times 10^{-5}cm^2sec^{-1}$ (about 9 times decrease) whereas for trehalose and NMA, the drop in its

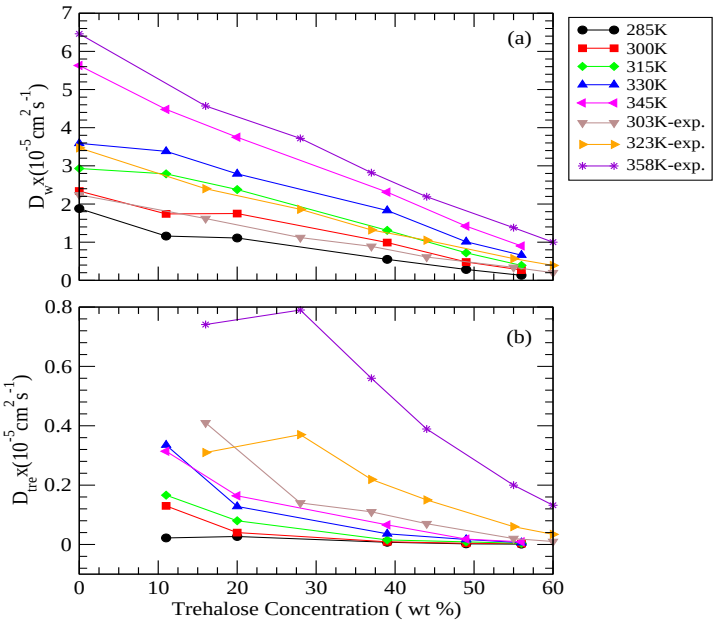

Figure 3A-17. *Diffusion coefficient of (a) water and (b) trehalose for different temperature. The experimental values of diffusion coefficient are taken from reference 157.*

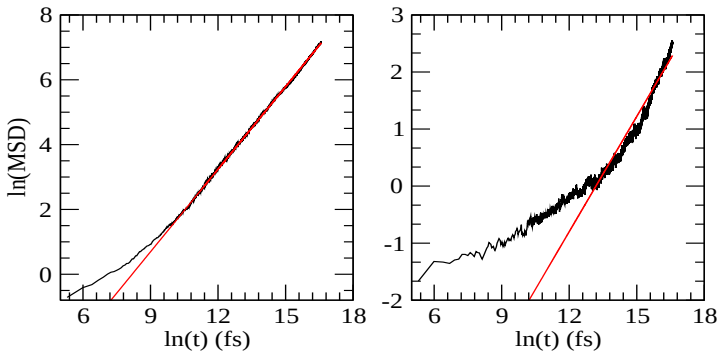

Figure 3A-18. *Black line represents log-log plot of mean-squared displacement (MSD) vs. time for water (left panel) and for trehalose (right panel) for system S5 at 285 K temperature. The slope of the curve becomes unity once the molecules reach the diffusive regime. The red line has unit slope.*

values are 18 times and 17 times respectively. Moreover, for all temperature considered here, the ratio of D_{tre} and D_w decreases, as trehalose concentration is increased. This estimated ratio of diffusion coefficient values is well agreement with the previous reported results of NMR experiment [157]. The sharp decrease in the D_{tre} values with increasing trehalose concentration is in good agreement with the sharp increase in the trehalose viscosity values

[158]. For a given trehalose concentration, as expected, the diffusion coefficient values of all species increases as temperature is increased. Since the appearance of so called "boson" peak in the log-log plot of MSD is an indicator of glass transition temperature, we have shown the log-log plot of MSD of water and trehalose for system S5 at 285 K temperature in Figure 3A-18. The non appearance of the "boson" peak suggests that the most concentrated trehalose concentration considered here is still above the glass transition temperature.

■ SUMMARY AND CONCLUSIONS

We investigated solvation characteristics of NMA in aqueous trehalose solutions with a regime of trehalose concentrations. For each trehalose concentration, we considered five different temperatures ranging from 285 K to 345 K and the pressure of each system was kept at 1 atm. Various structural, dynamical and hydrogen bond properties together with sugar-sugar cluster structure analyses are calculated. We found the off-set of temperature induced breaking of water structure by trehalose molecules and the presence of more water molecules (when compared to expected number of water molecules calculated explicitly from the water number density for different systems) near to the hydrophobic methyl groups of NMA as trehalose concentration is increased.

From hydrogen bond analyses, we found that NMA molecules prefer to act as a donor in NMA-water hydrogen bonds where its carbonyl oxygen atom preferably forms hydrogen bonds with water hydrogen. In regard to effect of temperature on this type of hydrogen bond, it is observed that the average number of NMA-water hydrogen bond decreases slightly with increasing temperature. On the other hand, keeping temperature fixed on increasing trehalose concentration, as expected, the average number of NMA-water hydrogen bond decreases and the same for NMA-trehalose increases. Here we note that, we did not observe any strong temperature dependence of trehalose-NMA average number of hydrogen bonds. But, it is interesting to observe that at a given temperature, total hydrogen bond number formed by a single NMA molecules with solution species water and trehalose remain essentially unchanged. This finding directs us toward the replacement of NMA-water hydrogen bonds by equal number of NMA-trehalose hydrogen bonds on addition of trehalose and supports water replacement hypothesis [55].

A further insight in to the trehalose's hydrogen bonding ability to different solution species revealed that trehalose hydroxyl oxygen (O2, O3, O4 and O6) and hydrogen atoms are mostly involved in this process. This is because of the fact that the solvent molecules cannot be positioned in the vicinity of the glycosidic oxygen of (1-1)-linked disaccharide.

For a given trehalose concentration, temperature induced breaking in the water-trehalose hydrogen bond is observed. Keeping temperature fixed, as we increase trehalose concentration the average number of water-trehalose hydrogen bond increases. Contrary to these observations, strikingly, water-water and trehalose-trehalose hydrogen bond analyses show the retention of these bonds even at high temperatures for concentrated trehalose solutions. These findings lead us to suggest that some of the water (and trehalose) molecules that are free due to the temperature induced breaking of trehalose-water hydrogen bonds compensate the breaking of water-water hydrogen bonds at higher temperature. In order to probe sugar-sugar hydrogen bond network, we, further, extended our study to the estimation of trehalose cluster structure analyses. At a given temperature, on addition of more and more trehalose molecules the growth of trehalose cluster is observed. It is worth to mention that, even for the highest trehalose concentration, the percolation of trehalose hydrogen bond network has not been achieved [155]. This is because of the presence of fairly large number of NMA molecules in our study.

Our calculated diffusion coefficient values for different solution species show trehalose induced slowing down of the translational motion and the effect is more prominent for NMA and trehalose than that of water. We, further, compared our simulation results with the available experimental diffusion coefficient values for water and trehalose. We find that our results are in consistent with the experimental diffusion coefficient values considering the fact the presence of NMA molecules in our simulated systems. Moreover, in accordance with the results of the NMR experiments [157], we also found that at a given temperature, the ratio of diffusion coefficient values of water and trehalose increases with increasing trehalose concentration. As per the expectation, for a given trehalose concentration, the value of the diffusion coefficient increases as temperature is increased.

Therefore, from our study we conclude that in the trehalose induced retention of native conformation of protein against temperature-induced denaturation two factors play major roles: (i) The compensation of lost water-protein hydrogen bonds by the formation of nearly equal number of trehalose-protein hydrogen bonds (support water replacement hypothesis) and (ii) The reduction in the translational dynamics of water molecules in presence of trehalose. Since, the dynamics of protein and its surroundings water molecules are coupled, a great reduction in water dynamics influences protein's dynamical fluctuations. Besides these, at higher temperature the retention of water-water and trehalose-trehalose hydrogen bond when trehalose concentration is also high plays an indirect role by making water molecules less available for protein.

Part B:

Trehalose's Effect on Amide Solvation in Aqueous Urea Solution

Overview: We perform here MD simulation of NMA in aqueous urea and/or trehalose solution to provide underlying mechanism of the inhibiting effect of trehalose on the urea denatured protein. The site-site rdfs and hydrogen bond properties indicate that in binary urea solution the replacement of NMA-water hydrogen bonds by NMA-urea hydrogen bonds. On the other hand, in ternary urea and trehalose solution, trehalose does not replace the NMA-urea hydrogen bonds significantly; rather, it forms hydrogen bonds with the NMA molecule. The calculation of preferential interaction parameter shows that at the NMA surface, trehalose molecules are preferred and the preference for urea decreases slightly in ternary solution with respect to the binary solution. The exclusion of urea molecules in the ternary urea-NMA-trehalose system causes alleviation in van der Waals interaction energy between urea and NMA molecules. Our findings also reveal: (a) trehalose and urea induced second shell collapse of water structure, (b) a reduction in the mean trehalose cluster size in ternary solution and (c) slowing down of translational motion of solution species in presence of osmolytes. These results provide a molecular explanation as how trehalose counteracts urea-conferred protein denaturation.

■ INTRODUCTION

As discussed in Part A of the present chapter, much attention has been directed toward understanding the hydration of NMA. However, the effects of osmolyte on NMA hydration are yet to be investigated thoroughly. In 2010, Wei *et al.* [38] reported the effects of three different osmolytes, two denaturants, urea and tetramethylurea (TMU), and one protectant, TMAO, on the hydration of NMA molecules on the basis of classical MD simulations. They showed that TMAO weakened the interaction between water and the carbonyl group, whereas both urea and TMU enhanced this interaction. They also found that hydration of NH group was found to be weaker as compared to the CO group in pure water as well as in the presence of osmolytes [38]. Again, the effect of osmolytes on water−water interaction was reported. But, the authors did not address direct interactions between NMA and osmolyte.

In the work described in this part, we first investigate the hydration characteristics of NMA in pure water system and then in binary and ternary solutions of urea and trehalose to find the role of trehalose on urea-induced modification of NMA hydration. We first examine NMA-water interaction and then direct NMA-trehalose interaction. We put our attention on structural, energetic, and dynamical properties of solution molecules in binary and ternary solutions.

The remainder of this part is organized into three sections. The models and simulation details are briefly described in the next section. This is followed by a section whereof we discuss our results, and our conclusions are summarized in the last section.

■ MODELS AND SIMULATION METHOD

To understand the mechanism of protein conformation protection by trehalose against urea denaturation, we have performed classical MD simulation of NMA in pure water as well as binary and ternary solutions of urea and trehalose. The four different systems considered here are presented in Table 3B-1. The Packmol program was used to prepare the initial configurations of our systems [129]. The different force field model used for NMA, trehalose and water are discussed in part A of this chapter. Urea is considered according to Smith model [170]. All the solution properties were investigated by performing MD simulations in a cubic box using AMBER12 [90] suite of programs at 300K.

The details of choice of different force field and simulation protocols were identical to those described in **Chapter 2**. In brief, the reasonable initial structures for the

production run of our systems were obtained by energy minimization for the 5000steps, where first 2500 step in steepest descent method and followed by the same number of steps in conjugate gradient method. After that, the systems were heated up slowly from 0 K to 300 K for 100 ps in NVT ensemble and then the systems were equilibrated in NPT ensemble for 2 ns. For calculating different structural and hydrogen bond properties, we have conducted the 40 ns production runs for all the systems in NPT ensemble and one atmospheric pressure. After that, for calculating diffusion coefficients of different solution species, we continued for another 15 ns NVE ensemble simulation.

Table 3B-1. Overview of Simulations[a]

System	N_N	N_U	N_T	N_W	volume (nm^3)	M_U	M_T	w_T%
NW	20	0	0	1000	32.15	0	0	0
NU	20	250	0	950	48.25	8.60	0	0
NT	20	0	35	950	43.22	0	1.34	41
NUT	20	250	35	800	56.04	7.41	1.04	45

[a] N_N, N_U, N_T, N_W, and w_T% are the number of NMA, urea, trehalose, water molecules and weight percentage of trehalose respectively and M_U and M_T are the molar concentrations of urea and trehalose for the above systems.

■ RESULTS AND DISCUSSION

Interaction of NMA with the Solution Species: In order to characterize the solvation of solute NMA molecules in presence and absence of osmolytes urea and trehalose it is important to investigate the interactions of different atomic sites of NMA with different solution species. Since, the different site-site rdfs involving different atomic sites of solute and solvent molecules provide very good qualitative information about the interactions between them, in this section we concentrate on the selected rdfs involving different atomic sites of NMA and solution molecules. The same are presented in Figures 3B-1−3B-4.

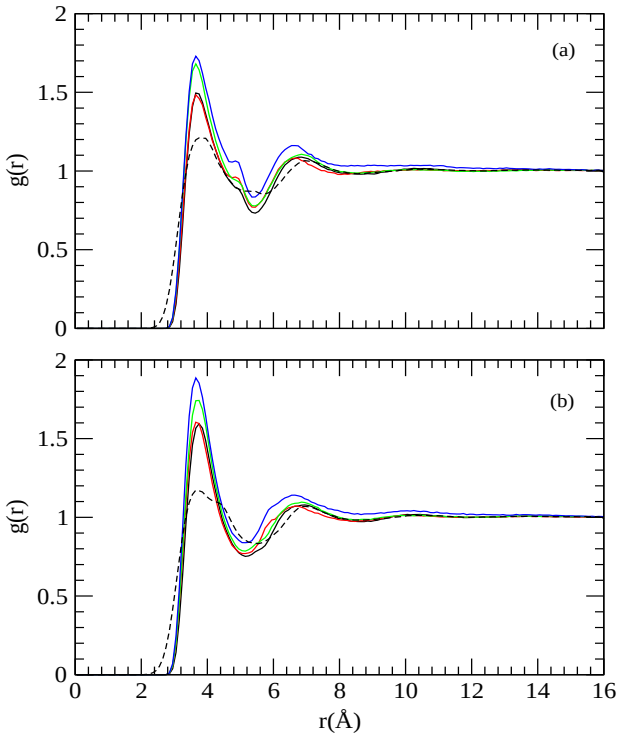

Figure 3B-1. *Solid lines represent site-site distribution functions between NMA methyl groups and water oxygen atom. (a) is for $Me_1 - O_w$ rdf and (b) represents $Me_2 - O_w$ rdf. Dashed lines are for NMA methyl-water hydrogen rdfs for system NW. NW (black), NU (red), NT (green) and NUT (blue).*

The hydration characteristics of the NMA methyl groups in pure water at one atmospheric pressure were discussed in Part A of this chapter. As shown in Figure 3B-1 (a) and (b), we noticed that the addition of urea has very little effect on methyl group and water rdfs. On the other hand, the presence of trehalose molecules in solution causes an enhancement in the first peak height suggesting an improved hydration of NMA methyl groups.

A good measurement of hydrogen bonding interactions between NMA and water, albeit indirectly, can be obtained from the site-site distribution functions involving the hydrophilic carbonyl oxygen and amide hydrogen of NMA with water oxygen and hydrogen atoms. The same are displayed in Figure 3B-2. Note that, the quantitative measurements of average number of these hydrogen bonds are discussed below.

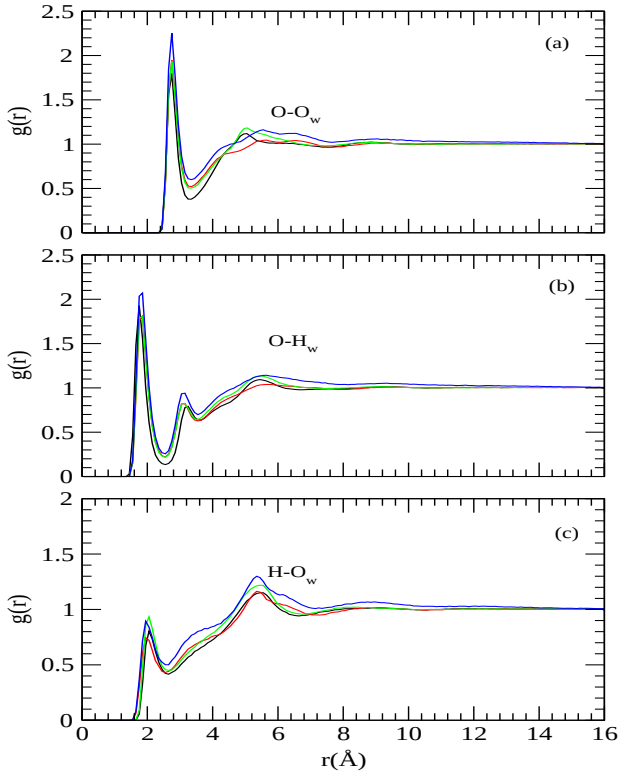

Figure 3B-2. *Site-site distribution functions involving carbonyl oxygen and amide hydrogen NMA with water. NW (black), NU (red), NT (green) and NUT (blue).*

Now considering the rdfs between water hydrogen and water oxygen with NMA oxygen in pure water system first (see Figure 3B-2 (a) and (b)), we find the appearance of first contact peak in rdf profiles at about 1.75 and 2.75 Å respectively, suggesting $CO\cdots H_wO_w$ hydrogen bonding interaction [195]. The first minimum at about 3.35 Å in $O-O_w$ rdf indicates the outer limit of the first shell and it decreases to a little more than the half of the bulk water density, which indicates a strong radial water structuring around the carbonyl oxygen of NMA. The rdf involving NMA hydrogen-water oxygen ($H-O_w$) (Figure 3B-2 (c)) has a characteristics hydrogen bonding peak at 2.05 Å and the weakness of the first peak height suggests the relatively weaker hydration of amide hydrogen atom by water molecules. Now, focusing on the effect of osmolytes urea and trehalose individually (systems NU and NUT) on these distribution functions it is observed that in comparison to pure water system, both of them enhance the first peak height of $O-O_w$ and $O-H_w$ rdfs and make the first valley shallower. In mixed urea/trehalose system (system NUT) the first peak height is further getting enhanced and the first valley becomes more shallower. On the other

hand, in presence of urea there is a modest depletion in the first peak height of $H - O_w$ pair correlation function whereas this rdf shows only slight awareness of the presence of trehalose.

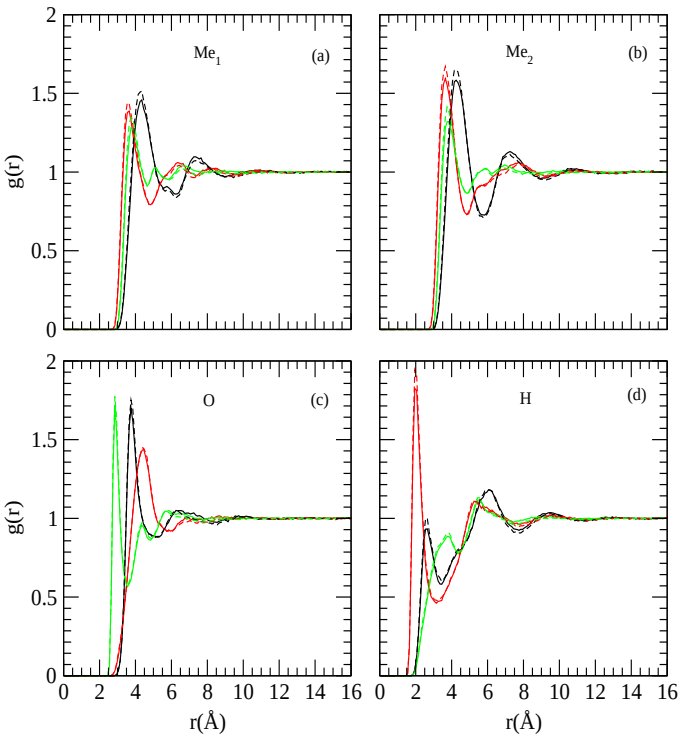

Figure 3B-3. *Site-site distribution functions between NMA and urea in aqueous urea (solid) and in mixed urea/trehalose (dashed) solutions. Black, red and green lines are for carbon (C_u), oxygen (O_u) and nitrogen (N_u) of urea.*

Figure 3B-3 demonstrates the interactions of NMA atomic sites with the urea atomic sites. Considering the rdfs involving the atomic sites of urea and the two methyl groups (Me_1 and Me_2), we observed that both the methyl groups exhibit similar tendency towards urea molecule. Moreover, the orientation of urea molecules in the vicinity of these hydrophobic methyl groups of NMA is similar to that observed in case of methane and neopentane [123, 134]. Further, the very similar locations of the rdfs of urea oxygen (O_u)-NMA methyl and urea nitrogen(N_u)-NMA methyl implies the no preference of these atomic sites of urea near to the methyl groups of NMA. These locations and the magnitudes of the first peaks in the corresponding rdfs suggest the direct interaction of urea with NMA methyl groups. Moreover, in comparison to urea carbon, slightly more closer approach of these two atomic sites of urea toward the methyl groups of NMA is also quite visible. As expected the

distribution of urea molecules around the carbonyl oxygen and amide hydrogen (see Figure 3B-3) indicates the presence of hydrogen bonding interactions between NMA and urea molecules. For carbonyl oxygen the position of first peak of N_u rdf is much closer than C_u and O_u atoms, suggesting the preference of urea nitrogen near to the NMA oxygen. Additionally, amide hydrogen shows preference towards the urea oxygen indicating the latter accepts the amide hydrogen of NMA in NMA-urea hydrogen bonding interaction. Interestingly, all these rdfs reveal a modest depletion in the urea density near NMA atomic sites up on addition of trehalose.

The information about the interactions between different atomic sites of NMA and trehalose molecules are probed by means of selected site-site distribution functions and these are displayed in Figure 3B-4.

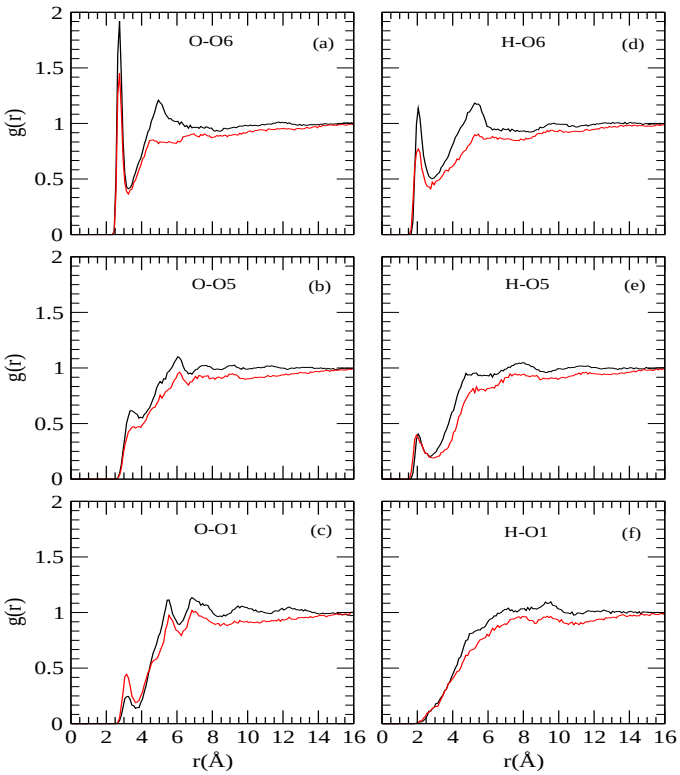

Figure 3B-4. *Site-site distribution functions involving trehalose hydroxyl oxygen (O6) with amide oxygen (left panel) and hydrogen (right panel) of NMA for systems NT (black) and NUT (red).*

Since, both NMA and trehalose molecules possess groups that participate in hydrogen bonding interactions, here, we discuss the rdfs involving different trehalose oxygen and the carbonyl oxygen and amide hydrogen of NMA for the systems NT and NUT. As discussed

previously, the rdfs of trehalose hydroxyl oxygen atoms O2, O3 and O4 with the amide group of NMA behave in similar fashion as that of O6 atom, therefore, the rdfs involving O6, O1 and O5 oxygen atoms of trehalose are considered in Figure 3B-4. The presence of much stronger first peaks of $O - O6$ and $H - O6$ rdfs (see Figure 3B-4 (a) and (d)) at 2.75 and 1.95 Å suggests that in the hydrogen bonding interaction between NMA and trehalose molecules, it is the hydroxyl O6 (and O2, O3 and O4) oxygen atom which actively participate. The appearance of peaks with high magnitudes, further, demonstrates that trehalose molecules can interact directly with the NMA molecules through its hydroxyl oxygen atoms. The small peak height of distribution functions involving ring oxygen atom (O5) (as well as glycosidic oxygen atom, O1) of trehalose and the amide group of NMA (Figure 3B-4 (b), (c), (e) and (f)) implies much weaker interactions between these atomic sites. Now, for aqueous urea/trehalose mixture, as per the expectation, we find that the NMA-trehalose hydrogen bonding interaction decreases in presence of urea. Moreover, from the peak heights of NMA oxygen-trehalose oxygen and NMA hydrogen-trehalose oxygen distribution functions it is apparent that in NMA-trehalose hydrogen bonding interactions, NMA molecule is preferably acting as a donor rather than acceptor. This observation is further supported by the hydrogen bond properties calculations (discussed later).

A more insights in to the solvation of NMA molecules by water as well as osmolytes urea and trehalose molecules are obtained by estimating the number of different solution species viz. water, urea and trehalose (central atom only) in the NMA solvation shell. The average number of molecules present around different atomic sites of NMA is calculated from the corresponding site-site distribution function, $g(r)$, by using Eq. 2.3. From the estimations of above coordination number values, the total number different solution species that are present in the NMA solvation shell of radius 6 Å are calculated as a function of distance. In Figure 3B-5, we show the change in RCN (running coordination number) value for different solution species as a function of distance. Since the size of a water molecule is significantly smaller than the osmolytes urea and trehalose, a much larger radii of exclusion is also observed for these osmolytes. As a result, from the purely geometric point of view, the exclusion of urea and trehalose molecules is observed from a certain volume shell of NMA. Nevertheless, the presence of considerable amount of osmolytes urea and trehalose molecules in the NMA solvation is quite evident and the abundance of the former is relatively higher than the latter (Figure 3B-5 (a)). As is evident that the number of water molecules in the solvation shell is much higher in pure water system than in aqueous osmolyte solutions. The addition of trehalose and urea causes exclusion of water molecules

from NMA solvation shell and the effect is much more pronounced for the former than later. In specific, for system NT, the presence of two trehalose molecules in the solvation shell causes an exclusion of about 24 water molecules. On the other hand, addition of urea alone to pure water system (system NU), displaces 34 water molecules (by 17 urea molecules) from NMA solvation shell. These suggest, the displacement of 12 and 2 water molecules respectively, with the incorporation of one trehalose and one urea molecules in the NMA solvation shell. Due to the presence of more number of urea molecules, the total number of excluded water molecules are much higher for NU system than NT system (34 against 12). As a result of exclusion of higher number of water molecules for system NU the total number of solution species in the solvation shell decreases more for this system (see Figure 3B-5 (b)). These observations are further confirmed from the atomic density analysis discussed below.

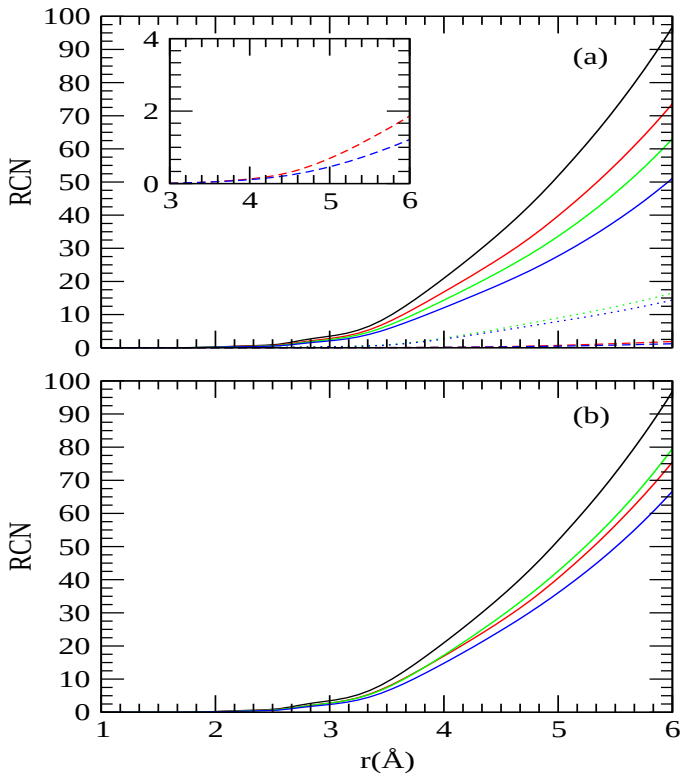

Figure 3B-5. *Top: Total number of water (solid), urea (dotted) and trehalose (dashed) molecules in the solvation shell of NMA as a function of distance. Bottom: Total number of solution species in the solvation shell of NMA as a function of distance. NW (black), NU (red), NT (green) and NUT (blue).*

From the above discussions, it is quite evident that in NMA solvation shell, water

molecules are replaced by osmolytes urea and trehalose molecules. In view of this it would be interesting to carry out atomic density analysis of different solution species around NMA. Using VMD, [132] the mass density maps of water, urea and trehalose molecules with a cell side of 0.5 Å within 3.5 Å of NMA molecule are calculated at different time intervals and these are shown in Figure 3B-6. The presence of large water density around NMA in pure water system and removal of water molecules on addition of urea and trehalose (as reflected in the depletion of water density) are also quite visible. Further, in consistent with the total number of excluded water molecules from the solvation shell of NMA (see above), the reduction in the water density around NMA is relatively higher for NU system than that for NT system. Further, on incorporation of trehalose in NU system (system NUT), in addition to depletion in water density, remarkably, some urea molecules are also replaced, albeit, in small amount, from the solvation shell. These findings are in accordance with the calculations of average number of different solute NMA-solution species hydrogen bonds (see below).

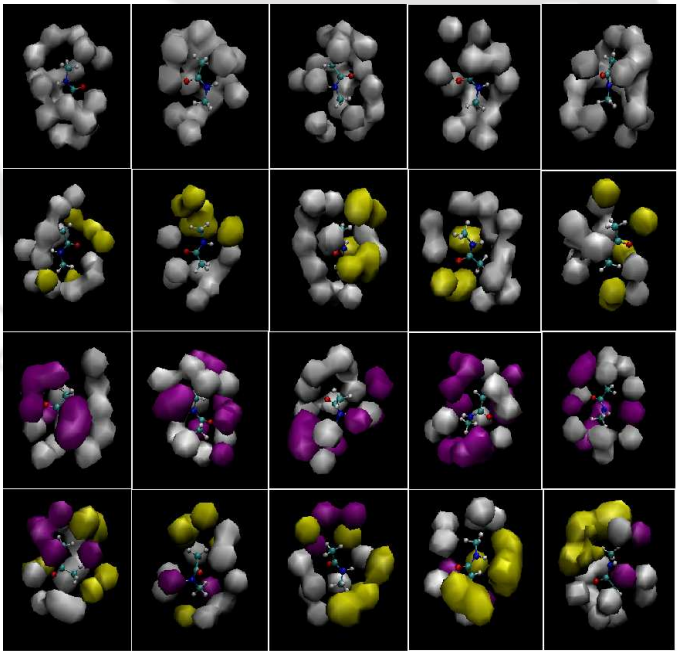

Figure 3B-6. *Contours of water oxygen, urea oxygen and trehalose hydroxyl O6 density within 3.5 Å around NMA. The systems NW, NT, NU and NUT are from top to bottom, respectively. From left to right are for 0 ns, 10 ns, 20 ns, 30 ns and 40 ns time intervals.*

Preferential Interaction: In order to have deeper insights in to the interactions of NMA

molecules with the solvent molecules, by considering preferential interaction parameters, we have also examined the local environment of NMA and compared it with that of the bulk solution. Following previous works, [84, 171] the time-averaged normalized ratio of water ($g_{ow}(r)$), trehalose ($g_{ot}(r)$) and urea ($g_{cu}(r)$) are calculated by using Eq. 2.7-2.9.

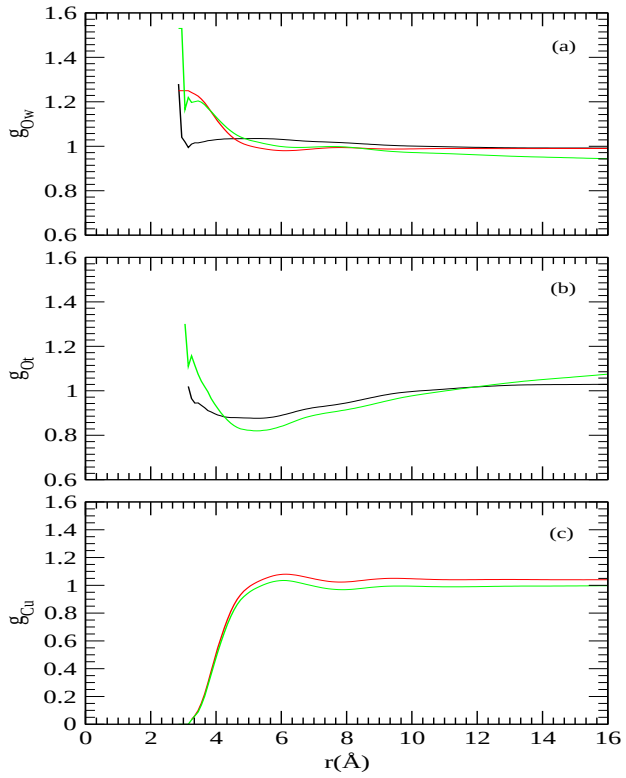

Figure 3B-7. *Time-averaged normalized fractions of water, urea and trehalose as a function of distance from the NMA center of mass. NT (black), NU (red), NUT (green).*

In the close proximity of NMA, if the ratio g_{ow}(r) is greater than one the NMA is preferentially hydrated by water molecules, conversely, water is preferentially excluded from NMA surface, if the value of g_{ow}(r) is lower than one. In Figure 3B-7, we have shown the normalized ratio of water oxygen, urea carbon and trehalose hydroxyl oxygens as function of distance from NMA center of mass. Focusing on the evolution of $g_{ow}(r)$ as distance changes, we notice that in the vicinity of NMA the value of $g_{ow}(r)$ is greater than 1 for all systems considered. Further, the effects of trehalose and urea alone (systems NT and NU) on $g_{ow}(r)$ are very much comparable to each other and the values for both these systems are slightly above 1. This suggests a modest preference for water molecules of NMA molecules in binary water/osmolyte systems. Interestingly, in mixed trehalose/urea

ternary system the value of $g_{ow}(r)$ increases sharply implying that NMA molecules prefer to be hydrated by water molecules. As revealed by the magnitude $g_{ot}(r)$, the presence of urea molecules in the ternary system increases NMA's preference for trehalose in its solvation shell. On the other hand, the preferential interaction parameter, $g_{cu}(r)$, decreases slightly for mixed osmolyte urea/trehalose system (when compared to that of water/urea binary system) and its value becomes lower than one at short-r distance. Thus, from the above observations we make following conclusions: In mixed osmolyte systems, some of the urea molecules are expelled from the NMA solvation layer and NMA interacts preferentially with trehalose and water. As a result of this, the direct interactions between NMA and urea molecules are negated by trehalose molecules and NMA molecules are preferentially hydrated. We note that, these findings are in general accordance with the results of a recent MD simulation study of counteracting effect of trehalose on urea-induced denaturation of protein chymotrypsin inhibitor 2 (CI2) [84] except for the fact that in our study we find the presence of favorable NMA-trehalose interactions in the NMA solvation shell. Whereas the findings of Ref. 84 revealed the exclusion of trehalose molecules from CI2 and argue that in the counteracting effect of trehalose molecules (on urea induced protein denaturation) the preferential hydration (of trehalose) mechanism is operative.

Hydrogen Bond Properties: In order characterize the solvation pattern of NMA in different solutions, in this section, we have estimated the average number of hydrogen bonds formed by a NMA molecule with water, urea and trehalose by adopting a geometric criteria (see Part A of **Chapter 2** for method). Since all solution species including NMA can act as a donor as well as an acceptor, we further decompose each of the types of hydrogen bonds in to donor and acceptor contributions. Note that, we have abbreviated different types of hydrogen bonds as I_x-J_y where I and J can be N (for NMA), W (for water), U (for urea) and T (for trehalose). x and y can be a (for acceptor) and d (for donor). Further note that, the average number of hydrogen bonds are presented with respect to first species. For example, $N_a - W_d$ represents average number of NMA-water hydrogen bonds per NMA where water acts as donor and NMA acts as an acceptor and so on.

The average number of hydrogen bonds formed between NMA and different solution species are shown in Tables 3B-2. In consistent with the Figures 3B-2 and 3B-4, we find that in the formation of NMA-water and NMA-trehalose hydrogen bonds, NMA acts preferably as an acceptor where its carbonyl oxygen accepts hydrogen of water and trehalose hydroxyl groups. For example, in pure water (system NW) each NMA molecule forms 2.46 hydrogen bonds with water in which on average, it acts as an acceptor and a

donor for 1.8 and 0.66 hydrogen bonds respectively. Thus, in the formation NMA-water hydrogen bond, the carbonyl oxygen is solely dominating the hydrogen bond interaction. Addition of urea in to pure water system reduces both these numbers. As a result, the average number of NMA-water hydrogen bonds decreases. We further observe formation of considerable number of NMA-urea hydrogen bonds at the expense of NMA-water hydrogen bonds. In contrast to pure water system where the carbonyl oxygen of NMA is accepting two hydrogen atoms of water molecules, for system NU, remarkably, the carbonyl oxygen of each NMA is shared almost equally by one water and one urea molecule. Further, we noticed that the total number of hydrogen bonds formed by each NMA molecules with the solution species is 2.88 (NMA-water plus NMA-urea), whereas this number is 2.46 in pure water. Thus, urea removes the water molecules from the protein solvation shell by making some favorable contact with protein residues, which leads to protein denaturation. In the context of urea conferred protein denaturation, these findings support the direct interaction mechanism [17-19, 22].

Table 3B-2. Average number of hydrogen bonds (with respect to first species) between NMA-water, NMA-urea and NMA-trehalose[a]

Systems	NW	NU	NT	NUT
$N_a - W_d$	1.80	1.34	1.47	1.06
$N_d - W_a$	0.66	0.47	0.55	0.39
$Total_{NW}$	2.46	1.81	2.02	1.45
$N_a - T_d$	–	–	0.31	0.21
$N_d - T_a$	–	–	0.17	0.11
$Total_{NT}$	–	–	0.48	0.32
$N_a - U_d$	–	0.72	–	0.63
$N_d - U_a$	–	0.35	–	0.32
$Total_{NU}$	–	1.07	–	0.95
$Total$	2.46	2.88	2.50	2.77

[a] Different hydrogen bond types are defined in the text. $Total_{NW}$, $Total_{NT}$ and $Total_{NU}$ correspond to the total number of NMA-water, NMA-trehalose and NMA-urea hydrogen bonds per NMA molecule and $Total$ is the sum of the $Total_{NW}$, $Total_{NT}$ and $Total_{NU}$.

In binary trehalose solution (system NT), the average of NMA-water hydrogen bond also decreases from the pure water system. However, this loss is very well compensated by the formation equal number of NMA-trehalose hydrogen bonds. For example, the

number of $N_a - W_d$ per NMA reduces from 1.80 in pure water to 1.47 in binary trehalose solution and there is formation of 0.31 number of $N_a - T_d$ hydrogen bond. It suggests that trehalose is capable of replacing the NMA-water hydrogen bonds by equal number of NMA-trehalose bonds and this makes the total number of hydrogen bonds formed by a single NMA molecule in the binary trehalose is exactly similar to the pure water system. Now, it would be interesting to observe the influence of trehalose on NMA-water and NMA-urea average number of hydrogen bonds (system NUT). As per the expectation, there is reduction in the NMA-water hydrogen bond in mixed urea/trehalose osmolyte system than that of binary solutions. Considerable amount of presence of NMA-trehalose hydrogen bonds is also observed though this number is much lower than NMA-urea hydrogen bonds (0.32 against 0.95). Further, in the context of NMA-urea hydrogen bonds we observe that though there is a modest decrease in the NMA-urea hydrogen bond number but what is interesting is that the presence of trehalose does not reduce it significantly. These suggest that in the event of trehalose induced protection of urea conferred protein denaturation, trehalose does not prevent formation of protein-urea hydrogen bond completely. Rather, the replacement of protein-water hydrogen bonds by protein-trehalose hydrogen bonds has a major role in the trehalose induced protection of protein from the deleterious effect of urea.

Effect of Trehalose on NMA-Urea Interaction: As mentioned in the Introduction section of **Chapter 1** that the denaturing action of urea molecules can be explained by two different mechanisms namely *direct* and *indirect* mechanisms. Within the former, the interactions between protein and urea can further be sub-divided in to electrostatics and van der Waals interactions. In protein-urea electrostatic interactions the urea molecules interact directly with the protein backbone via hydrogen bonds or other electrostatic interactions. On the other hand, according to direct van der Waals/dispersion interactions urea interacts favorably with the protein amino acids through van der Waals interactions. Though there have been debates over which of the forces is dominant, [20, 196-198] these two direct interactions viz. electrostatics and van der Waals interactions between protein and urea are not always mutually exclusive. In this context it is worth noting that by means of MD simulation studies several attempts have been made in order to understand whether it is the direct electrostatic or van der Waals interactions between urea and protein or a combination of both that is responsible for urea-conferred protein denaturation [18, 33, 84, 199, 200]. By estimating dispersion and electrostatic interactions between each water/urea molecule (present in the first solvation shell of solute and bulk) with solute

protein/macromolecule separately it has been proposed that the favorable van der Waals interactions help to accumulate urea molecules in first solvation shell of the solute. The electrostatic interactions between the solute and solution species play only a minor role [18, 199, 200]. These observations are further supported by another MD simulation study of effect of trehalose on protein-urea system, which revealed that Lennard-Jones interactions rather than electrostatic interactions between urea and protein is responsible for urea-induced protein denaturation [84]. Contrary to these, Das and Mukhopadhyay [33] argued that the favorable electrostatic interactions between urea and protein causes protein denaturation. Thus, following the recent analysis of Zhang *et al.* [84] we have computed direct electrostatic and van der Waals interactions separately between urea and NMA for systems NU and NUT. We consider the interaction energies involving all urea and NMA molecules present in a given system. These energies are plotted as a function of simulation time (see Figure 3B-8).

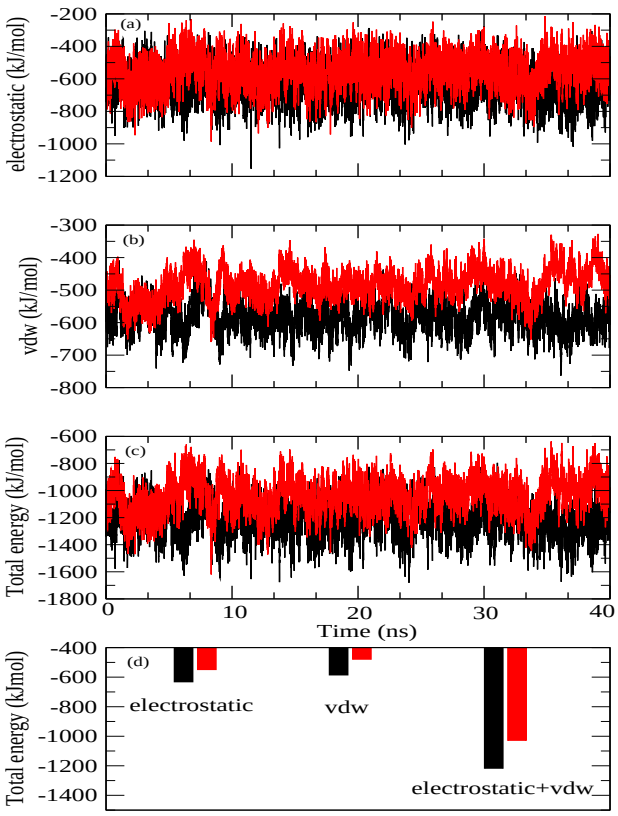

Figure 3B-8. *Intermolecular van der Waals (a), electrostatic (b) and (c) total interaction energies between urea and NMA molecules as a function of simulation time for systems NU (black) and NUT (red). (d) represents van der Waals, electrostatic and total interaction energies averaged over all simulation time.*

As is evident from Figure 3B-8 (a) that the addition of trehalose molecules does not affect urea-NMA electrostatic energy much. Interestingly, there is a modest enhancement (more positive) in the NMA-urea van der Waals energy for ternary NUT system when compared to binary NU system (Figure 3B-8 (b)). In the same Figure we also show total interaction energy as a function of time (Figure 3B-8 (c)) and the average van der Waals, electrostatic and total interaction energies between NMA-urea where averaging is done over the last 30 ns simulation time (Figure 3B-8 (d)). It is apparent that in comparison to binary NMA-urea system, the addition of trehalose in NMA-urea system makes NMA-urea interactions less favorable and a much enhanced (more positive) van der Waals interactions play a dominant role in to it, the effect of unfavorable electrostatic energy being a minor. As discussed above, since trehalose is known to protect the protein from the deleterious effect of urea, it can be inferred from the above observations that urea-protein direct van der Waals interactions play an important role. These findings are in line with the previous results [18, 199, 200].

Interactions Between Solution Species: It is equally important to examine the interactions among different solution species to understand the solvation of NMA in different binary and ternary solutions considered here. This is because, the interactions among water, urea and trehalose molecules influences the solvation of NMA molecules albeit, indirectly. In view of this, we also investigate the interactions between these solution species by considering selected site-site distribution functions and these are shown in Figures 3B-9−3B-11.

As discussed in previous chapter, trehalose molecule possesses hydrophilic hydroxyl groups that can form hydrogen bonds with both water and urea molecules. In Figure 3B-9, we present the rdfs involving trehalose hydroxyl oxygens (O2, O3, O4, O6), glycosidic oxygen (O1) and acetalic ring oxygen (O5) atoms and water oxygen (O_w) atom. It is noticed that each of the hydroxyl oxygen atoms of trehalose shows a characteristics hydrogen bond peak at about 2.75 Å . As revealed by Figure 3B-9 (a) and (e), since, water molecules can not be positioned around O1 and O5 oxygen atoms of trehalose effectively because of the purely geometrical reason, a comparatively lower water density is observed around these two trehalose's oxygen. Thus, in the hydrogen bonding interactions with water molecules (the same logic can be applied for trehalose-trehalose and trehalose-urea hydrogen bonding) the hydroxyl oxygen atoms of trehalose contribute mostly. We note that the appearance of typical hydrogen bond peaks in hydroxyl oxygens and water oxygen rdfs are already reported in literature and our results are in fair agreement with those results [137-139].

Furthermore, the heights of the first peak of these rdfs are getting enhanced in presence of urea (system NUT). Note that, for these distribution functions though the height of the first peak and first minimum increases in presence of urea, the number of first shell water molecules around trehalose decreases from 19.25 (in system NT) to 14.92 (in system NUT) (not shown). This anomaly in the coordination number value is attributed due to the effect of reduced water number density for system NUT. As a result, we observe a decrease in trehalose-water average hydrogen bond number as we move from system NT to system NUT (see below).

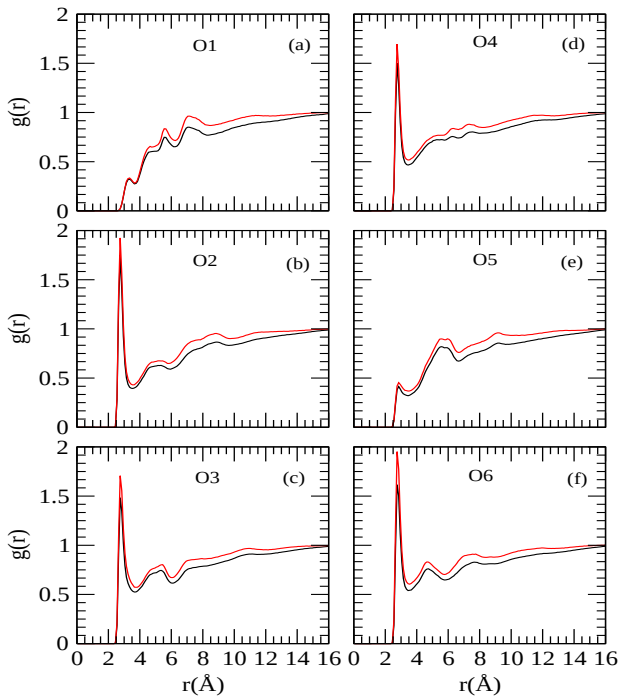

Figure 3B-9. *Site-site radial distribution functions of water oxygen around different oxygen atomic sites of trehalose for systems NT (black) and NUT (red).*

In Figure 3B-10 (a) and (b), we have shown the interaction of trehalose O6 oxygen with urea by considering selected site-site rdfs. The magnitude of the first peak height of these distribution functions confirm the presence of sufficient number of trehalose molecules around urea. The hydrogen bonding interaction between urea and trehalose molecules is also quite evident from rdfs involving oxygen (O_u) and hydrogen (H_u) of urea and trehalose O6. Further, the comparison of the first peak heights of O_u-O6 and H_u-O6 indicates that in the hydrogen bonding interaction between trehalose and urea, the later preferably acts as an acceptor. The distribution of water molecules around the urea atomic sites are displayed

in Figure 3B-10 (c) and (d). For system NU, the appearance of first contact peaks at 2.85 Å and 1.85 Å in urea oxygen-water oxygen ($O_u - O_w$) and urea oxygen-water hydrogen ($O_u - H_w$) rdf profiles, respectively, reflects the formation of urea-water hydrogen bond. It is also notable that the first peak in $O_u - H_w$ rdf is much stronger than the $H_u - O_w$ rdf, which indicates that urea prefers to be a hydrogen bond acceptor rather than a donor. The hydrogen bonding interaction between urea and water increases modestly for ternary system NUT as is evident from the enhanced peak height.

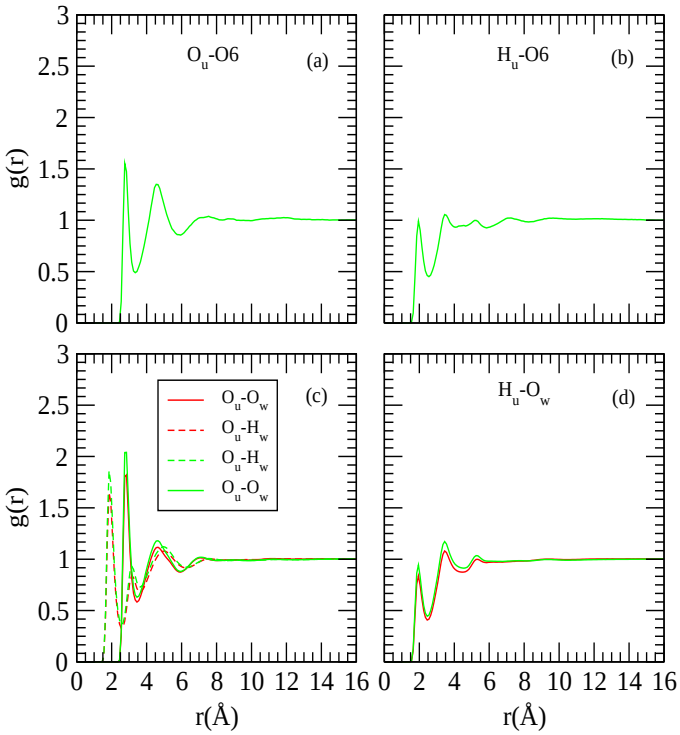

Figure 3B-10. *(a) and (b) respectively, are the site-site radial distribution functions of urea oxygen and hydrogen around trehalose hydroxyl oxygen O6. (c) and (d) are the site-site radial distribution functions involving urea and water. NU (red), NUT (green).*

In order to probe the effects of urea and trehalose on water structure, we examine water-water rdfs for different systems and these are shown in Figure 3B-11. The first peak of $O_w - O_w$ distribution function characterizes the first hydrogen bond neighbor and its second peak represents the tetrahedrally located second neighbor. They appear at 2.8 Å and 4.5 Å respectively. The locations of these peaks are in consistent with the previously reported results [123, 133]. Considering the effect of urea on this distribution function alone (system NU), we notice that the magnitude of the first peak is slightly enhanced keeping its location unchanged. However, urea makes the first valley shallower and the second peak

becomes less pronounced suggesting a modest second shell collapse in the water structure. The influence of trehalose on water structure in solutions containing trehalose is much more pronounced. In specific, trehalose makes the first peak height even more stronger and trehalose-induced collapsing of water structure is much more prominent in systems NT and NUT than that of binary urea solution.

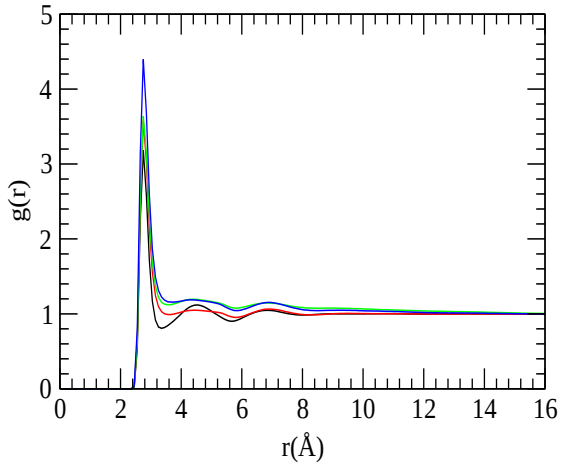

Figure 3B-11. *Site-site radial distribution functions involving water oxygen and water oxygen. NW (black), NU (red), NT (green) and NUT (blue).*

Further, insights in to the hydrogen bonding interactions between different solution species can be obtained by estimating the average number of hydrogen bonds formed by water, trehalose and urea molecules with other like or different solution species. In Table 3B-3, we have shown the calculated values of these hydrogen bonds for different systems.

Table 3B-3. HB_{W-W}, HB_{U-W}, HB_{U-U}, HB_{T-W}, HB_{T-T}, **and** HB_{U-T} **are the average hydrogen bond numbers (with respect to the first species) between water-water, urea-water, urea-urea, trehalose-water, trehalose-trehalose and urea-trehalose respectively**

System	NW	NU	NT	NUT
HB_{W-W}	3.37	2.48	2.78	1.81
HB_{U-W}	–	3.76	–	3.03
HB_{U-U}	–	1.31	–	1.20
HB_{T-W}	–	–	10.00	7.33
HB_{T-T}	–	–	2.45	1.43
HB_{U-T}	–	–	–	0.81

As can be seen that the average number of water-water hydrogen bonds reduces in aqueous osmolyte solutions. This is due to the formation of hydrogen bonds between water and the hydrogen bond active sites of osmolytes urea and trehalose. As a result of this, the average number of hydrogen bonds formed by these osmolytes with the like molecules also decreases. A close look in to the urea-urea and trehalose-trehalose hydrogen bond numbers in binary NU and NT systems reveals that the self-association propensity of urea molecules through hydrogen bonding interactions is somewhat lower than that of trehalose -trehalose self-association. Further, what is remarkable is that in ternary solution, the presence of trehalose molecules causes a reduction in the urea-water hydrogen bond number. There is about 0.73 number of urea-water hydrogen bond, which is lost by per urea molecule as one moves from system NU to NUT. Further, the reduction of 0.11 urea-urea hydrogen bond is also observed for mixed urea/trehalose osmolyte system. And these lost hydrogen bonds by urea molecules are well compensated by the formation of 0.81 urea-trehalose hydrogen bond leaving the NMA-urea hydrogen bonds almost unaffected. Therefore, these act as a corroborative evidence that the protection of protein molecules (by trehalose) does not come from the removal of urea molecules (by trehalose molecules) from the protein surface. So, what trehalose does is it dehydrates the protein surface by removing water molecules from it and forms hydrogen bonds with protein by direct interactions.

Trehalose Clusters and Diffusion Coefficients: The formation of trehalose cluster and its effect on the dynamical properties of the solution species are discussed in Part A of this chapter. Therefore, to observe the self-aggregation propensity of trehalose molecules and how the dynamical properties of different molecules are affected in presence of osmolytes, in this section, we calculate the trehalose clusters (for systems NT and NUT) and diffusion coefficients of NMA and different solution species using Eq. 2.5 and 2.6, respectively.

We have presented the change in $< n_{tre} > / N_{tre}$ (where N_{tre} is the total number of trehalose molecules present in a given system) as a function of trehalose concentration in Table 3B-4. Together with this, in the same table we show the diffusion coefficient values of water (D_W), trehalose (D_T), urea (D_U) and NMA (D_N) for different systems. We find the values of $< n_{tre} > / N_{tre}$ for system NT and NUT, are 0.42 and 0.25, respectively. A little lower value of $< n_{tre} > / N_{tre}$ for system NUT is due to the formation significant trehalose-urea hydrogen bonds. We note that, the value of mean trehalose cluster size for system NT is in line with Part A of this chapter. Moreover, we notice that for binary NT system the percolation of trehalose hydrogen bond network is yet to be achieved. This is due to the consideration of lower trehalose concentration in this study and the presence of

NMA molecules in the system. We also note that the change in $< n_{tre} > /N_{tre}$ values for systems NT and NUT are in accordance with trehalose-trehalose (per trehalose) hydrogen bond formation for these systems discussed above (see Table 3B-4).

Table 3B-4. D_W**,** D_T**,** D_U **and** D_N **correspond to the translational diffusion coefficient values of water, trehalose, urea and NMA respectively.** $< n_{tre} > /N_{tre}$ **is the normalized mean cluster size**[a]

System	D_W	D_T	D_U	D_N	$< n_{tre} > /N_{tre}$
NW	2.43	–	–	1.24	–
NU	2.38	–	1.15	0.77	–
NT	1.89	.03	–	0.37	0.42 (±0.04)
NUT	1.27	.03	0.35	0.36	0.25 (±0.02)

[a] Diffusion coefficient are the times of $10^{-5} cm^2 sec^{-1}$. The standard errors calculated using the block average over 2 ns are given in parentheses.

Now, focusing on the dynamical properties, we observe a sharp decrease in the diffusion coefficient values of all solution species with the addition of osmolytes. A more insight in to these values reveal that trehalose induced retardation of translational motion of water and NMA molecules is significantly larger than that of urea. The presence of both osmolytes in the system (system NUT) decreases these diffusion coefficient values further. In this context, it is worth noting that trehalose induced significant drop in the diffusion coefficient value of water molecules (due to formation of stable water-trehalose hydrogen bonds) that are present within 5.5 Å of solute molecule is already reported elsewhere [159]. The temperature dependent diffusion coefficient measurements of binary water-trehalose mixtures shows that the activation energy for the diffusive motion falls in the typical hydrogen bond energy range [160]. We also observe that the translational dynamics of trehalose remains essentially unchanged for both binary NT and ternary NUT system. On the other hand, the diffusion coefficient of urea decreases from $1.15 \times 10^{-5} cm^2 sec^{-1}$ in binary NU system to $0.35 \times 10^{-5} cm^2 sec^{-1}$ in ternary NUT system. This means that dynamics of urea molecules is also greatly affected in presence of trehalose.

■ SUMMARY AND CONCLUSIONS

To explore the mechanism of trehalose induced counteraction of urea conferred protein de-

naturation, we have performed all atoms MD simulation study to characterize the solvation of NMA in binary and ternary solutions of urea and trehalose. The site-site rdfs between the methyl groups of NMA and water oxygen indicates that binary urea solution has very little effect on the solvation of methyl groups of NMA as compared to the pure water. On the other hand, trehalose enhance the solvation of methyl groups of NMA in both binary trehalose and ternary urea/trehalose solution. Further, the distributions of water hydrogen and oxygen around the NMA oxygen and hydrogen suggest the presence of hydrogen bonding interaction between NMA and water. These rdfs also suggest the relatively weaker hydration of NMA hydrogen by water molecules. The NMA-urea site-site rdfs indicate the direct interaction of urea and NMA in binary urea solution and interestingly, urea density decreases modestly near to NMA molecules upon addition of trehalose. Moreover, the preferential interaction parameter calculations also imply a slight depletion of urea molecules in the vicinity of NMA molecule in ternary urea/trehalose mixture. The depletion of the urea molecules in the close proximity of NMA molecules leads to an enhancement (more positive) in the urea-NMA van der Waals interaction energy. On the other hand, preference for trehalose in the solvation shell of NMA increases in that solution.

Investigation of hydrogen bonding properties of NMA with the solution species showed that in the hydrogen bonding between NMA and water, the former preferably acts as an acceptor in which its carbonyl oxygen atom accepts water hydrogen. Our results also demonstrated that a large number of NMA-water hydrogen bond is replaced by the NMA-urea hydrogen bond in binary urea solution, more specifically, the carbonyl oxygen of NMA is shared between one water and one urea molecule. Again, when compared to pure water system, the total number of hydrogen bonds formed by a single NMA molecule with other solution species is higher in binary urea solution. These findings support the direct interaction mechanism of urea conferred protein denaturation. Just like urea, in binary solution, trehalose also replaces water molecules from the NMA surface, but this replacement is lower than that for the aqueous urea solution. Remarkably, the total number of hydrogen bond formed by one NMA molecule with trehalose in binary trehalose solution is nearly equal to the number of NMA-water hydrogen bonds broken. This keeps total number of hydrogen bonds formed by a single NMA molecules with the solution species essentially unchanged as one moves from system NW to system NT. However, on addition of trehalose to urea solution (system NUT), NMA-urea hydrogen bond number decreases slightly relative to the binary urea solution and trehalose compensates the NMA-water hydrogen bonds by forming NMA-trehalose hydrogen bonds. These observations direct us to propose that

the counteracting effect of trehalose on urea-conferred protein denaturation comes from the replacement of protein-water hydrogen bonds by protein-trehalose hydrogen bonds (lending support from water replacement hypothesis). This essentially reduces the availability of water molecules (at the protein surface) to form hydrogen bonds with protein backbone and as a result the protein native structure is preserved. Furthermore, the formation of large number of trehalose-water hydrogen bonds also suggests the preferential solvation of trehalose molecules by water molecules, which indirectly reduces the availability of water molecules further.

The cluster structure analysis shows that trehalose cluster size decreases from binary trehalose solution to ternary trehalose solution. The value of the mean cluster size for different trehalose containing systems suggests that the percolation of trehalose hydrogen bond network has not been achieved at this concentration of trehalose. The calculation of translational diffusion coefficients shows trehalose induced slowing down of translational motion of all solution species and the effect is more pronounced for NMA and water molecules.

Therefore, the present study explicitly elucidates the counteracting effects of trehalose on urea-induced unfolding of protein and also explains the underlying mechanism of counteracting effect of trehalose at high urea concentration. Finally, these conclusions may improve further our understanding of compatibility and counteracting effects of osmolytes on proteins in protein science.

Chapter 4

Counteracting Action of Trehalose and Conformational Stability of Polypeptide Chain

"It has been recognized that hydrogen bonds restrain protein molecules to their native configurations, and I believe that as the methods of structural chemistry are further applied to physiological problems it will be found that the significance of the hydrogen bond for physiology is greater than that of any other single structural feature."

– Linus Pauling, Nature of the Chemical Bond and the Structure of Molecules and Crystals (1939)

So far, our focus has been on the effects of temperature and osmolyte on solvation of hydrophobic and amide groups. It is necessary to extend the investigation to more realistic protein systems. Protein denaturation is a process that involves the disruption of both the secondary and tertiary structures on application of some external stresses. Since the denaturation reactions are not strong enough, it does not break the peptide bonds (sequence of amino acids), rather it disrupts the normal alpha-helix and beta sheets in a protein and unfolds it into a random shape. This chapter deals with a polypeptide chain that contains 15 amino acid residues. Due to high protein unfolding times, complete unfolding of protein is usually difficult even in presence of urea, and often high temperature has to be used to observe protein unfolding. So to see the folding and unfolding of proteins, high temperature and high urea concentration are used in this study. The folded state of a protein is considered as of having maximum helicity and represents a typical α-helix of proteins where backbone cannot interact freely with the surrounding solution species. Therefore, we interest in the finding of molecular level explanation of trehalose-induced protein stabilization and counteraction of temperature-induced and urea-conferred protein denaturation. The work presented in this chapter is motivated by this necessity.

The chapter is divided into two parts. In Part A, we focus on the counteraction of trehalose on temperature induced protein denaturation. Part B, on the other hand, concentrates on trehalose's influence on urea-conferred protein denaturation.

Part A:

Trehalose's Counteraction of Polypeptide against Temperature Denaturation.

Overview: To investigate the underlying mechanism by which trehalose acts as a bioprotectant against thermal denaturation of protein in aqueous solution, we carry out classical MD simulations at two different temperatures. In view of this, we report here the thermal denaturation process of a 15-residue S-peptide analogue at 360 K and the counteracting ability of trehalose of varying concentrations at that temperature. In order to verify the conformational stability of the peptide at ambient temperature condition, we also carry out a separate simulation of peptide-water binary system at 300 K. The goal is to provide a molecular level understanding of how trehalose protects protein at elevated temperature. The C_α-rmsd calculation shows that in pure water, the peptide is stable at 300 K and its unfolding is observed at 360 K. However, in peptide-water-trehalose ternary system, the value of C_α-rmsd decreases as trehalose concentration is increased. Remarkably, at the highest trehalose concentration considered here, the value of C_α-rmsd at 360 K is similar to that of water-peptide binary system at 300 K. Further, the calculations of radius of gyration of C_α-atoms and helical percentage of the peptide residues support the above observations. The total number of hydrogen bonds formed by the peptide with solution species (trehalose and water) remains constant, though the peptide water hydrogen bond decreases and peptide trehalose hydrogen bond increases with increasing trehalose concentration. This finding suggests replacement of water molecules by trehalose molecules and supports water replacement hypothesis. The calculations of preferential interaction parameter show that at the peptide surface, trehalose molecules are slightly more preferred over water and for the most concentrated solutions, a prominent exclusion of water and enrichment of trehalose molecules is observed. We also observed: (i) trehalose induced second shell collapse of water structure, (ii) the growth of trehalose cluster as concentration is increased and (iii) trehalose induced slowing down of the translational motion of both water and trehalose, the effect being more pronounced for the latter. Implications of these results for counteracting mechanism of trehalose are discussed.

■ INTRODUCTION

Protein protection against the high temperature is a subject of long-standing interest. It has been reported that trehalose is very effective in the stabilization of macromolecules against thermal inactivation [46, 76, 201-203]. Raman Scattering and Differential Scanning Calorimetry (DSC) studies of the effect of trehalose on thermal denaturation of lysozyme showed the bioprotecting ability of trehalose on thermal denaturation of protein [76]. Further, Lerbret *et al.* [77] reported that trehalose stabilizes the lysozyme from thermal denaturation because of the two complementary effects. Firstly, trehalose has destructuring effect on tetrahedral H-bond network of water, which is in agreement with the previous water-sugar solution study [78, 79]. Secondly, trehalose preserves the hydration shell of protein and are excluded from the protein surface, which is in agreement with the preferential hydration hypothesis [59]. However, an investigation of thermal stabilization of RNase A in presence trehalose shows that at low temperature trehalose molecules are excluded from protein surface, but at high temperature trehalose interacts with the RNase A and thereby stabilize the protein [72]. Further, several studies carried out by Timasheff and coworkers [204, 205] at higher temperature (50 °C) also showed that trehalose binds to the protein during thermo-stabilization. A very recent investigation at room temperature said that the distribution of trehalose around the surface of lysozyme is non-uniform and trehalose forms patches on the protein surface and suggest that both water entrapment and water replacement hypotheses are valid [206].

As mentioned above and in **Chapter 1**, it is clear that the molecular mechanism of trehalose towards understanding of bioprotection is not fully understood. In view of this, our goal is to provide the molecular level understanding of how aqueous trehalose solution protects proteins and counteracts the deleterious effect of temperature. We have carried out MD simulation for 15-residue model peptide in absence and presence of trehalose at low and high temperature. In order to see the conformational stability of the peptide, we consider peptide-water binary solutions in absence of trehalose at 300 K. On the other hand, to examine the thermal denaturation of the peptide and the counteracting effect of trehalose, we consider systems with a regime of trehalose concentrations at 360 K. It is also important to mention that only nine residues (4-12) of the peptide are in the α-helical regions. Therefore, we focus on the counteracting effect of trehalose on the residues 4-12. We have first examined the atom positional rmsd of C_α-atom, radius of gyration, and helical percentage of the helix. Thereafter, in order to have some deeper insights in

to the interactions of different solution species, we have first examined different site-site rdfs, hydrogen bond properties and trehalose cluster structure. Finally, the influence of trehalose on the translational dynamics of the solution species viz. water and trehalose are investigated.

The organization of the rest of the chapter is as follows. We first present the models and details of simulations. Results are discussed thereafter, and the last section includes concluding remarks with a brief summary.

■ MODELS AND SIMULATION METHOD

We carried out classical MD simulation of a 15 residue S-peptide to understand the counteracting effect of trehalose on temperature denaturation of protein. First, to verify the peptide conformational stability at ambient temperature condition, in a preliminary survey, a system consisting of water and the peptide (without trehalose) was simulated at 300 K temperature. After that, to investigate the bioprotecting ability of trehalose at somewhat higher temperature another set of simulations with different trehalose concentrations were carried out at 360 K. An overview of the systems simulated here are shown in Table 4A-1.

Table 4A-1. Overview of Simulations[a]

System	N_P	N_{tre}	N_{wat}	volume (nm^3)	w_{tre}%	Temperature
S0	1	0	1000	31.79	0	300
S1	1	0	1000	33.14	0	360
S2	1	10	1000	36.79	16	360
S3	1	20	1000	40.60	28	360
S4	1	50	1000	51.39	49	360
S5	1	75	1000	60.37	59	360

[a] N, N_P, N_{tre}, N_{wat} and w_{tre}% are the number of peptide, trehalose, water molecules and weight percentage of trehalose, respectively.

The initial configurations of our systems were prepared using the Packmol program [129]. For all the simulations, GLYCAM06 force field [120] was adopted for trehalose and for water SPC/E model was used [121]. For the helical structure of S-peptide, the initial coordinates were taken from the X-ray structure of Ribonuclease S (PDB Code: 2RNS) [207].

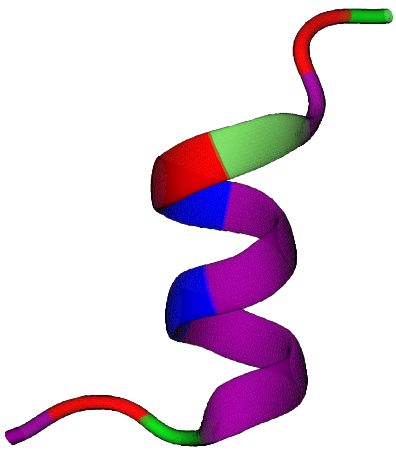

Figure 4A-1. *Initial structure of the helical peptide. Blue, red, and purple colors are for positive, negative, and nonpolar residues, respectively. The peptide sequence is:*

ALA-GLU-THR-ALA-ALA-ALA-LYS-PHE-LEU-ARG-GLU-HIS-MET-ASP-SER

In order to obtain a good initial structure, after extracting the first 15 residues from it a few minor modifications were made (by replacing the residues LYS1, GLU9, and GLN11 by ALA1, LEU9, and GLU11 and followed by protonation to give a zwitterionic form with N-terminal NH_3^+ and C- terminal COO^- groups). The modified initial structure of this helix along with the sequence of amino acids is shown in Figure 4A-1. Histidine was deprotonated and one Na^+ ion was used to neutralize the peptide. This model peptide was described according to the AMBER ff12SB all atom parameter set.

The solution properties were investigated by carrying out classical MD simulation using AMBER12 suite of programs [90]. To obtain a reasonable initial structure, energy minimization for 5000 steps with the first 2500 steps in steepest descent method followed by 2500 steps in conjugate gradient method were performed. Note that the energy minimization which relieves bad van der Waals' contacts, was carried out in two steps, at first holding the peptide fixed by using harmonic restraints (force constant = 500.0 kcal mol^{-1} $Å^{-2}$) and next the whole system was minimized by removing the restraints on peptide. Subsequently, in order to avoid void formation, each system was heated slowly from 0 K to the desired temperature for 100 ps in NVT ensemble with weak restraints (force constant = 10.0 kcal mol^{-1} $Å^{-2}$) on the peptide and then the systems were equilibrated in NPT ensemble without any restraints on peptide for 2 ns at one atmospheric pressure. For calcu-

lating different structural properties, the production runs were performed for 30 ns in NPT ensemble at one atmospheric pressure and in a cubic box. Finally, in order to calculate the diffusion coefficients of different solution species the simulations were, continued for another 20 ns simulation run in NVE ensemble. The choice of different force fields and simulation protocols are discussed in **Chapter 2**.

■ RESULTS AND DISCUSSION

Protein Conformation in Different Solutions: To probe the effect of increased temperature and trehalose concentration on the peptide conformation, the atom positional rmsd of the C_α carbon atoms of backbone of residues 4-12 from the initial structure is calculated.

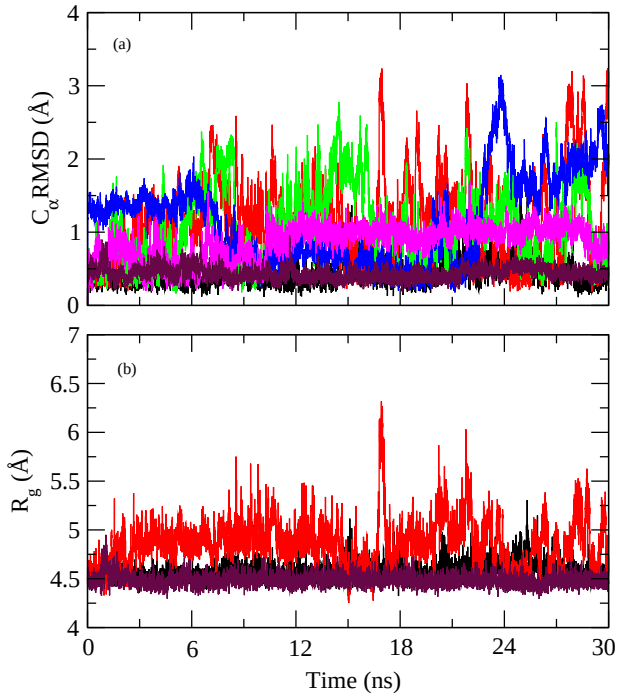

Figure 4A-2. *(a) The atom positional root mean square deviation (rmsd) and (b) radius of gyration of the C_α carbon atoms of backbone of residues 4-12. S0 (black), S1 (red), S2 (green), S3 (blue), S4 (magenta) and S5 (maroon).*

In Figure 4A-2 (a) we show the rms deviations of all the systems simulated here as a function of simulation time. In absence of trehalose, the C_α rmsd of the protein residues at 300 K fluctuates at about 0.45 Å (averaged over simulation time) indicating that the helix of residues 4-12 is stable. On the other hand, because of the additional kinetic energy

available at higher temperature (360 K), a considerably large deviations in the rms deviation is observed and its value reaches to 1.18 Å . The observed rms deviations are in consistent with that reported elsewhere [208, 209]. The addition of trehalose to the protein water solution at higher temperature reduces the conformational changes of peptide as seen from decreased C_α rmsd value. In specific, the average C_α rmsd for system S2−S5 decreases as the concentration of trehalose increases. Interestingly, for system S5, the C_α rmsd is similar to that of system S0 at 300 K. These results indicate the counteracting effect of trehalose on temperature-induced protein denaturation. The temperature-induced modifications of the peptide conformation both in presence and absence of trehalose has also been analyzed by calculating the radius of gyration of C_α atoms of residues 4-12. In Figure 4A-2 (b), we have shown the radius of gyrations for systems S0, S1 and S5 only. In order to have proper visual clarity other systems are left off. It is apparent that the radius of gyration values for systems S0 and S5 are very much comparable whereas the same for the system S1 is much higher.

In order to validate the observed conformational changes further, the secondary structural propensities for residues 4-12 were calculated using DSSP method of Kabsch and Sander [210]. In Table 4A-2, we have presented the helical percentages of the residues 4-12 for all systems. It is observed that in pure water at 300 K the helix is relatively stable (residues 4-9), with only minor deviations from the helical structure. Again, it shows the higher stability of the helix near to the N-terminus residues, which is consistent with the Tirado-Rives's observation [208]. The higher helical propensity of N-terminus residues (notably for ALA4, ALA5, and ALA6) is also in agreement with previous observations [211, 212]. Now, considering the helical percentage of peptide residues in pure water at 360 K, as evident from the helical percentage values of the different residues, we noticed that the peptide rapidly loses its native conformation and shows more unfolded structure. The helical percentage of peptide residues increases with the addition of trehalose molecules at 360 K. For system S5, more interestingly, we observed that helix is more stable up to residue 4-11. The conformational changes in the peptide in pure water system at elevated temperature (system S1) as well as for system with highest trehalose concentration (i.e., system S5) are further confirmed by the snapshots taken at 10 ns interval (see Figure 4A-3). In the same figure we have also shown the structural changes of the peptide at 300 K and in order to have good visual clarity, for all snapshots the solution species (i.e., water and trehalose) are not considered. At 360 K, the changes in the peptide conformation in absence of trehalose and the retention of the peptide conformation in presence of trehalose

molecules are quite evident from this figure. These results suggest the counteracting effect of trehalose on thermal-induced protein denaturation. Moreover, some other structural parameters e.g. native contacts, hydrogen bonds etc. are analyzed below in order to have the molecular insights into the protective action of trehalose on thermal denaturation of the peptide.

Table 4A-2. Helical percentage of residues 4-12 over the simulation time

residues	S0	S1	S2	S3	S4	S5
4	97.35	65.24	68.56	88.67	90.00	98.05
5	97.63	68.94	71.02	90.23	91.49	98.07
6	99.55	76.37	84.00	93.20	97.69	99.58
7	99.67	84.45	86.11	94.55	99.43	99.60
8	99.28	78.29	80.87	92.65	97.56	99.49
9	98.07	64.26	65.19	69.02	90.52	97.64
10	84.65	50.63	43.89	73.68	44.08	97.61
11	54.54	41.70	34.54	57.60	24.32	94.05
12	14.61	26.97	11.59	26.72	17.44	21.33

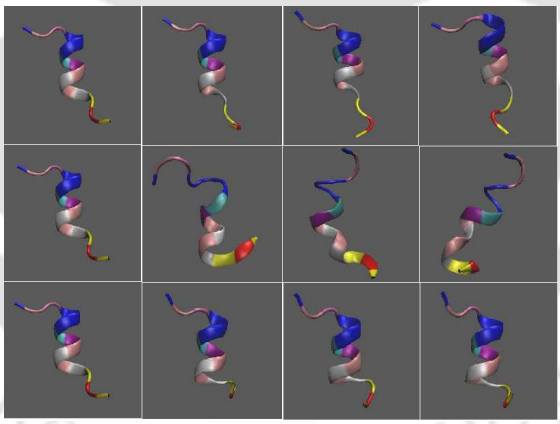

Figure 4A-3. *Snapshots of MD simulations of systems S0, S1 and S5 (from top to bottom). From left to right are for the snapshots of 0ns, 10ns, 20ns and 30ns.*

Protein Conformation in Different Solutions: To investigate the solvation of peptide residues, selected site-site rdfs between different atomic sides of the peptide and solution species are computed. Figure 4A-4 shows the distribution of water oxygen around the peptide heavy atoms and backbone oxygen and hydrogen atoms of residues 4-12. Focusing on the hydration of peptide heavy atoms in pure water at 300 K, we first observe a small first peak at about 2.85 Å which suggests the existence of hydrogen bonding interaction

between the peptide and water (see Figure 4A-4 (a)). A more pronounced second peak that appears at 3.85 Å implies the presence of non-hydrogen-bonding type interactions (e.g., hydrophobic hydration). The significantly lower than bulk water density near the peptide heavy atoms suggests the exclusion of water molecules from the peptide surface. Note that, the observed exclusion of water molecules is consistent with the notion that protein folds spontaneously in nature as water itself is a slightly bad solvent. The peptide hydration pattern at 360 K is qualitatively very similar to that of 300 K except for the fact that a slightly lower water density is observed above 3.7 Å . As trehalose concentration increases we observe a decrease in the peak heights implying a reduction in the water density near the peptide surface. This reduction in the water density is more prominent for system S5 where a large drop in the water density is observed at the close proximity of the peptide surface.

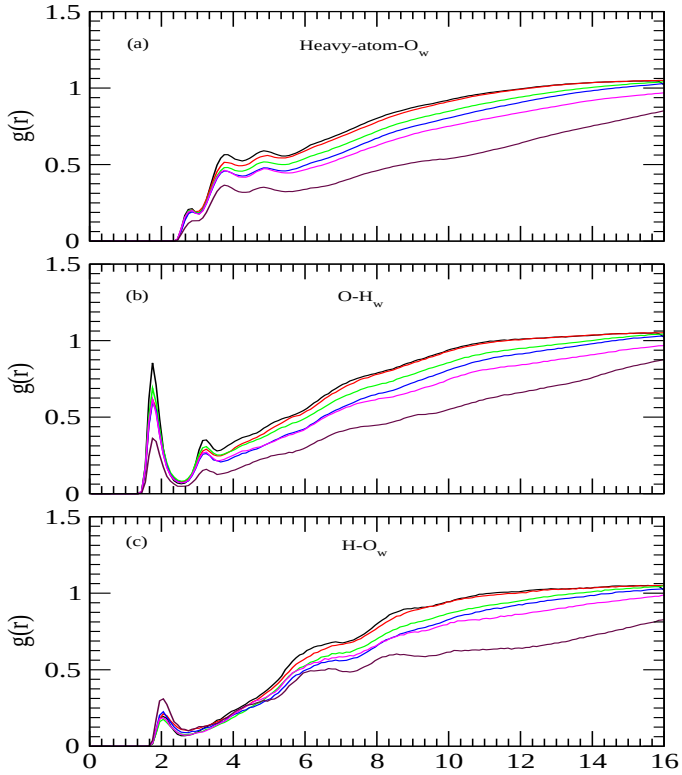

Figure 4A-4. *Site-site distribution functions involving: (a) water oxygen around the peptide heavy atoms, (b) water hydrogen around backbone oxygen atoms and (c) water oxygen around peptide backbone hydrogen atoms of residues 4-12, respectively. S0 (black), S1 (red), S2 (green), S3 (blue), S4 (magenta) and S5 (maroon).*

Now, comparing the water density around the peptide backbone oxygen and hydrogen atoms (Figure 4A-4 (b) and (c)), we find that the water density around the backbone oxygen is higher than that around the backbone hydrogen. In fact peptide backbone hydrogens are not easily accessible for water molecules as evident from small first peak height. Moreover, since a water molecule possesses one oxygen atom and two hydrogen atoms, the peptide-water hydrogen bonding interactions are solely dominated by backbone oxygen of the peptide. Further, in comparison to peptide backbone hydrogen-water oxygen rdf, the effect of trehalose concentration is much more prominent for peptide backbone oxygen-water hydrogen distribution function. In brief, addition of trehalose causes a sharp drop in the first peak height indicating a much reduced peptide-water hydrogen bonding interactions in concentrated trehalose solutions. These observations are in accordance with the calculated peptide-water hydrogen bond numbers discussed below. The examination of water distributions around the positively charged peptide side chains (LYS7 and ARG10) and the negatively charged side chain (GLU11) (see Figure 4A-5) reveal that both of them participate in hydrogen bonding interactions with water. Moreover, as revealed by the very strong first peak height, among the hydrogen bonding sites in the peptide, the negatively charged side chain has the strongest tendency for the hydrogen bonding interactions with water molecules. Further, the effect of either temperature or trehalose concentration is not very dramatic for positively charged side chain-water rdfs (except for system S5) whereas the same for negatively charged side chain-water distribution is more prominent. As can be seen, for the latter the addition of trehalose decreases the first peak (and second peak) height modestly with a more pronounced effect for system S5.

In order to obtain the distribution of trehalose molecules near the peptide surface the site-site rdfs involving peptide heavy atoms (of residues 4-12) and different oxygen atoms of trehalose are considered and they are shown in Figure 4A-6. The presence of considerable number of trehalose molecules near the peptide surface is quite evident from these figures. We also note that, though trehalose has larger excluded volume than the water, the densities of trehalose oxygen atoms in peptide-trehalose rdfs start to rise from the similar location as that of peptide-water rdfs. Moreover, the densities of trehalose hydroxyl oxygen atoms (i.e., O2, O3, O4 and O6) at around 4 Å of peptide are much higher than that of the water density implying trehalose's ability to reduce the water density in the close proximity of the peptide and its (trehalose's) preferential interaction with the peptide residues. This is further confirmed by the calculation of the RCN of solution species around the heavy atoms of the entire peptide using Eq. 2.3.

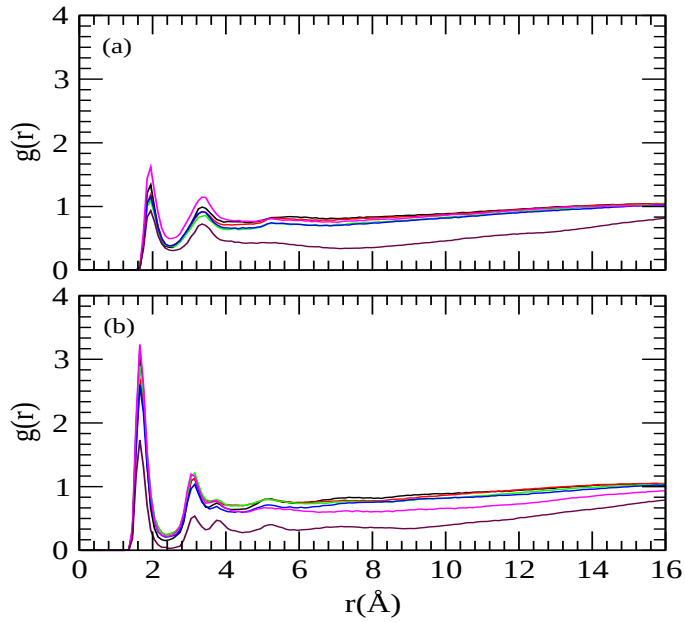

Figure 4A-5. *Site-site distribution functions involving: (a) water oxygen around positively charged peptide side chains (LYS7 and ARG10) and (b) water hydrogen around the negatively charged peptide side chain of residue GLU11. S0 (black), S1 (red), S2 (green), S3 (blue), S4 (magenta) and S5 (maroon).*

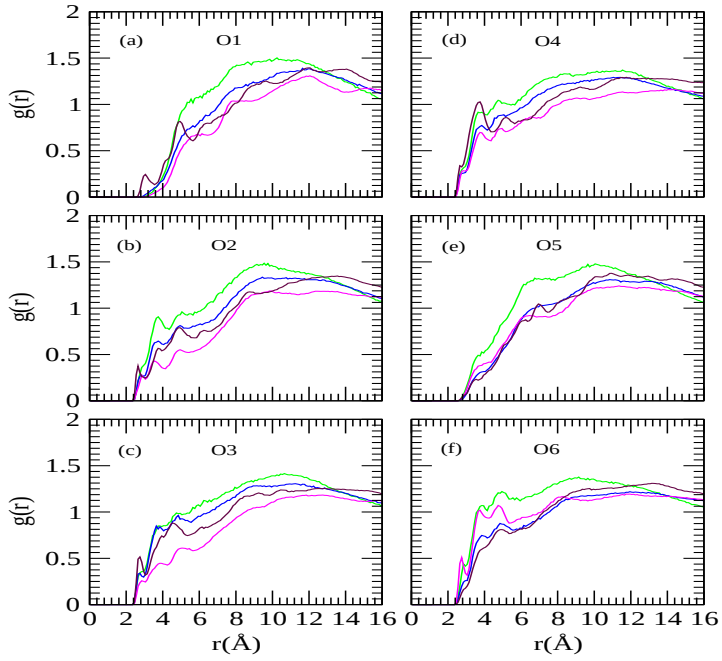

Figure 4A-6. *Site-site distribution functions between peptide heavy atoms (residues 4-12) and trehalose oxygen atoms. S2 (green), S3 (blue), S4 (magenta) and S5 (maroon).*

The values of RCN (as a function of distance) for water oxygen and O1 atom of trehalose around the peptide heavy atoms are displayed in Figure 4A-7. At a given distance, the addition of trehalose causes a decrease in the number of water molecules and an increase in the number of trehalose molecules. These findings are further supported from the calculations of peptide-water and peptide-trehalose hydrogen bond numbers discussed below where we find that on addition of trehalose, large number of peptide-water hydrogen bonds are replaced by peptide-trehalose hydrogen bonds.

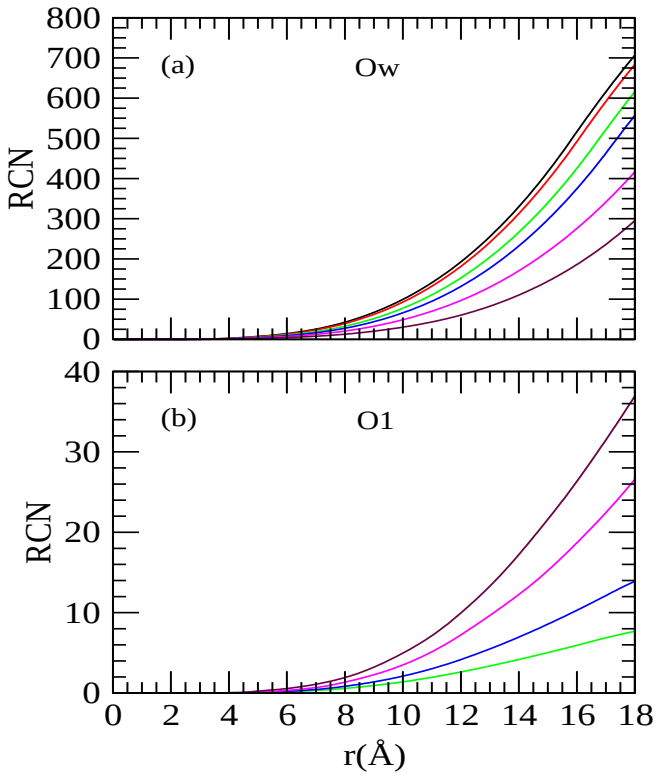

Figure 4A-7. *Running coordination numbers for (a) water oxygen and (b) trehalose central atom (O1) around the heavy atoms of the peptide. S0 (black), S1 (red), S2 (green), S3 (blue), S4 (magenta) and S5 (maroon).*

Preferential Interaction: The preferred peptide-trehalose (over peptide-water) interactions at concentrated trehalose solution are also confirmed from the calculations of preferential interaction parameters. In order to understand if the peptide surface is enriched by water or trehalose, we have calculated the time-averaged normalized ratio of solution species trehalose and water (i.e., $g_{ow}(r)$ and $g_{ot}(r)$) by using Eq. 2.7 and 2.8.

As discussed previously, in the close proximity of peptide, if the value of $g_{ow}(r)$ is greater than 1 then the peptide is preferentially hydrated by water molecules and opposite

to that, the relative depletion of water leads to the value of $g_{ow}(r)$ that is lower than 1. The values of $g_{ow}(r)$ and $g_{ot}(r)$ are shown in Figure 4A-8. As can be seen, for systems with low trehalose concentrations, trehalose molecules are slightly more preferred in the close proximity (within 3.5 Å) of the peptide surface. On the other hand, for the highest trehalose concentration (system S5), remarkably, exclusion of water molecules (and accumulation of trehalose molecules) is clearly visible. These findings validate the water replacement hypothesis [44, 213]. Here we also note that, Crowe *et al.* previously proposed that upon dehydration, the water molecules that were initially present in the protein hydration layer are replaced by trehalose molecules [45]. The hydration pattern of peptide residues were, further, characterized by estimating the number of water and trehalose molecules around the peptide heavy atoms of residues 4-12. For calculating the number of water and trehalose molecules around the peptide heavy atoms, we have considered the first solvation shell of 3.5 Å from the peptide heavy atoms and the values are presented in Table 4A-3.

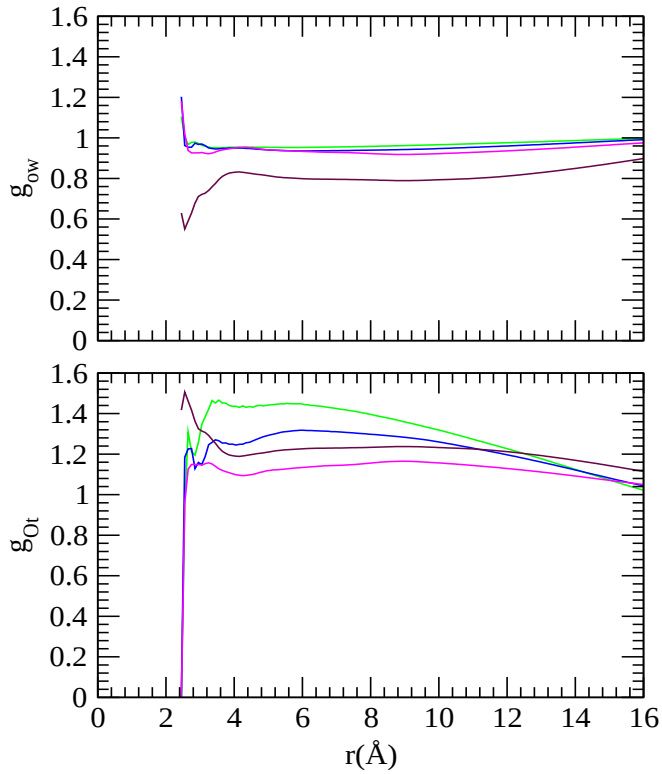

Figure 4A-8. *Time-averaged normalized fractions of water (top) and trehalose (bottom) as a function of the distance from the peptide heavy atoms of residue 4-12. S2 (green), S3 (blue),S4 (magenta) and S5 (maroon).*

The number of water molecules around the peptide heavy atom at 300 K is about 38.67, which is consistent with previously reported result for this peptide [214]. The hydration number around these heavy atoms decreases slightly as temperature increases from 300 K to 360 K, though the unfolding of the peptide is observed at 360 K. This decrease in the number is due to decrease in the water number density and increased temperature of the system. Interestingly, with the addition of trehalose, the hydration number decreases for systems S2-S5 and on the other hand number of trehalose molecules increases around the peptide heavy atom.

Table 4A-3. Average number of water and trehalose molecules within 3.5 Å of any heavy atom of the peptide residues

Systems	water	trehalose
S0	38.67	–
S1	35.97	–
S2	31.68	4.04
S3	26.96	5.81
S4	21.57	10.67
S5	14.06	12.95

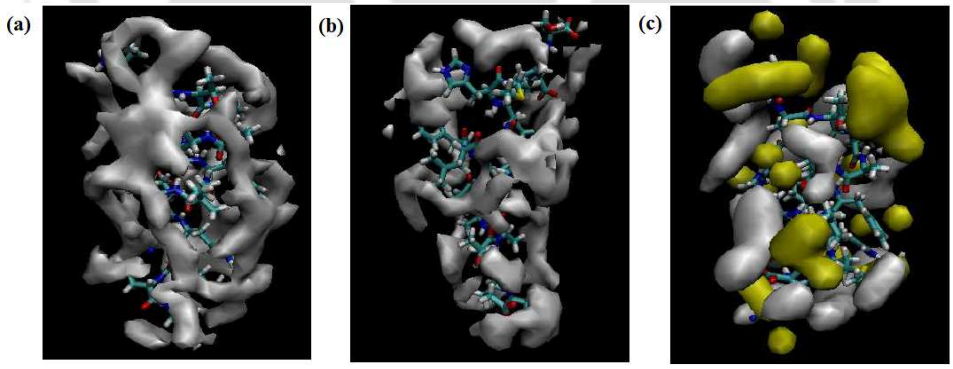

Figure 4A-9. *Contours of trehalose and water density within 3.5 Å around the peptide monomer for systems: (a) S0, (b) S1 and (c) S5. The colors grey and light green correspond to water and trehalose molecules respectively.*

In order to visualize the above observations further, we have carried out atomic mass density analysis using VMD. Figure 4A-9 displays the mass density map of water and trehalose molecules with a cell side of 0.5 Å within 3.5 Å around the peptide for systems S0, S1 and S5. From this contour diagram, it can be clearly seen that in comparison to system

S0, the water density around the peptide is slightly lower for system S1. The presence of considerably large number of trehalose molecules near to peptide surface and exclusion of water molecules from the surface are also quite visible for system S5. Thus, from the above observations, we conclude that in the process of protein stabilization by trehalose at high temperature, trehalose molecules are preferred over water in the peptide solvation shell.

Interaction Between Solution Species: The sugar-sugar, sugar-water and water-water interactions play an important role in the bioprotection phenomenon. In brief, it is believed that in aqueous sugar solution the formation of extended sugar-sugar hydrogen bond network affects the dynamical properties of the solution species very strongly. Further, since protein-water dynamics are coupled, trehalose induced slowing down of the surrounding water dynamics influences protein dynamics. As claimed in some previously reported results, [70, 173] the trehalose induced stabilization of biomolecules comes because of this retardation of the surrounding water molecules. Further, it has been already reported that in comparison to other oxygen atoms, the hydroxyl groups of trehalose are well hydrated with well defined hydration peak in the corresponding trehalose hydroxyl oxygen and water oxygen rdfs [137-139].

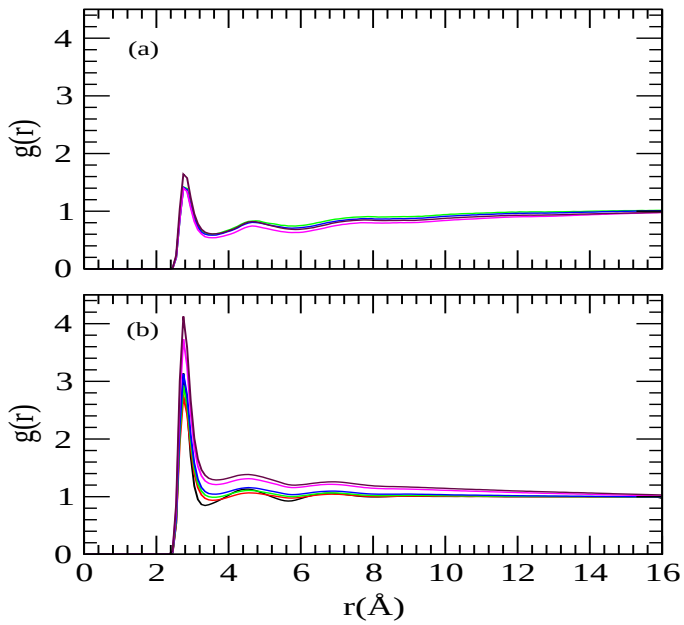

Figure 4A-10. *Site-site radial distribution function between (a) water oxygen and trehalose hydroxyl oxygen O6 and (b) water oxygen and water oxygen. S0 (black), S1 (red), S2 (green), S3 (blue), S4 (magenta) and S5 (maroon).*

In view of this, in Figure 4A-10 (a), we have shown the rdfs of hydroxyl oxygen (O6) with respect to water oxygen. Note that, since rdfs of other hydroxyl oxygen atoms (O2, O3 and O4) with water oxygen behave in similar fashion as that of O6 hydroxyl atom, therefore, we restrict ourselves to O6 hydroxyl atom-water oxygen rdf only. As can be seen, the rdf involving hydroxyl O6 and water oxygen has a sharp peak at about 2.75 Å indicating the presence of hydrogen bonding interactions between water and trehalose. Considering the effect of trehalose concentration, we find that the first peak is not much affected as trehalose concentration increases for up to system S4. After that, the addition of trehalose does nothing to decrease the the peak heights rather it appears to be enhanced modestly and makes the first valley slightly shallower.

Table 4A-4. Number of first shell water molecules around the different hydroxyl hydrogen of trehalose[a]

		System					
	Coordination number (CN)	S0	S1	S2	S3	S4	S5
1GA	$O1O_w$	–	–	0.60	0.47	0.53	0.42
	$O2O_w$	–	–	2.32	2.05	1.72	1.69
	$O3O_w$	–	–	3.40	2.88	2.15	2.17
	$O4O_w$	–	–	2.63	2.29	1.67	1.74
	$O5O_w$	–	–	0.68	0.72	0.52	0.47
	$O6O_w$	–	–	2.87	2.52	1.98	1.91
0GA	$O2O_w$	–	–	2.57	2.32	1.85	1.65
	$O3O_w$	–	–	2.81	2.75	2.24	1.90
	$O4O_w$	–	–	2.59	2.35	1.76	1.63
	$O5O_w$	–	–	0.67	0.72	0.51	0.54
	$O6O_w$	–	–	2.83	2.33	1.85	1.86
	Total	–	–	23.97	21.40 (21.83)	16.78 (17.16)	15.98 (14.61)

[a] The values given in the parentheses represent the water coordination number if the only change with added trehalose came through the number density of water.

To probe the effects of trehalose concentration on trehalose O6-water oxygen rdfs in more detail, we extend our investigation further by estimating the number of first shell water molecules around different oxygen atoms of trehalose molecules and the results for the same are presented in Table 4A-4. We immediately see that in comparison to the glycosidic and ring oxygen atoms, trehalose hydroxyl oxygen atoms are interacting more with water molecules and the effect of change in trehalose concentration is more prominent for the latter. Moreover, though the addition of trehalose has negligible effect in regard to change in

peak height of trehalose O6-water oxygen rdf, as is evident from Table 4A-4 that the number of first shell water molecules around trehalose oxygen decreases as trehalose concentration increases. However, to nullify the effect of reduced water density and to probe the effect of change in trehalose concentration exclusively, we have estimated the coordination numbers by assuming that trehalose oxygen-water oxygen pair distribution functions are unchanged by the addition of trehalose molecules and these are given in the parentheses of the same table (Table 4A-4). For the systems S3 and S4, the coordination number does not change much than that expected from the water density change. But, for system S5 the number of water molecules in the first solvation shell of water estimated from Eq. 2.3 is in slight excess than the expected coordination number values. The above observations direct us to suggest that addition of trehalose causes breaking of some of the trehalose-water hydrogen bonds and are further confirmed by the calculation of average number trehalose-water (per trehalose) hydrogen bonds. What is more that, as one moves from system S4 to S5, the average number of water-trehalose hydrogen bonds per trehalose molecule remains essentially unchanged (discussed below) and this fact acts as a corroborative evidence of exclusion of some water molecules from peptide surface.

The hydrogen bonding interactions between water molecules and the possible effects of trehalose concentrations on to it can be probed by considering water-water rdfs. Figure 4A-10 (b) represents distribution function involving water oxygens. The first peak and second peak that appear at about 2.75 Å and 4.45 Å respectively, characterizes H-bonded first neighbor and tetrahedrally located second neighbor. The positions of these peaks are similar to those already reported in the literature [214, 215]. We further noticed that for binary water-peptide systems, the peak height decreases with increasing temperature and the position of the first minimum is shifted towards longer distances. The second peak that was quite visible at 300 K is almost disappeared at higher temperatures. These observations of the effect of temperature on water structure observed in this study are consistent with the previously reported simulation results [216]. Now, at 360 K, on increasing trehalose concentration we observe a sharp increase in the first peak height and the first peak valley appears at about 3.4 Å becomes much shallower which in turn makes the second peak less pronounced. Such changes in $O_w - O_w$ rdfs suggest the second shell collapse of water structure as trehalose concentration is increased.

Hydrogen Bond Properties: To examine peptide solvation more closely, we estimate the average number of hydrogen bonds formed by the peptide with the solution species viz. water and trehalose. Together with this, we also calculate the average number of

hydrogen bonds formed by each water and trehalose molecule with other water and trehalose molecules. The hydrogen bond number is calculated by adopting a geometric criteria (see **Chapter 2**). The number of different type of hydrogen bonds such as water-water (WW), water-trehalose per trehalose (WT) trehalose-peptide (TP), water-peptide (WP), trehalose-trehalose (TT) and the intramolecular peptide hydrogen bonds are summarized in Table 4A-5.

Table 4A-5. Average number of hydrogen bonds for different systems for different species. P, W and T represent peptide, water and trehalose molecules respectively[a]

Systems	HB_{PP}	HB_{WP}	HB_{TP}	HB_{WT}	HB_{WW}	HB_{TT}
S0	4.95	25.08	0.00	0.00	3.35	0.00
S1	3.95	23.48	0.00	0.00	3.20	0.00
S2	4.10	21.31	3.02	12.16	3.07	0.95
S3	4.46	18.14	4.08	9.48	2.98	1.59
S4	4.40	14.63	9.22	8.15	2.80	2.61
S5	5.24	8.61	12.56	8.10	2.57	2.85

[a] The average number of hydrogen bonds are represented with respect to the second species. For example, HB_{WT} is the average number of water-trehalose hydrogen bonds per trehalose and so on.

Considering the folded and unfolded states of peptide in pure water at 300 K and 360 K, we observe the loss of peptide-peptide intramolecular hydrogen bond within the helix. The number of peptide-peptide intramolecular hydrogen bond is 4.95 at 300 K and it is 3.95 at 360 K suggesting the breaking of helical structure of the peptide at higher temperature. On the other hand, the stabilising effect of trehalose on temperature-denatured peptide is quite evident from the average number of peptide-peptide hydrogen bonds. We find that this hydrogen bond number increases with increasing trehalose concentration. This finding of increased number of peptide-peptide intramolecular hydrogen bonds supports our C_α-rmsd and radius of gyration calculations discussed above. The average number of peptide-water hydrogen bonds in absence of trehalose for two temperatures 300 K and 360 K are 25.08 and 23.48, respectively. Despite the fact that the peptide is unfolded at higher temperature, the peptide-water hydrogen bond decreases. This is an obvious effect for thermal-induced protein unfolding process [217]. Further, the average peptide-water hydrogen bond number decreases as the concentration of trehalose increases. This decrease in the number of peptide-water hydrogen bond is compensated by the nearly equal number of trehalose-peptide hydrogen bonds. For example, the average number of water-peptide hydrogen bond is 23.48 for system S1 and on addition of 10 trehalose molecules (system

S2) this number reduces to 21.31. This makes a loss of 2.17 water-peptide hydrogen bonds that are compensated by three trehalose-peptide hydrogen bonds. This observation holds true for all other systems considered here. Therefore, we emphasize that trehalose preferentially interacts with the peptide in the protein stabilization mechanism as suggested by preferential interaction hypothesis. Here it is important to mention that our findings are in contradiction with the results of vapor pressure osmometry studies of different osmolyte solutions containing different structure protectant osmolytes such as glycine betaine, proline, trimethylamine-N-oxide (TMAO), glycerol, trehalose and k^+Glu^- where exclusion of these osmolyte molecules from the surface of bovine serum albumin (BSA) was observed [218]. Further, their calculations of preferential interaction parameters revealed that it is the betaine molecule which shows maximum exclusion, on the other hand glycerol molecules are the least excluded from the protein surface. In this context we note that, Timasheff *et al.* [204] reported that in temperature dependence protein stabilization trehalose molecules preferentially bind to native protein compared to unfolded protein and gives rise to the stabilization. Finally, it seems that at higher temperature, the replacement of water molecules (by trehalose molecules) from the peptide does play a role in peptide stabilization and supports water replacement hypothesis [55]. In regard to the average number of hydrogen bonds formed by a water molecule with other like molecules we find that these hydrogen bonds decrease on addition of trehalose molecules and this fact acts as a corroborative evidence to that observed in the water-water distribution functions.

Trehalose Clusters: The mean trehalose cluster size, $< n_{tre} >$, is calculated using Eq. 2.5 (see **Chapter 2**) and Figure 4A-11 represents the normalized mean trehalose cluster size $< n_{tre} > / N_{tre}$ (where N_{tre} is the total number of trehalose molecules in a system) as a function of trehalose concentration. Notwithstanding the error bars, we notice that as trehalose concentration increases, the value of $< n_{tre} > / N_{tre}$ increases sharply indicating the growth of trehalose clusters. For the highest trehalose concentration considered here, the value of $< n_{tre} > / N_{tre}$ reaches to 0.7 implying that the percolation of trehalose hydrogen bond network has not been achieved. As discussed in previous chapter, the percolation of trehalose hydrogen bond network has been achieved at 66 wt% trehalose concentration in binary water-trehalose solution [155]. The discrepancy in the percolation of trehalose hydrogen bond network reported here may be due to the presence of peptide and slightly lower trehalose concentration. It is evident from Table 4A-5 that the peptide-trehalose hydrogen bond number increases with increasing trehalose concentration, which may affect the formation of trehalose-trehalose hydrogen bond network. Further, the average number

of trehalose-trehalose hydrogen bond increases with increasing trehalose concentration and this is consistent with the increased growth of trehalose cluster at high trehalose concentration.

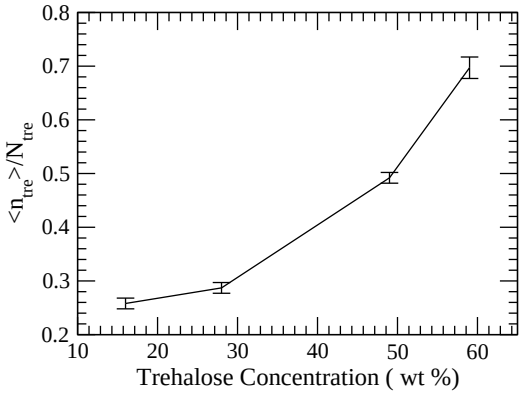

Figure 4A-11. *The normalized mean trehalose cluster size* $< n_{tre} >/N_{tre}$ *for different systems. The standard errors are calculated using the block average over 2 ns.*

Diffusion Coefficients: We have calculated the translational diffusion coefficients of water and trehalose for different systems using Eq. 2.6 (see **Chapter 2**). The diffusion coefficient values of water (D_w) and trehalose (D_{tre}) for different systems are presented in Table 4A-6. For pure water systems, as expected, we find a sharp increase in the diffusion coefficient value for water as temperature is increased from 300 K to 360 K. Considering the fact that we have peptide in our systems, the diffusion coefficient of water at 300 K temperature is in agreement with the experimental diffusion coefficient reported earlier [157]. In regard to the effect of trehalose, we find that trehalose has pronounced effect on the dynamical properties. For example, as trehalose concentration is increased from 16% to 59% the diffusion coefficient of water decreases from $4.98 \times 10^{-5} cm^2 sec^{-1}$ to $1.95 \times 10^{-5} cm^2 sec^{-1}$ (2.5 times decrease) and for trehalose, the diffusion coefficient decreases from $0.23 \times 10^{-5} cm^2 sec^{-1}$ to $0.02 \times 10^{-5} cm^2 sec^{-1}$ (11.5 times decrease). Thus, compared to water the effect of trehalose on the retardation of translational motion is more prominent for trehalose molecules. Indeed, the ratio of D_w and D_{tre} increases sharply with increasing trehalose concentration. This finding is in accordance with the NMR experiment results [157]. Further, the sharp decrease in the D_{tre} value, particularly at higher trehalose concentration, is consistent with the sharp increase in its viscosity value [158]. In this context it is worth noting that the formation of stable water-trehalose hydrogen bonds and trehalose induced significant decrease in the diffusion coefficient of water molecules that are present near to 5.5 Å of a

solute molecule has already been reported [159]. Trehalose induced slowing down of translational and rotational motion of surrounding water molecules has also been observed in recent Terahertz absorption measurements [69].

Table 4A-6. D_w, D_{tre} **correspond to diffusion coefficient of water, and trehalose respectively**

System	D_w $(10^{-5} cm^2 sec^{-1})$	D_{tre} $(10^{-5} cm^2 sec^{-1})$
S0	2.17	—
S1	5.74	—
S2	4.98	0.23
S3	4.58	0.19
S4	2.51	0.05
S5	1.95	0.02

■ SUMMARY AND CONCLUSIONS

Classical MD simulations have been used to investigate the role of aqueous trehalose solutions on the conformational stability of a model 15-residue peptide at higher than ambient temperature condition. At 1 atm pressure and 360 K temperature, trehalose concentrations ranging from 0% to 59% were used. A separate simulation of system consisting water and peptide (in absence of trehalose molecules) at 300 K temperature was also carried out in order to assess the stability of peptide at the ambient condition.

From the C_α-rmsd calculation for different systems we noticed that in pure water, peptide loses its helical structure at high temperature. Interestingly, high trehalose concentration can off-set the thermal-induced peptide conformational changes. This observation is further supported by the calculation of radius of gyration of C_α-atoms and the estimation of helical percentage of the peptide residues 4-12. The interesting observations that we made are that, at 360 K temperature, the value of C_α-rmsd for the system with the highest trehalose concentration matches well with that of peptide-water binary system at 300 K. The snapshots of different systems at 10 ns intervals also indicate the retention of peptide helical conformation at higher temperature in concentrated trehalose solution.

To provide the molecular level understanding of the counteracting effect of trehalose on temperature induced protein denaturation, we have computed the site-site rdfs involving different solution species. From the rdfs of peptide heavy atoms and water oxygen it is observed that on addition of trehalose water density decreases around the peptide heavy atoms. Moreover, the distributions of water oxygen and hydrogen atoms reveal that the backbone hydrogens are not easily accessible for water molecules to interact. This implies that in the peptide-water hydrogen bonding interactions it is the backbone oxygens that involve predominantly. Further, as evidenced from the peptide backbone-water distribution functions that in presence of trehalose it is the peptide backbone-water hydrogen rdfs that are affected more compared to backbone-water oxygen rdf. In specific, on increasing trehalose concentration the peak height of the former decreases sharply suggesting a reduction in the hydrogen bonding interactions between the peptide and water molecules. These findings are consistent with the results of calculated average number of hydrogen bonds between peptide and the solution species. Moreover, among the hydrogen bonding sites, the negatively charged side chain of the peptide is more inclined towards hydrogen bonding interactions with the solution species than the positively charged side chain.

The distribution functions involving peptide and different atomic sites of trehalose show the presence of large number of trehalose molecules in the close proximity of peptide surface. To obtain a physical picture of peptide's preference for different solutions species near to its surface, we, further, calculate preferential interaction parameters. For low trehalose concentrations, the estimation of these parameters as a function of distance from the peptide surface suggests that trehalose molecules are slightly more preferred over water molecules at the surface. Interestingly, at the highest trehalose concentration studied here, we observe high preferential exclusion of water molecules and accumulation of trehalose molecules at the surface. This fact is further confirmed by the calculation of average number of water-peptide and trehalose-peptide hydrogen bonds in different system. We find that the peptide-water hydrogen bond decreases with trehalose concentration and remarkably, these hydrogen bonds are replaced by nearly equal number of peptide-trehalose hydrogen bonds and the total number of hydrogen bonds formed by the peptide with the solution species remains essentially unchanged. The atomic density analyses also show the depletion in the number of water molecules and enrichment of the peptide surface by trehalose molecules. These observations support water replacement hypotheses proposed earlier [55].

The calculated diffusion coefficient values suggest trehalose induced slowing down of translational motion of all solution species and the effect is more pronounced for trehalose

than water. Though we have observed higher diffusion coefficient value for water at higher temperature, the translational dynamics of water are greatly reduced with the addition of trehalose. In accordance with the results of NMR experiments [157], we also observe that for a particular temperature, the ratio of water and trehalose diffusion coefficient values increases with concentration. Furthermore, in the log-log plot of mean squared displacement vs. time (not shown) we did not see any so-called "boson" peak for the most concentrated trehalose solution as reported earlier [139]. This fact implies that the most concentrated aqueous trehalose solution considered in our study is still above the glass transition temperature. We have also examined the effect of trehalose concentration on the growth of trehalose cluster at high temperature. We find that the growth of the cluster increases with concentration. The values of normalized mean cluster sizes for different systems indicate that percolation of trehalose hydrogen bond network has not been achieved for highest trehalose concentration considered here [155]. Thus, without excluding trehalose induced slowing down of translational dynamics of solution species, we conclude that the prominent effect of trehalose's counteracting effect on the thermal denaturation of our model peptide arises due to exclusion of water molecules (and enrichment of trehalose molecules) at the peptide surface and the replacement of peptide-water hydrogen bonds by peptide-trehalose hydrogen bonds.

Part B:

Trehalose's Effect on Polypeptide against Urea Denaturation

Overview: Molecular dynamics simulations are performed to investigate the counteracting effect of trehalose against urea induced denaturation of S-peptide analogue. The calculations of C_α-rmsd, radius of gyration and solvent accessible surface area reveal that the peptide loses its native structure in aqueous 8 M urea solution at 310 K and this unfolding process is prevented in presence of trehalose. Interestingly, the native structure of the peptide in ternary mixed urea/trehalose solution is similar to pure water system. The estimation of helical percentage of peptide residues as well as peptide-peptide intramolecular hydrogen bond number for different systems also support the above findings. Decomposition of protein-urea total interaction energy in to electrostatic and van der Waals contributions shows that the presence of trehalose molecules makes the latter contribution unfavorable without affecting the former. These observations are further supported by preferential interaction calculations. Further, the hydrogen bond analyses show that with the addition of urea molecules to peptide-water system, the formation of peptide-urea hydrogen bonds takes place at the expense of peptide-water hydrogen bonds. In ternary mixed osmolytes system, due to formation of considerable amount of peptide-trehalose hydrogen bonds some urea molecules are excluded from the peptide surface. This essentially reduces the interaction between peptide and urea molecules and due to this we notice a reduction in the number of peptide-urea hydrogen bond. Interestingly, the total number of peptide-solution species hydrogen bond in pure water system is very similar to that for mixed osmolytes system. From these observations we infer that in ternary solution, peptide-solution species hydrogen bonds are shared by water, urea and trehalose molecules. The presence of trehalose in mixed osmolyte system causes a significant reduction in the translational dynamics of water molecules. We discuss these results to understand the molecular explanation of trehalose's counteracting ability on urea-conferred protein denaturation.

■ INTRODUCTION

Urea is considered as a potent chemical protein denaturant. Many classical MD simulations were used extensively to study the urea-conferred denaturation of proteins and polypeptides [18, 38-41, 84, 197, 219-224]. Simulations of the protein CI2 in 8 M urea at 60°C by Bennion and Daggett [41] showed that protein rapidly unfolds in urea solution through expansion of the hydrophobic core. They also said that urea interact directly with the peptide backbone, and the average residence times for urea around the protein hydrophobic and hydrophilic residues is higher than the corresponding water residence times [41]. Moreover, Berne and co-workers [18] found from the μs MD simulations of hen egg-white lysozyme in 8 M urea solution that the dispersion interactions between urea and the protein fractions (the backbone and side-chains) is stronger than water. It causes the intrusion of urea into the protein interior and to urea's preferential binding to all regions of the protein. Further, many simulations focused on small peptides to reduce the complexity in the interactions between solution species and protein residues and provides many useful information [40, 174, 225, 226]. Pettitt and co-workers [225] simulated a decaalanine peptide with different conformation in binary urea solution and showed that protein denaturation is governed by vdW interaction. Addition of urea to pure water was shown to stabilize the extended states more than the compact helix through enhancement of more favorable protein−urea vdW interactions [225].

In recent years, the behavior of protein in aqueous solutions of urea and/or trehalose emerges as a major topic of research. Trehalose's counteracting effectiveness against the urea-conferred protein denaturation has not been studied in great details. Only recently, a few attempts have been made to understand the mechanism of the counteracting effect of trehalose on urea-induced denaturation of protein [82-84]. A MD simulation study by Zhang *et al.* [84] reported that trehalose's effectiveness exists in 1:8 molar ratio of trehalose and urea. They reported the direct interaction mechanism of urea-conferred protein denaturation. They further said that in ternary mixed trehalose/urea solution trehalose-induced protection of biomolecules comes from trehalose-induced enhancement in the water structure as well as preferential exclusion of urea and trehalose molecules from the protein surface. It is found that the exclusion of urea from the protein surface in presence of trehalose is due to the alleviation of Lennard-Jones interactions between urea and hydrophobic side chains of protein. Note that, though the results of these studies are in general consistent with each other but they lack in exploring other mechanisms

such as trehalose-induced slowing down of dynamical properties of solution species and proper quantitative estimation of average number of hydrogen bonds between protein and water molecules. The information about the later i.e., protein-water hydrogen bonds along with protein-trehalose and protein-urea hydrogen bonds provide meaningful information that could have directed us to examine if water replacement hypothesis has any role in to trehalose-induced protection of biomolecules. This fact encourages us to examine the counteracting effect of trehalose in great details. To study the molecular mechanism of urea induced counteraction, here, we have considered a 15-residue model peptide in pure water, binary urea and ternary urea/trehalose solution. The effect of urea on this protein has been studied extensively for protein folding and unfolding process [208, 209, 214]. The peptide is shown to be stable in pure water at 278 K and it unfolds completely at 385 K and partially in 8 M urea solution at 278 K [209]. To observe relatively more unfolding of the peptide in 8 M urea, we simulate the systems at 310 K, and counteracting effect of trehalose is observed in urea/trehalose mixture at that temperature. As discussed in part A of this chapter that nine residues (4-12) of the S-peptide analogue are in α helical conformation. Thus, here, we have estimated the rmsd and radius of gyration (R_g) of C_α atoms and helical percentage of residues 4-12 only. After that, we have compared the properties of the peptide in ternary urea/trehalose solution with the two other controlled simulations (pure water and 8 M urea solution). Thereafter, we considered selected site-site rdfs and hydrogen bond numbers to shed light on molecular mechanism. Finally, we explore the effect of trehalose on the translational motion of the solution species.

The rest of the chapter is as follows. We first present the models and details of simulations. After that results are discussed in the next section and this is followed by our concluding remarks with a brief summary.

■ MODELS AND SIMULATION METHOD

To investigate the counteracting ability of trehalose on urea induced protein denaturation, classical MD simulation studies have been performed considering 15 residues S-peptide in three different solutions. The stability of the peptide is examined by considering first a pure water system and then we consider an aqueous 8 M urea system at 310 K. After that a ternary aqueous solution consisting of osmolytes urea and trehalose is constructed to examine the counteracting ability of trehalose. The overviews of our systems are shown in Table 4B-1.

The starting configurations for different systems are prepared using Packmol pro-

gram [129]. The different force field parameters for water, trehalose and modified 15-residue S-peptide analogue are similar to the part A of this chapter. And, urea is considered according to Smith model [170]. To make the peptide uncharged one Na^+ ion is added.

Table 4B-1. Overview of Our Systems[a]

System	N_P	N_U	N_T	N_W	volume (nm^3)	M_U	M_T
PW	1	0	0	1100	35.28	0	0
PUW	1	250	0	1000	49.83	8.33	0
PUTW	1	250	35	800	56.18	7.40	1.04

[a] N_P, N_U, N_T, and N_W, refer to number of peptide, urea, trehalose, and water molecules respectively and M_U and M_T are the molar concentrations of urea and trehalose for the different systems.

All MD simulations are carried out using AMBER12 [90] suite of programs. First 5000 steps energy minimization is performed in which steepest decent method is used for first 2500 steps and followed by same number of steps in conjugate gradient method. Note that, during the energy minimization, we have performed two step minimization to relieve bad van der Waals contacts, first holding the peptide fixed by using harmonic restraints (force constant = 500.0 kcal mol $^{-1}$ Å^{-2}) and then removing the restraints on peptide. Subsequently, each system is heated slowly from 0 K to 310 K temperature in NVT ensemble for 100 ps where we use weak restraints (force constant = 10.0 kcal mol^{-1} Å^{-2}) to avoid the void formation in a cubic box. After that, we equilibrate the systems (without putting any constraints on peptide) for 2 ns in NPT ensemble and at 1 atm pressure. After the equilibration, we perform the production runs (in NPT ensemble) for 200 ns. Finally, we continued another 20 ns simulation run in NVE ensemble to calculate the diffusion coefficients of different solution species. The other simulation protocols and choice of different force field are discussed in **Chapter 2**.

■ RESULTS AND DISCUSSION

Protein Conformation in Different Solutions: To understand the counteracting effect of trehalose against the denaturing effect of urea on the peptide, the rmsd of C_α carbon of residues 4-12 are calculated for pure water, binary urea and ternary urea and trehalose solutions and the same are shown in Figure 4B-1 (a). In pure water, the rmsd of C_α carbon of peptide fluctuates at around 0.64 Å. It implies that the peptide remains in

helical conformation in pure water during the simulation time. In binary urea solution, the C_α rmsd is similar to that of pure water system up to 95 ns and then it increases rapidly, which indicates the denaturation of the peptide in urea solution. This urea induced peptide denaturation is in agreement with the previous simulation results [209, 227]. Interestingly, in ternary urea and trehalose solution, the C_α rmsd remains similar to that of pure water system over the simulation time, suggesting that trehalose can efficiently counteract the denaturing effect of urea.

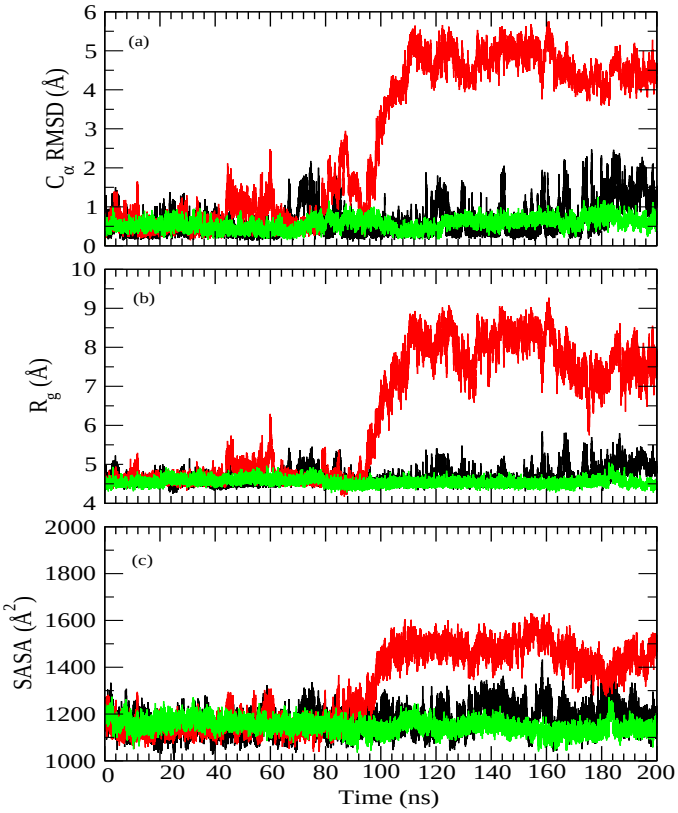

Figure 4B-1. *(a) The C_α-rmsd (root mean square deviation) and (b) the radius of gyration (R_g) of C_α carbon atoms of residues 4-12 vs. simulation time. (c) Solvent accessible surface area (SASA) of backbone of residues 4-12 vs. simulation time. The abbreviations PW (black), PUW (red) and PUTW (green) correspond to peptide-water, peptide-urea-water and peptide-urea-trehalose-water systems respectively.*

In support of the above observations, the radius of gyrations of the C_α atoms of residues 4-12 are estimated (see Figure 4B-1 (b)). It is apparent that the radius of gyrations of C_α-atoms in pure water and urea/trehalose mixture systems are very much comparable, whereas they increase after 95 ns for binary urea system. Further, we have calculated the values of solvent accessible surface area (SASA) for residue 4-12 and the same are shown

in Figure 4B-1 (c) as function of simulation time. The probe radius of 1.4 Å is used for water molecules. As is evident that SASA value for the system PW does not change as simulation progresses whereas there is a large enhancement in the SASA value for PUW system after 95 ns. These findings indicate that for the latter system the peptide residues are more exposed to the solvent molecules as compared to the former once the peptide gets denatured. The very similar SASA values for ternary PUTW system and PW system implies that trehalose molecules offset urea-conferred denaturation.

Table 4B-2. Helical Percentage of Residues 4-12 for Different Systems

residues	PW	PUW	PUTW
4	89.13	34.84	89.78
5	92.07	36.04	90.26
6	96.68	38.41	96.77
7	96.57	38.82	96.80
8	95.69	39.76	98.56
9	91.03	35.83	92.29
10	79.32	30.79	84.66
11	68.58	29.51	83.15
12	45.71	3.69	60.54

To probe the changes in the helical structure of the peptide of residues 4-12 for different solutions, the secondary structure is determined by DSSP method of Kabsch and Sander [210]. For all the systems we calculate the percentage of helicity of residues 4-12 (see Table 4B-2). In pure water, there is no significant conformational change in the helix, especially residues 4-9 are relatively stable and only minor deviation is observed for residues 10-12. In line with the previously reported results of Tirado-Rives's [208] we also find that the helix near to N-terminus residues has higher stability. Further, in accordance with previous observations [211, 212] we also observe the presence of high helical propensity of N-terminus residues (in particular for ALA4, ALA5, and ALA6). The percentage of helicity of peptide residues confirm that the peptide's native conformation is lost and the peptide gets denatured in binary urea solution. Trehalose can offset the denaturing effect of urea in ternary urea/trehalose solution and the helical structure of residues 4-12 is maintained.

In this regard, we also show the snapshots of peptide conformational changes in pure water, binary urea solution as well as ternary urea/trehalose solution systems at 50 ns time interval (see Figure 4B-2). It is evident that the conformation of the peptide changes from helix to coil in urea solution and the peptide retained its helical structure in pure water and ternary mixed osmolytes solution. All these findings indicate that trehalose can

counteract the urea conferred protein denaturation. In the following sections we present some other important structural and dynamical parameters such as the native contacts, preferential interaction parameters, hydrogen bond, diffusion coefficients etc. These parameters provide insights into the counteracting mechanism of trehalose on urea induced peptide denaturation in molecular level.

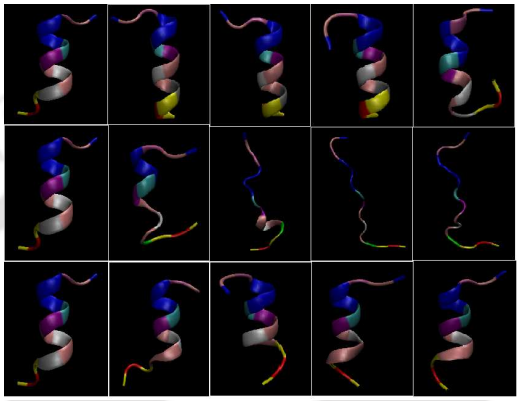

Figure 4B-2. *Snapshots for systems PW (top row), PUW (middle row) and PUTW (bottom row). For time 0, 50, 100, 150 and 200 ns, the snapshots are displayed from left to right.*

Radial Distribution Functions: To obtain the details of peptide solvation in different systems, we have computed site-site rdfs between peptide and solution species. Considering the hydration of peptide, the rdfs of water oxygen around the heavy atoms of peptide are calculated and they are shown in Figure 4B-3 (a). In pure water the appearance of first peak at about 2.85 Å indicates the presence of peptide-water hydrogen bond interaction. The relatively more prominent second peak at about 3.85 Å corresponds to hydrophobic hydration. Furthermore, these peak densities are significantly lower than the bulk density implying that water molecules are expelled from the peptide solvation shell. Note that, in nature protein folds spontaneously and exclusion of water molecules is expected. The distribution of water oxygen around the first peak of peptide heavy atoms in binary urea solution is relatively higher than pure water system. However, in ternary urea and trehalose solution, the height of the first peak is similar to the binary urea solution.

In Figure 4B-3 (b) and (c), we have shown the distribution functions involving the atomic sites of water and peptide backbone oxygen and hydrogen atoms. In pure water, we notice that first peak of water oxygen density around the backbone hydrogen is lower than the water hydrogen around the backbone oxygen. Thus, the backbone oxygens are

relatively more accessible to water molecules for hydrogen bonding interaction. Therefore, the backbone oxygen of the peptide is mostly involved in hydrogen bonding interactions between the peptide and water. Now, considering the effect of urea on these distribution functions, we observe a considerable rise of first peak height of water density around the peptide oxygen and hydrogen atoms, suggesting an increase of hydrogen bonding interaction between water and peptide in presence of urea. However, the peak density is lower than the bulk density. This enhanced hydration is likely due to the unfolding of the peptide in urea solution. Whereas, the addition of trehalose in to peptide-urea system causes a reduction in the water density around the peptide backbone hydrogen and oxygen atoms. This is due to the fact of preservation of the peptide native conformation in presence of trehalose.

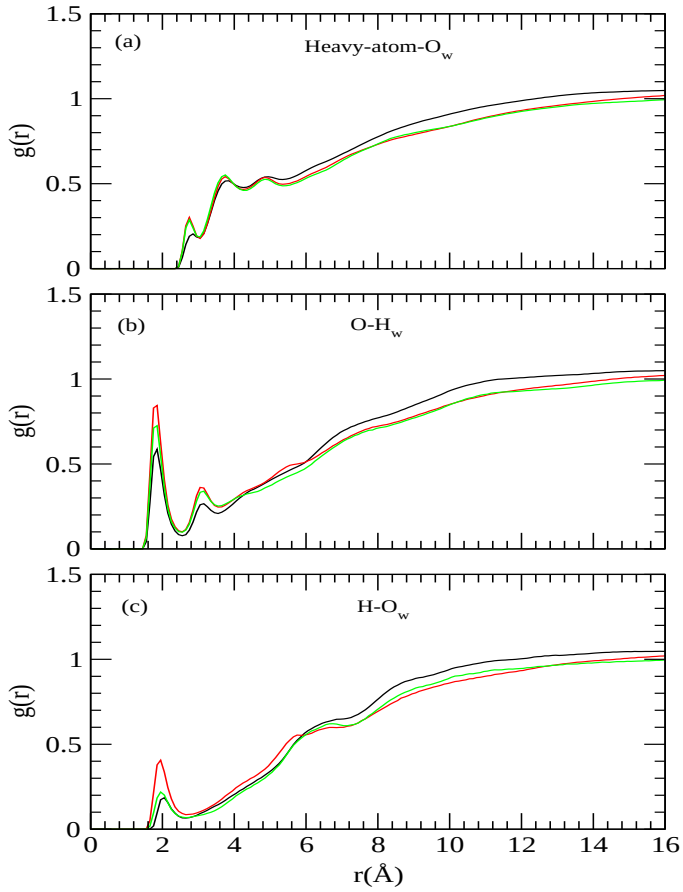

Figure 4B-3. *(a) and (b) refer to site-site distribution functions involving water oxygen and water hydrogen with respect to peptide heavy atoms and backbone oxygen of residues 4-12 respectively. (c) refer to site-site distribution functions between oxygen atom of water and hydrogen atoms of peptide backbone of residues 4-12. PW (black), PUW (red) and PUTW (green).*

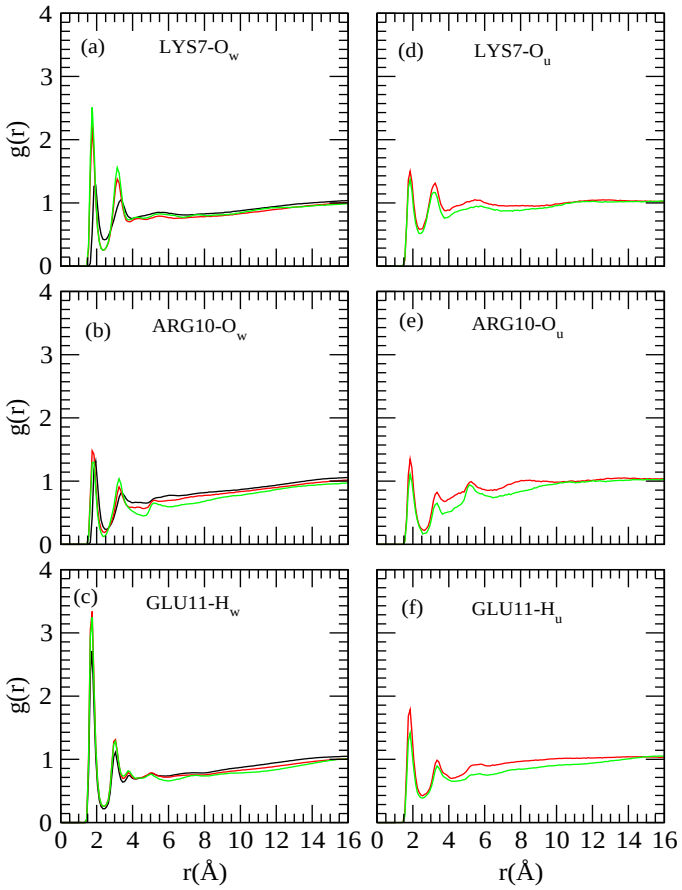

Figure 4B-4. *(a) and (b) refer to site-site distribution functions involving water oxygen and positively charged residues LYS7 and ARG10. (c) refers to rdf involving water hydrogen and negatively charged GLU11 residue. (d) and (e) are site-site distribution functions of urea oxygen around positively charged LYS7 and ARG10 residues and (f) represents distribution functions involving urea hydrogen and negatively charged residue GLU11. PW (black), PUW (red) and PUTW (green).*

we also have examined the water distribution around the positively charged peptide side chains (LYS7 and ARG10) and negatively charged side chain (GLU11) (see Figure 4B-4 (a)-(c)). As can be seen that both positively and negatively charged peptide side chains involve in hydrogen bonding interactions with water molecules. Moreover, in comparison to the pure water system, in mixed osmolytes solution (system PUTW) the heights of the first and second peak of the rdf involving positively charged side chain (LYS7) and water oxygen are getting enhanced and the first minimum becomes more deeper. Whereas, considering the effect of urea alone (system PUW), we notice that the magnitudes of these peaks are enhanced keeping the first valley remains unchanged. In case of distribution func-

tion involving positively charged side chain ARG10 and water oxygen we observe negligible influence of the presence of osmolytes on to it. Again, the distribution of water hydrogen around the negatively charged side chain (GLU11) is similar for both the binary and ternary solutions, but lower for pure water system. By comparing these three distribution functions (i.e., LYS7-water oxygen, ARG10-water oxygen and GLU11-water hydrogen) we find that the negatively charged side chain (GLU11) has the maximum tendency to form hydrogen bond with water molecules. Interestingly, these rdfs further reveal that the addition of trehalose in binary urea solution (system PUTW) increases the hydrogen bonding interaction between water and positively charged lysine side chain (LYS7) of the peptide. For other two side chains (i.e., ARG10 and GLU11), the interactions between them with water molecules remains unaffected as one moves from system PUW to system PUTW. The presence of hydrogen bonding interactions between oxygen and hydrogen atoms of urea and the positively and negatively charged side chains are also quite evident from the respective pair-correlation functions (see Figure 4B-4 (d)-(f)). In binary urea solution, the appearance of characteristic hydrogen bond first peak at 1.85 Å indicates the direct interaction of urea with peptide side chains. However, in presence of trehalose, the hydrogen bonding interaction between these side chains and urea decreases. These observations suggest the expulsion of urea molecules from the peptide surface by trehalose molecules and thereby a reduction in the denaturing effect of urea.

Further, since trehalose molecule possesses hydroxyl oxygen (and hydrogen) atoms that can participate in hydrogen bonding interactions with these side chains of the peptide we, therefore, probe this hydrogen bonding interaction by considering distribution functions involving O6 hydroxyl oxygen (and hydroxyl hydrogen) of trehalose and LYS7, ARG10 and GLU11 of peptide and the same are shown in Figure 4B-5 (a)-(c). In the same figure (Figure 4B-5 (d)-(f)) we have also shown the rdfs between heavy atoms of the peptide and hydroxyl oxygen and hydrogen atoms of trehalose. We note, the previous studies revealed that trehalose hydroxyl oxygens, O2, O3, O4 and O6, mostly participate in hydrogen bond formation. As discussed previously, the rdfs of all these hydroxyl oxygens behave in similar fashion. In view of this, we, hereby, show the rdfs involving O6 hydroxyl oxygen of trehalose and positively and negatively charged side chains of the peptide. The appearance of a strong peak at about 1.8 Å in Figure 4B-5 (a) and (c) suggests the presence of hydrogen bonding interactions between trehalose hydroxyl oxygen (and hydroxyl hydrogen) of trehalose with the peptide side chains LYS7 and GLU11. Comparing these two rdfs with the corresponding distribution functions involving urea oxygen and hydrogen atoms (Figure 4B-5 (a), (c)

vs. Figure 4B-4 (d), (f)) we notice that the distributions of urea oxygen and trehalose O6 around the peptide residue LYS7 are very similar. This implies that the interactions between LYS7 residue with trehalose and urea molecules are comparable. Together with this, a depletion in the first peak height of urea oxygen-LYS7 residue rdf in mixed osmolytes solution suggests that trehalose molecules remove some urea molecules efficiently from the peptide surface and occupy those vacant positions. Further, the interactions between trehalose and GLU11 side chain of the peptide are much stronger than that for urea.

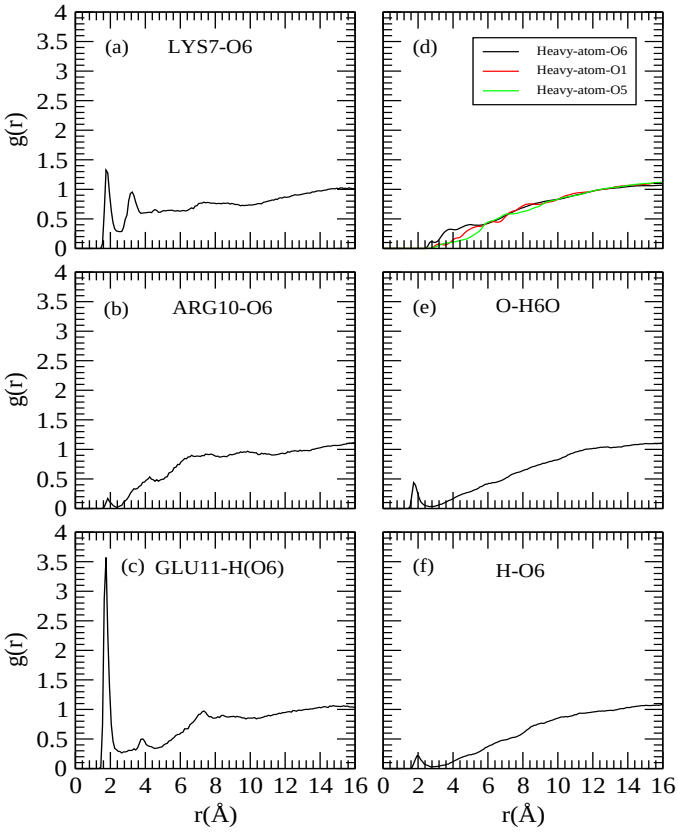

Figure 4B-5. *Site-site distribution functions (for protein-urea-trehalose-water system) involving: (a) and (b) for trehalose O6 oxygen and positively charged side chains (LYS7 and ARG10), (c) trehalose hydrogen attached to O6 oxygen and the negatively charged residue GLU11, (d) trehalose hydroxyl oxygen (O6), glycosidic oxygen (O1) and ring oxygen (O5) around the peptide heavy atoms, (e) trehalose hydroxyl hydrogen attached to O6 around peptide backbone oxygen and (f) trehalose hydroxyl oxygen (O6) around backbone hydrogen.*

Now considering the rdfs involving peptide heavy atoms and trehalose's oxygen (Figure 4B-5 (d)) we notice that the density of trehalose oxygen atom (O6) in peptide-trehalose

rdf starts at the same position as that of peptide-water rdfs. The first peak for trehalose hydroxyl oxygen atom(O6) around the peptide heavy atoms appears at 2.75 Å, which indicates the peptide-trehalose hydrogen bonding interaction. The peptide heavy atom-acetalic ring oxygen (O5) rdf behaves in similar fashion as that of peptide heavy atoms and glycosidic oxygen (O1) rdf. Moreover, in Figure 4B-5 (e) and (f), the location of the first peak indicates that hydroxyl oxygen and hydroxyl hydrogen of trehalose also participate in the hydrogen bonding interaction with the backbone oxygen and hydrogen of peptide.

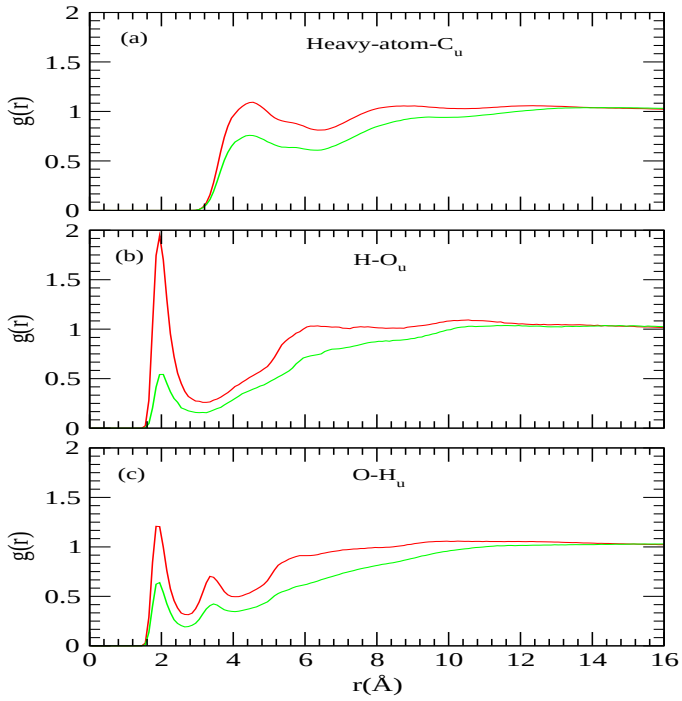

Figure 4B-6. *Site-site distribution functions involving: (a) urea carbon and the peptide heavy atoms (b) urea oxygen and peptide backbone hydrogen (c) urea hydrogen and backbones oxygen. PUW (red) and PUTW (green).*

Next, we calculate the site-site distribution functions between urea and the peptide heavy atoms of residues 4 to 12 for different systems (see Figure 4B-6). These rdfs provide information about the distribution of urea molecules around peptide heavy atoms. The distribution of urea carbon around the heavy atoms of the peptide is shown in Figure 4B-6 (a). As can be seen that this rdf starts to rise from 2.75 Å and the first peak appears at 4.55 Å. Trehalose-induced changes on this rdf is quite prominent. In specific, a prominent reduction in the peak height is observed in mixed osmolytes system suggesting the decrease of urea density around the peptide. Further, a strong hydrogen bonding interaction between

urea oxygen and hydrogen with the peptide backbone hydrogen and oxygen (see Figure 4B-6 (b) and (c)) is also visible for binary urea solution system. This hydrogen bonding interaction of urea and peptide supports the direct interaction mechanism of urea induced protein denaturation [19-23]. Now, concentrating on trehalose's effect, we find that peptide-urea interaction decreases substantially in ternary urea/trehalose solution.

The hydration pattern of the peptide residues in different solutions are further characterized by computing the number of different solution components i.e., water, urea and trehalose around the heavy atoms of residues 4-12. These numbers are calculated by considering a cutoff distance of 3.5 Å from the heavy atoms of the peptide and these are shown in Table 4B-3. We find that in pure water system, the number of water molecules around the peptide heavy atoms is 36.68. In binary urea solution this number decreases to 26.07 and with a loss of 10.61 water molecules at the peptide surface. This hydration number decreases further to 21.32 in mixed osmolytes system. A drop in the number of water molecules in the peptide solvation shell is expected purely due to reduced water number density in osmolyte solutions. To nullify the effect of reduced number density of water we calculate the coordination numbers assuming that the only change with added osmolytes came through the reduced number of water molecules and these numbers are also presented in the parentheses of Table 4B-3.

Table 4B-3. Coordination numbers for the water, urea and trehalose around the heavy atoms of residues 4-12[a]

Systems	water	urea	trehalose
PW	36.68	–	–
PUW	26.07 (23.61)	24.45	–
PUTW	21.32 (16.75)	15.21 (21.68)	4.95

[a] The coordination numbers are calculated by considering a cut off distance of 3.5 Å . The numbers given in parentheses are the coordination numbers obtained due to number density change alone of different species.

From these normalized hydration number values, we find that hydration of the peptide increases slightly (when compared to the "expected" coordination number values) in binary urea solution. This is a consequence of unfolding of peptide in binary urea solution. Interestingly, in ternary urea/trehalose solution, we observe a much higher hydration number than the "expected" value. Further, by considering the number of urea molecules that are present within 3.5 Å of peptide surface (see Table 4B-3) we find that the addition of

trehalose causes expulsion of some of the urea molecules from the peptide solvation shell. Moreover, we also observe the existence of few trehalose molecules in the peptide solvation shell in ternary solution. From these findings we infer that trehalose reduces the number of urea molecules from the solvation shell of peptide by entering into the peptide solvation shell. Trehalose induced exclusion of urea molecules from the protein surface along with the exclusion of trehalose and trehalose-induced preferential hydration of peptide has already been reported elsewhere [84].

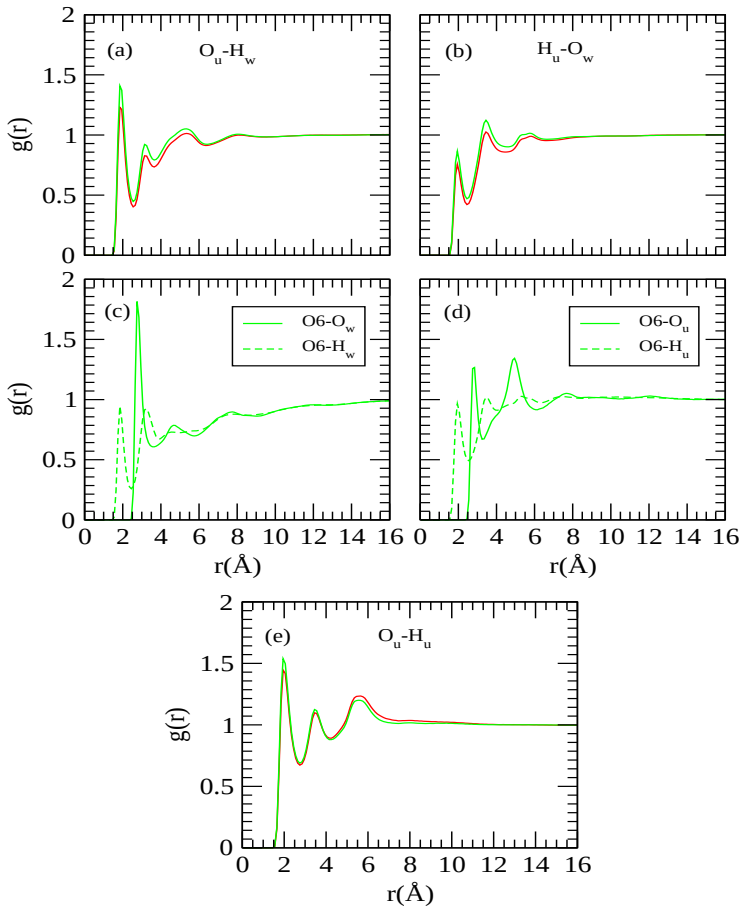

Figure 4B-7. *Site-site distribution functions involving: (a) urea oxygen-water hydrogen, (b) urea hydrogen-water oxygen, (c) O6 hydroxyl oxygen of trehalose-water atomic sites oxygen and hydrogen, (d) O6 hydroxyl oxygen of trehalose and urea (hydrogen and oxygen) and (e) urea hydrogen and urea oxygen. Lines in red and green are for systems PUW and PUTW, respectively. Rdfs involving: (a) urea carbon and the peptide heavy atoms (b) urea oxygen and peptide backbone hydrogen (c) urea hydrogen and backbones oxygen. PUW (red) and PUTW (green)*

To obtain more insights of the counteracting effect of trehalose, we have calculated

the rdfs between the solution species. These are presented in Figure 4B-7. The appearances of first contact peaks at about 1.85 Å and 1.95 Å for $O_u - H_w$ and $H_u - O_w$, respectively (see Figure 4B-7 (a) and (b)) in binary urea solution indicates the formation of urea-water hydrogen bond (where the subscript u and w correspond to urea and water respectively). The much higher magnitude of first peak for $O_u - H_w$ rdf in comparison to the $H_u - O_w$ rdf suggests that in the hydrogen bond interaction with water urea prefers to act as an acceptor rather than a donor. In mixed osmolytes solution, the peak heights of these rdfs are enhanced. Again, from Figure 4B-7 (c), we observe a significant hydrogen bonding interaction between trehalose and water molecules. We also notice the presence of an effective hydrogen bonding first peak between trehalose hydroxyl oxygen and urea (oxygen and hydrogen) (see Figure 4B-7 (d)). This hydrogen bonding interaction can be considered as one of the reason for the depletion of urea molecules from the peptide surface. The urea-urea interaction does not show much awareness of the presence of trehalose molecules in ternary solution (see Figure 4B-7 (e)).

As claimed by the results of the previous studies, [38, 228] the protein stabilization is associated with the increase in water structure and its hydrogen bonging network. To find the effect of osmolytes on the water structure, the water-water rdfs for different systems are calculated and these are displayed in Figure 4B-8. The locations of the first and second peak at 2.75 Å and 4.55 Å respectively, in pure water system, characterize the H-bonded first neighbor and tetrahedrally located second neighbor [214, 215]. Focusing on the effect of urea alone, we find that the first peak height increases without changing the peak position. In this binary solution, the much shallower first valley in this rdf causes the tetrahedral peak less prominent. Such changes in the $O_w - O_w$ rdf by urea are in line with the earlier works [38]. In urea/trehalose mixture the first peak height increases further and the second shell collapses suggesting a disruption in the water structure. It is worth to mention that from the calculations of water tetrahedral parameters Idrissi *et al.* observed urea-induced breaking of tetrahedral peak in the distribution function [229]. Interestingly, a recent MD simulation study of aqueous urea solutions reveals that in presence of urea water molecules are replaced by urea molecules and water maintains its tetrahedral network when one or more vertices of the tetrahedron is occupied by urea oxygen [230]. In the context of effect of trehalose on tetrahedral network of water molecules we note that the results of a recent study showed the breaking of water structure in presence of trehalose [231]. These findings are in line with our observation that both urea and trehalose breaks the water structure though the effect of the latter is much more pronounced than the former.

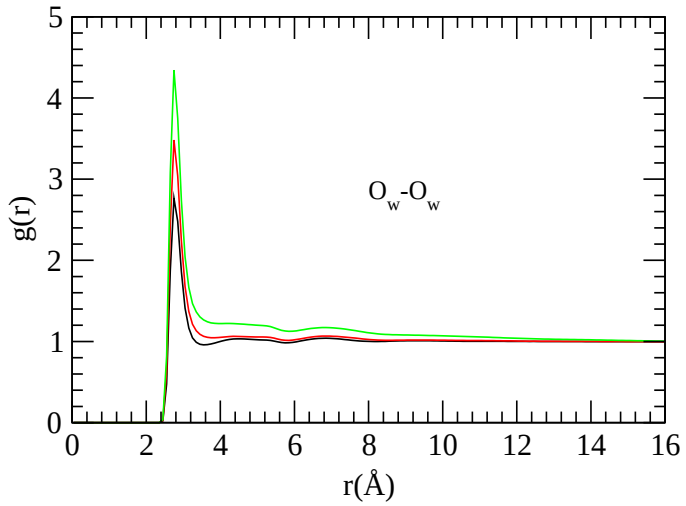

Figure 4B-8. *Site-site distribution functions involving water oxygen and water oxygen. PW (black), PUW (red) and PUTW (green)*

Preferential Interaction: Commonly, preferential exclusion of protective osmolytes such as TMAO etc. from the protein surface is considered as the reason of stabilizing effect of osmolytes [59]. The structure-protectant osmolyte molecules are excluded from the protein surface, which in turn increases the hydration of the protein and the thermodynamic stabilization of the protein are enhanced. In view of this it would be interesting to estimate the preferential interaction parameters, which provides the information about the enrichment (or exclusion) of solution species at the peptide surface. As discussed in **Chapter 2**, we have calculated the time averaged local distribution of water, urea and trehalose molecules (i.e., $g_{ow}(r)$, $g_{cu}(r)$ and $g_{ot}(r)$) by using 2.7−2.9. The relative ratio of $g_{ow}(r)$, $g_{cu}(r)$ and $g_{ot}(r)$ as a function of distance from the peptide surface are shown in Figure 4B-9. In urea solution (Figure 4B-9 (a)), $g_{ow}(r)$ is greater than one up to a distance of 4.05 Å from the protein surface and then it started to decrease. On the other hand, due to larger excluded volume of urea, the value of $g_{cu}(r)$ becomes greater than one at somewhat larger distance. In binary urea solution, $g_{cu}(r)$ starts to decrease from 5.65 Å to larger distance and from this distance $g_{ow}(r)$ starts to increase. In comparison to $g_{ow}(r)$, the relatively higher (as well as greater than one) value of $g_{cu}(r)$ suggests that protein is preferentially interacts by urea molecules in close proximity. This acts as a corroborative evidence of what we have seen in the calculations of number of urea molecules in the first coordination shell of the peptide (see Table 4B-3) where large accumulation of urea molecules in the peptide

solvation shell was observed. These results also support the denaturation of the peptide by urea molecules in which the direct mechanism is operative.

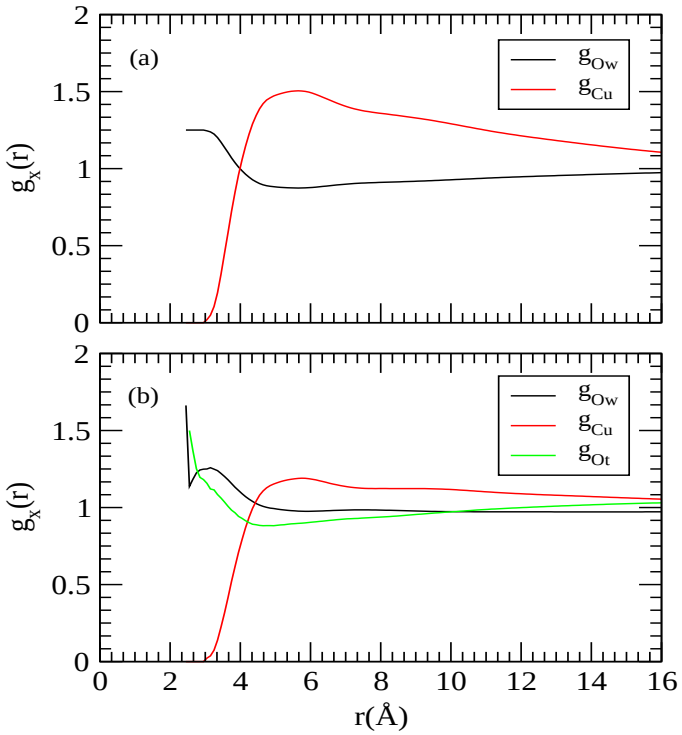

Figure 4B-9. *Time-averaged normalized fractions of water (g_{Ow}), urea (g_{Cu}) and trehalose (g_{Ot}) as a function of the distance from the peptide heavy atoms of residue 4-12. (a) For system PUW and (b) for system PUTW.*

On the other hand, in ternary urea/trehalose solution ((Figure 4B-9 (b)), the value of $g_{ow}(r)$ is greater than one and its value is higher than that of the $g_{cu}(r)$ in the close proximity of the protein. Considering the affinity of the peptide for trehalose molecules we find that at the vicinity of the peptide surface the value of $g_{ot}(r)$ is greater than one. Further, the change in its value with distance is very similar to that for water. Therefore, in mixed osmolytes solutions water and trehalose molecules are equally preferred by the peptide. Moreover, in the close proximity of peptide, the value of $g_{ow}(r)$ is higher for ternary solution than that for binary urea solution suggesting more preference for water molecules near to the peptide surface in presence of trehalose. It is also interesting to note that, $g_{cu}(r)$ value is lower for urea/trehalose mixture than binary urea solution. These results suggest that urea molecules are depleted from the protein surface in presence of trehalose. In this context it is worth noting here that our observation of trehalose-induced depletion of urea molecules

at the peptide surface are in line with the previously reported simulation results [84]. But, at the same time we note that in the context of trehalose's preference at the protein surface our results differ to them. In specific, contrary to the observations reported in Ref. 84 we observe a higher affinity for trehalose molecules (as high as that for water molecules) at the peptide surface.

Peptide-Urea Interactions and the Role of Trehalose: It is widely accepted that urea-induced protein denaturation can be explained by (i) *direct interaction mechanism* or (ii) *indirect interaction mechanism* (iii) or a combination of both (i) and (ii). The former can further be sub-divided in to electrostatic and van der Waals interactions between protein and urea molecules. The direct protein-urea electrostatic interaction suggests urea molecules interact directly with the protein backbone via H-bonds or other electrostatic interactions. Whereas, according to protein-urea direct van der Waals interactions urea molecules interact favorably with the amino acid residues of the protein through dispersion interactions. In order to understand which of these two direct interactions is dominant several studies have been carried out without any definitive conclusive results [20, 196-198]. Note that, these two direct urea-protein interaction mechanisms are not always mutually exclusive. Thus, it is important to examine the role of urea on protein denaturation from the energetics of protein-urea interaction and the role of trehalose molecules on to it. Following earlier work [84] we have decomposed the total urea-peptide interaction energy in to electrostatic and van der Waals contributions for systems PUW and PUTW. Figure 4B-10 displays the direct peptide-urea van der Waals and electrostatic energies as simulation progresses. We find that peptide-urea electrostatic energies are very similar for both PUW and PUTW systems and they do not change much with the simulation time. In contrary, the van der Waals energy for PUW system decreases from approximately -300 kJ/mol to -500 kJ/mol after 95 ns. For example, the average van der Waals and electrostatic energies are weakened by 140 kJ/mol and 81.5 kJ/mol as one moves from PUW system to PUTW system. The averaging was done for last 30 ns of simulation run. These results are in accordance with the findings of some previously reported results [225, 232, 233] where it has been found that addition of urea causes an enhancement of solvent-protein (or solute) van der Waals interactions without affecting the electrostatic interactions much. Interestingly, as trehalose is added (for system PUTW) the van der Waals interactions between peptide and urea are weakened (more positive). This is because of the fact that the presence of trehalose molecules in ternary PUTW system results in a depletion of urea molecules in the solvation shell of the peptide (see above) which in turn leads to an enhancement (more

positive) peptide-urea van der Waals interactions.

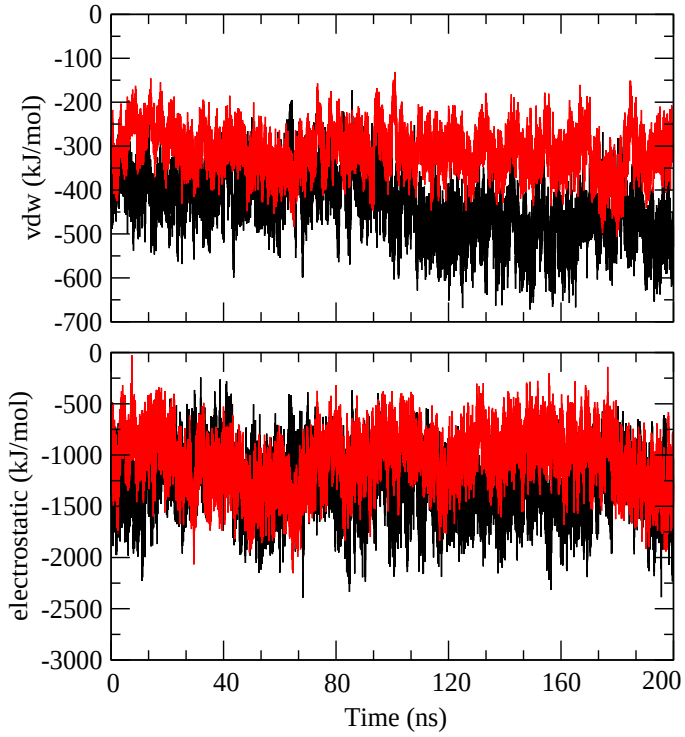

Figure 4B-10. *Intermolecular van der Waals (top) and electrostatic (bottom) energies between peptide and urea molecules as a function of simulation time for systems PUW ((black) and PUWT (red).*

Hydrogen Bond Properties: Hydrogen bonding interaction among the solution species plays an important role in protein stabilization. Therefore, the average peptide-water, peptide-urea and peptide-trehalose hydrogen bond numbers are estimated to examine the peptide solvation closely. Note that the information about the folding and unfolding state of the peptide can also be obtained from intra-protein hydrogen bonds. Moreover, we also determine the average hydrogen bond numbers between solvents and cosolvents (like water-water, water-urea and urea-trehalose etc). The average hydrogen bond numbers between the reference molecule and other molecules are calculated by adopting a geometric criteria (see **Chapter 2**). The different types of hydrogen bonds calculated in this study are summarized in Table 4B-4. In binary urea solution, the number of intramolecular hydrogen bonds in the helix of the peptide is 2.89, whereas the same is 5.70 in pure water system. It suggests the loss of helical structure of the peptide in binary urea solution. Remarkably, in ternary urea and trehalose solution, the number of intramolecular hydrogen bonds in helix of the peptide is exactly same as that of pure water system, which indicates the counteracting

effect of trehalose on urea conferred protein denaturation. Thus, the native conformation of the peptide is preserved in mixed urea/trehalose system. The retention of helical structure of the peptide acts as a corroborative evidence of what we observe in the calculations of C_α-rmsd and radius of gyration discussed above. Therefore, the helical structure of the peptide is well maintained in ternary urea/trehalose solution. The average peptide-water hydrogen bond number in pure water is 23.58 and its value decreases to 19.30 and 13.02 in binary and ternary solutions, respectively. The decrease of peptide-water hydrogen bond might be due to the formation of peptide-urea and peptide-trehalose hydrogen bonds. We find a large number of formation of urea-peptide hydrogen bonds in binary urea solution (which is about 13.63), without replacing that many number of water molecules from the peptide surface. This high accumulation of urea molecules causes the denaturation of the peptide in binary urea solution. The exclusion of urea from the peptide surface can also be observed from the large decrease of peptide-urea hydrogen bond number in presence of trehalose. For example, the peptide-urea hydrogen bond decreases from 13.63 to 7.62 when moving from binary urea solution to urea/trehalose mixture. This exclusion of urea molecules from the peptide surface is also supportive to the preferential interaction parameter calculations discussed above. We further note that the average hydrogen bond numbers formed between peptide and trehalose molecules is 4.05. Considering the fact that we have 35 trehalose molecules (against 250 urea molecules) this hydrogen bond number is significant. What is remarkable is that the total hydrogen bond number formed by peptide with water and urea increase as we move from system PW to PUW (29.28 against 35.28). But, in ternary urea/trehalose system (i.e., PUTW) this number (i.e., 30.40) is very similar to that for PW system. Remember that the number of peptide-peptide intramolecular hydrogen bonds is the same for the system PW and PUTW. These observations together with the fact that considerable amount of formation of peptide-trehalose hydrogen bonds direct us to propose that the sharing of peptide-solution species hydrogen bonds (between water, urea and trehalose molecules) contributes towards the stabilization of peptide conformation. Obviously, this proposed mechanism indirectly implies the removal of some of the urea molecules due to incorporation of trehalose molecules in the peptide solvation shell. At the same time, we note that this proposed mechanism differs from the previously reported results [84] where it was claimed that the preferential exclusion of trehalose molecules (and negligible contribution of protein-trehalose hydrogen bonds) is solely responsible for protein stabilization.

Table 4B-4. Average Number of Hydrogen bonds[a]

Systems	PW	PUW	PUTW
HB_{PP}	5.70	2.89	5.71
HB_{WP}	23.58	19.30	13.02
HB_{UP}	—	13.63	7.62
HB_{TP}	—	—	4.05
HB_{total}	29.28	35.82	30.40
HB_{WW}	3.33	2.63	2.30
HB_{WU}	—	3.43	2.74
HB_{WT}	—	—	6.90
HB_{UT}	—	—	5.61

[a] The peptide, water, urea and trehalose molecules are abbreviated as P, W, U and T respectively. The average number of hydrogen bonds (HB) are defined with respect to second species, i .e., HB_{WP}, HB_{TP} etc. represent the number of peptide-water (per peptide), peptide-trehalose (per trehalose) etc. HB_{total} is sum of HB_{PP}, HB_{WP}, HB_{UP} and HB_{TP}.

The average number of hydrogen bonds formed between trehalose and urea per trehalose is 5.61 in ternary trehalose solution. The formation of hydrogen bonds between urea and trehalose molecules can also be seen from the direct interaction of trehalose hydroxyl oxygen and urea oxygen rdf (see Figure 4B-7 (d)). This strong urea-trehalose hydrogen bonding interaction has a role in reduction of peptide-urea hydrogen bond number. We also notice the formation of large number of water-trehalose hydrogen bonds (6.90 per trehalose). The presence of significantly large number of urea-trehalose allows us to infer that the preferential solvation of trehalose molecules by urea molecules causes a reduction in the urea molecules in peptide solvation shell that are available to attack the peptide and thereby prevents its denaturation [84]. This phenomenon is similar to that of TMAO's counteracting effect against the deleterious effect of urea on protein conformation [234, 235], which states that TMAO molecules are preferentially solvated by urea through hydrogen bonding interactions and as a result the urea concentration on protein surface is reduced. This causes a reduction in the urea-protein interaction.

Diffusion Coefficients: As discussed in previous chapter, the formation of hydrogen bonded sugar network in aqueous solution influences the dynamics of the solution components. Therefore, we have computed the diffusion coefficients using Eq. 2.6. In Table 4B-5, we have presented the diffusion coefficients of water (D_w), urea (D_u) and trehalose (D_{tre}). We find that the diffusion coefficient of water D_w in pure water system is 5.18. The value of D_w decreases from 3.17 to 1.35 for binary and ternary solution, respectively. The D_w

decreases 1.63 times in binary urea solution and 3.83 times in ternary solution as compared to the pure water system. This retardation of water dynamics is due to the sugar-water hydrogen bonding interaction. In this context, it is worth to mention that according to previously reported results [159] trehalose forms stable hydrogen bonds with water molecules and thereby reduces the dynamics of water molecules present in the solvation shell of solute. Moreover, the slowing down of translational and rotational motion of surrounding water molecules by trehalose molecules is also observed from recent Terahertz absorption measurements [69]. Moreover, due to urea-trehalose hydrogen bonding interactions, the dynamics of urea decreases in ternary urea and trehalose solution.

Table 4B-5. The calculated values of diffusion coefficients for water (D_w), urea (D_u) and trehalose (D_{tre})

System	D_w $(10^{-5}cm^2sec^{-1})$	D_u $(10^{-5}cm^2sec^{-1})$	D_{tre} $(10^{-5}cm^2sec^{-1})$
PW	5.18	—	—
PUW	3.17	1.40	—
PUWT	1.35	0.41	0.03

■ SUMMARY AND CONCLUSIONS

In this part of this chapter, all atom MD simulations have been performed to investigate the counteraction of urea induced denaturation of S-peptide analogue by trehalose. From the C_α-rmsd calculation, it is found that the peptide unfolds completely in binary urea solution. By introducing trehalose to urea solution, the native structure of the peptide is well maintained. Again, the analysis of radius of gyration of C_α-atoms, solvent accessible surface area and the estimation of helicity of the residues 4-12 of the peptide are in line with the above observations. This retention of peptide helical conformation in ternary urea and trehalose solution is also noticed from the snapshots of the peptide taken at 50 ns time interval.

To understand the trehalose's counteracting effect on urea conferred protein denaturation, the site-site distribution functions considering different solution species are computed. The distributions of water molecules around the backbone hydrogens and oxygens reveal that water molecules can not easily access the backbone hydrogen atoms for hydrogen bonding interaction and in likelihood, backbone oxygen involves mostly in the hydrogen

bonding interaction with the water. The distributions of water around the positively and negatively charged side chains indicate that it is the negatively charged side chain, which has strong tendency to from hydrogen bonds with water molecules. We also notice that in comparison to the binary urea solution the distribution of urea carbon atom around the heavy atoms of peptide decreases in ternary solution. Moreover, the rdfs involving the positively and negatively charged side chain of peptide with urea oxygen and hydrogen atoms demonstrate the presence of the hydrogen bonding interaction between urea and peptide. This hydrogen bonding interaction decreases in ternary mixed urea/trehalose solution. Further, the distribution functions between these side chains (in particular LYS7 and GLU11) of the peptide and trehalose hydroxyl oxygen and hydroxyl hydrogen atoms suggest the strong trehalose-peptide hydrogen bonding interactions (as strong as that for water).

Further, we have calculated preferential interaction parameters to understand the preference of solution species towards peptide. In binary urea solution, in the vicinity of the peptide, the accumulation of urea molecules suggests that the direct interaction mechanism is operative in urea-conferred denaturation of peptide. In ternary solution, the preference of urea molecules decreases and water and trehalose molecules become more preferred at the peptide surface. To confirm this fact the number of water, urea and trehalose molecules are calculated in the peptide hydration shell. We notice that hydration of peptide decreases as osmolytes are added. The estimation of number of urea molecules in the peptide solvation shell implies a reduction in the number of urea molecules on addition of trehalose. We also find the existence of considerable amount of trehalose in the solvation shell. Further, the decomposition of urea-peptide direct interactions in to electrostatic and van der Waals contributions further reveals that the presence of trehalose in peptide-urea-trehalose solution makes the van der Waals peptide-urea interactions more unfavorable when compared to peptide-urea system without affecting peptide-urea electrostatic interactions much. We also observe depletion of water-peptide hydrogen bonds on incorporation of osmolytes. This is because of the formation of peptide-osmolyte hydrogen bonds in osmolyte solutions. The addition of a second osmolyte trehalose in to binary urea solution, decreases urea-peptide hydrogen bonds efficiently. In this context we note that, in contradiction to the previously reported results [84], we find significant amount of trehalose-peptide hydrogen bonds. Further, our study makes two important revelations: (i) the calculations of intramolecular peptide-peptide hydrogen bond number for different systems shows that the number of intra-peptide hydrogen bonds are very similar for pure water system and

ternary mixed osmolytes systems, (ii) the total number of hydrogen bonds that a peptide forms with different solution components in pure water and in ternary solutions are nearly equal. The latter observation together with the different peptide-solution species hydrogen bond numbers suggest that the peptide-water hydrogen bonds that were present in pure water system are now being shared by water, urea and trehalose molecules in ternary solution. This further directs us to propose that in the counteraction of urea-induced protein denaturation by trehalose molecules following two factors play significant role: (i) removal of urea molecules from the peptide surface by trehalose molecules (replacement of some of the urea-peptide hydrogen bonds by trehalose-peptide hydrogen bonds is also observed) and (ii) trehalose makes the urea-protein direct van der Waals interactions unfavorable Moreover, in ternary solution the formation of large number of water-trehalose and urea-trehalose hydrogen bonds further imply the solvation of trehalose molecules by water and urea. This observation lends support to the preferential solvation model, which states that in the counteraction of urea-conferred protein denaturation by the structure protectant osmolyte it is the preferential solvation of the osmolyte that prevents the attack of urea and water molecules indirectly.

The calculations of translational diffusion coefficients indicate the trehalose induced reduction of translational dynamics of solution components. As expected, we also notice that the diffusion coefficient of water is higher in absence of osmolytes and its value decreases as osmolytes are added. But, a significant reduction of water dynamics is observed for the system containing trehalose molecules.

Therefore, it can be concluded that in trehalose solution the retention of native conformation of biomolecules is ascribed primarily to replacement of some urea molecules by trehalose molecules (possibly due to the stabilization of urea in the bulk by hydrogen bonding with trehalose). This prevents the urea-conferred denaturation originating from the energy lowering due to primarily urea-biomolecule van der Waals attractive interaction. The great reduction of the translational dynamics of water molecules caused by the trehalose addition, which could be relevant to an increase in the solvent crowding, would also be a contributor.

Chapter 5

Summary and Our View on Trehalose's Protein Protecting Action

"We are at the very beginning of time for the human race. It is not unreasonable that we grapple with problems. But there are tens of thousands of years in the future. Our responsibility is to do what we can, learn what we can, improve the solutions, and pass them on."

– Richard P. Feynman

To explore the underlying mechanism of protein stabilization by trehalose at low and high temperature and in presence of urea, we systematically investigated solvation characteristics of various functional groups comprising proteins by employing classical MD simulation technique. We started our investigations using neopentane as model hydrophobic group. We have found that trehalose dissolved the neopentane molecules at low temperature and this dissolvation in presence of trehalose is reduced when the temperature is high. Thus, trehalose act as stabilizing co-solute when the temperature is high. Preferential exclusion of trehalose molecules from the neopentane solvation shell was observed with increasing trehalose concentration and high temperature has negligible effect on it. An investigation of temperature dependence structural properties of NMA (the smallest amide that represents the solvent-exposed protein backbone) and hydrogen bonds with solution species showed the replacement of NMA-water hydrogen bonds by equal number of NMA-trehalose hydrogen bonds. In the NMA-water and NMA-trehalose hydrogen bonding interactions the carbonyl oxygen of NMA participates strongly in the hydrogen bonding interaction. Our simulation of peptide at high temperature confirmed that trehalose can counteract the temperature-induced protein denaturation. We have observed the unfolding of the peptide at high temperature and this unfolding of peptide at high temperature was reduced in presence of trehalose. As a consequence, peptide maintained its intramolecular hydrogen bonds in presence of trehalose and thereby its helical structure. Interestingly, in the close proximity of the peptide trehalose molecules were more preferred over water. We also found that peptide-water hydrogen bonds were replaced by nearly equal number of peptide-trehalose hydrogen bonds. Therefore, it induced the reduction of the solvent exposed structure of the protein. The significant importance in the context of temperature-induced protein denaturation is the water replacement hypothesis [55] that causes the protein stabilization.

Urea also destabilized the hydrophobic interactions between the neopentane molecules. Correlating with the urea conferred enhancement of hydration of neopentane and its counteraction by trehalose, we observed that trehalose and urea both were excluded from the neopentane surface and trehalose helped to increase the hydrophobic association of neopentane molecules slightly. The analyses of hydrogen bond properties of NMA with the solution species showed that large number of NMA-water hydrogen bonds were replaced by NMA-urea hydrogen bonds. Specifically, the carbonyl oxygen of NMA was shared by water and urea in binary urea solution (which were occupied by water alone in pure water system). Moreover, total number of hydrogen formed by NMA molecule in binary urea solution was higher compared to that of pure water system. These results indicated direct interaction of

urea with protein residues in urea-conferred protein denaturation. That the direct protein-urea interaction plays an important role in protein denaturation by urea was also confirmed from simulations of the peptide. In binary solution of urea, water density was reduced near the peptide and urea also occupied the depleted hole created by water molecules through favorable van der Waals interaction and making preferential interaction with the peptide residues. While the peptide was dehydrated with consequent reduction of peptide-water hydrogen bonds, total number of heavy atom contacts as well as the hydrogen bond number between the peptide and solution species also increased in the presence of urea due to direct interaction of urea with the peptide residues. On other hand, upon addition of trehalose to binary urea solution, the site-site rdfs and preferential interaction parameter calculation indicated the modest decrease of urea density near to the NMA and peptide. Moreover, the depletion of urea molecules from the close proximity of peptide (or NMA) in presence of trehalose was confirmed from the decrease of favorable van der Waals interaction between urea and protein (or NMA). In the mean time, the decrease of peptide-urea (or NMA-urea) hydrogen bond relative to the binary urea solution was reflected from the slight reduction (more positive) electrostatic energy between them. This decrease of peptide-urea hydrogen bonds was well compensated by the formation of peptide trehalose hydrogen bonds. In this context, these observations direct us to propose that the counteracting effect of trehalose on urea-conferred protein denaturation comes from the replacement of peptide-urea hydrogen bonds by peptide-trehalose hydrogen bonds (supporting water replacement hypothesis).

To shed light on the mechanism of protein stabilization, we also examined various structural, and dynamical properties of the aqueous solutions. Computations of site-site rdfs showed the collapse of the water second shell in the presence of both urea and trehalose and this collapse of water second shell was also observed with the increasing temperature. Such changes by urea and trehalose indicate the urea's and trehalose's ability to act as a water structure breaker. Our analysis of hydrogen bond properties also provided the evidence for the water structure breaking capacity of both urea and trehalose. However, the effect of trehalose on water structure was more significant than the urea. As claimed previously [78, 79] the effect of trehalose on water structure is consistent with trehalose role on protein stabilization. Investigation of solvation characteristics of trehalose by solution species revealed the solvation of trehalose by both water and urea. Trehalose molecules, which participated approximately 10 to 13 hydrogen bonds with water in its binary solution, showed its inability to maintain these hydrogen bonds as urea was added and these hydrogen bonds (trehalose-water) were replaced by trehalose-urea hydrogen bonds. We observed that

hydrogen bonds formed by trehalose with water and urea were very strong. This observation supports the preferential solvation model, which states that in the counteraction of urea-conferred protein denaturation by the structure protectant osmolyte, it is the preferential solvation of the osmolyte that prevents the attack of urea and water molecules indirectly.

The calculations of translational diffusion coefficients indicated the trehalose induced slowing down of translational motion of all solution species. The diffusion coefficient of water is higher in absence of osmolytes and its value decreases in presence of osmolyte. The reduction of water and trehalose dynamics is more significant in presence of trehalose. Hence, without excluding the importance of slowing down of solution species and its indirect effect on water structure, we conclude that trehalose's ability to protect proteins at high temperature and in presence urea arises mainly due to the replacement of water molecules by trehalose molecules from the solvation shell of protein and supports water-replacement hypothesis.

Bibliography

1. Y. Zhou, C. Zhang, G. Stell and J. Wang *J. Am. Chem. Soc.* **125**, 6300 (2003).
2. M. S. Li, D. K. Klimov and D. Thirumalai *Comp. Phys. Comm.* **147**, 625 (2002).
3. Y. Xu, T. Wang and F. Gai *Chem. Phys.* **323**, 21 (2006).
4. W. Kauzmann *Adv. Protein Chem.* **14**, 1 (1959).
5. A. Pastore, S. R. Martin, A. Politou, K. C. Kondapalli, T. Stemmler and P. A. Temussi *J. Am. Chem. Soc.* **129**, 5374 (2007).
6. O. Gursky and D. Atkinson *Protein Sci.* **5**, 1874 (1996).
7. E. Paci and M. Karplus *Proc. Natl. Acad. Sci. U.S.A.* **97**, 6521 (2000).
8. Y. S. Djikaev and Eli Ruckenstein *Phys. Chem. Chem. Phys.* **10**, 6281 (2008).
9. A. Hédoux, R. Ionov, J.-F. Willart, A. Lerbret, F. Affouard, Y. Guinet, M. Descamps, D. Prévost, L. Paccou and F. Danéde *J. Chem. Phys.* **124**, 014703 (2006).
10. A. K. Lala and P. Kaul *J. Biol. Chem.* **267**, 19914 (1992).
11. K. Kuwajima *Proteins* **6**, 87 (1989).
12. J. Baum, C. M. Dobson, P. A. Evans and Claire Hanley *Biochemistry* **28**, 7 (1989).
13. P. L. Privalov *J. Mol. Biol.* **258**, 707 (1996).
14. V. Daggett Chem Rev. **106**, 1898 (2006).
15. A. Kumar and P. Venkatesu Chem Rev. **112**, 4283 (2012).
16. D. R. Robinson and W. P. Jencks *J. Am. Chem. Soc.* **87**, 2462 (1965).
17. W. K. Lim, J. Rösgen and S. W. Englander *Proc. Natl. Acad. Sci. U.S.A.* **106**, 2595 (2009).
18. L. Hua, R. Zhou, D. Thirumalai and B. J. Berne *Proc. Natl. Acad. Sci. U.S.A.* **105**, 16928 (2008).

19. B. J. Bennion, M. L. DeMarco and V. Daggett *Biochemistry* **43**, 12955 (2004).

20. E. P. O'Brien, R. I. Dima, B. Brooks and D. Thirumalai *J. Am. Chem. Soc.* **129**, 7346 (2007).

21. R. D. Mountain and D. Thirumalai *J. Am. Chem. Soc.* **125**, 1950 (2003).

22. G. I. Makhatadze and P. L. Privalov *J. Mol. Biol.* **226**, 491 (1992).

23. C. Oostenbrink and W. F. v. Gunsteren *Phys. Chem. Chem. Phys.* **7**, 53 (2005).

24. Y. Nozaki and C. Tanford *J. Biol. Chem.* **238**, 4074 (1963).

25. P. Das and R. Zhou *J. Phys. Chem. B* **114**, 5427 (2010).

26. R. Zangi, R. Zhou and B. J. Berne *J. Am. Chem. Soc.* **131**, 1535 (2009).

27. M.-E. Lee and N. F. A. van der Vegt *J. Am. Chem. Soc.* **128**, 4948 (2006).

28. E. M. Duffy, P. J. Kowalczyk and W. L. Jorgensen *J. Am. Chem. Soc.* **115**, 9271 (1993).

29. D. O. Alonso and K. A. Dill *Biochemistry* **30**, 5974 (1991).

30. M. C. Stumpe and H. Grubmüller *Biophys. J.* **96**, 3744 (2009).

31. D. B. Watlaufer, S. K. Malik, L. Stoller and R. L. Coffin *J. Am. Chem. Soc.* **86**, 508 (1964).

32. E. G. Finer, F. Franks and M. J. Tait *J. Am. Chem. Soc.* **94**, 4424 (1972).

33. A. Das and C. Mukhopadhyay *J. Phys. Chem. B* **113**, 12816 (2009).

34. H. S. Frank and F. Franks *J. Chem. Phys.* **48**, 4746 (1968).

35. F. Vanzi, B. Madan and K. Sharp *J. Am. Chem. Soc.* **120**, 10748 (1998).

36. A. Idrissi, E. Cinar, S. Longelin and P. Damay *J. Mol. Liq.* **110**, 210 (2004).

37. L. Yang and Y. Q. Gao *J. Am. Chem. Soc.* **132**, 842 (2009).

38. H. Wei, Y. Fan and Y. Q. Gao *J. Phys. Chem. B* **114**, 557 (2010).

39. H. Wei, Q. Shao and Y. Q. Gao *Phys. Chem. Chem. Phys.* **12**, 9292 (2010).

40. H. Wei, L. Yang and Y. Q. Gao *J. Phys. Chem. B* **114**, 11820 (2010).

41. B. J. Bennion and V. Daggett *Proc. Natl. Acad. Sci. U.S.A.* **100**, 5142 (2003).

42. L. J. Borowitzka and A. D. Brown *Arch. Microbiol.* **96**, 3752 (1974).

43. R. D. Bowlus and G. N. Somero *J Exp. Zool.* **208**, 137 (1979).

44. J. H. Crowe, L. M. Crowe, A. E. Oliver, N. Tsvetkova, W. Wolkers and F. Tablin *Crobiology* **43**, 89 (2001).

45. J. H. Crowe, J. F. Carpenter and Crowe LM *Annu. Rev. Physiol.* **60**, 73 (1998).

46. J.-A. Seo, A. Hédoux, Y. Guinet, L. Paccou, F. Affouard, A. Lerbret and M. Descamps *J. Phys. Chem. B* **114**, 6675 (2010).

47. A. Patist and H. Zoerb *Colloids Surf. B: Biointerfaces* **40**, 107 (2005).

48. M. Watanabe *Appl. Entomol. Zool.* **41**, 15 (2006).

49. J. F. Carpenter, M. J. Pikal, B. S. Chang and T. W. Randolph *Pharm Res.* **14**, 969 (1997).

50. B. Roser *Trend. Food Sc. Technol.* **2**, 166 (1991).

51. T. Higashiyama *Pure. Appl. Chem.* **74**, 1263 (2002).

52. J. H. Crowe, L. M. Crowe, W. F. Wolkers, A. E. Oliver, X. Ma, J. -H. Auh, M. Tang, S. Zhu, J. Norris and F. Tablin *Integr. Comp. Biol.* **45**, 810 (2005).

53. J. L. Green and C. A. Angell *J. Phys. Chem.* **93**, 2880 (1989).

54. C. A. Angell *Chem. Rev.* **102**, 2627 (2002).

55. J. F. Carpenter and J. H. Crowe *Biochemistry* **28**, 3916 (1989).

56. J. H. Crowe, S. B. Leslie and L. M. Crowe *Cryobiology* **31**, 355 (1994).

57. S. D. Allison, B. Chang, T. W. Randolph and J. F. Carpenter *Arch. Biochem. Biophys.* **365**, 289 (1999).

58. P. S. Belton and A. M. Gil *Biopolymers* **41**, 957 (1994).

59. S. N. Timasheff *Biochemistry* **41**, 13473 (2002).

60. S. Paul and S. Paul *J. Chem. Phys.* **139**, 044508 (2013).

61. A. K. Sum, R. Faller and J. J. de Pablo *Biophys J.* **85**, 2830 (2003).

62. M. Doxastakis, A. K. Sum and J. J. de Pablo *J. Phys. Chem. B* **109**, 24173 (2005).

63. C. S. Pereira and P. H. Hünenberger *J. Phys. Chem. B* **110**, 15572 (2006).

64. A. Skibinsky, R. M. Venable and R. W. Pastor *Biophys J.* **89**, 4111 (2005).

65. R. D. Lins, C. S. Pereira and P. H. Hünenberger *Proteins: Struct. Funct. Bioinf.* **55**, 177 (2004).

66. G. Cottone, G. Ciccotti and L. Cordone *J. Chem. Phys.* **117**, 9862 (2002).

67. C. Branca, S. Magazù, G. Maisano, P. Migliardo, V. Villari and A. P. Sokolov *J. Phys.: Condens. Matter* **11**, 3823 (1999).

68. C. Branca, S. Magazù, G. Maisano and P. Migliardo *J. Chem. Phys.* **111**, 281 (1999).

69. M. Heyden, E. Bründermann, U. Heugen, G. Niehues, D. M. Leitner and M. Havenith *J. Am. Chem. Soc.* **130**, 5773 (2008).

70. S. Magazù, V. Villari, P. Migliardo, G. Maisano and M. T. F. Telling *J. Phys. Chem. B* **105**, 1851 (2001).

71. T. Hottiger, C. De Virgilio, M. N. Hall, T. Boller and A. Wiemken *Eur. J. Biochem.* **219**, 187 (1993).

72. J. K. Kaushik and R. Bhat *J. Biol. Chem.* **278** 26458 (2003).

73. M. Sola-Penna and J. R. Meyer-Fernandes *Arch. Biochem. Biophys.* **360**, 10 (1998).

74. T. Uchida, M. Nagayama and K. Gohara *J. Cryst. Growth* **311**, 4747 (2009).

75. A. Hédoux, F. Affouard, M. Descamps, Y. Guinet and L. Paccou *J. Phys.: Condens. Matter* **19**, 205142 (2007).

76. A. Hédoux, J.-F. Willart, R. Ionov, F. Affouard, Y. Guinet, L. Paccou, A. Lerbret and M. Descamps *J. Phys. Chem. B* **110**, 22886 (2006).

77. A. Lerbret, P. Bordat, F. Affouard, A. Hédoux, Y. Guinet and M. Descamps *J. Phys. Chem. B* **111**, 9410 (2007).

78. S. Magazù, C. Branca, A. Faraone, F. Migliardo, P. Migliardo and G. Romeo *Physica B: Condens. Matter* **301**, 126 (2001).

79. C. Branca, S. Magazù, F. Migliardo and P. Migliardo *Physica A* **304**, 314 (2002).

80. T. E. Dirama, J. E. Curtis, G. A. Carri and A. P. Sokolov *J. Chem. Phys.* **124**, 034901 (2006).

81. N. Katyal and S. Deep *Phys. Chem. Chem. Phys.* **16**, 26746 (2014).

82. A. Kumar, P. Attri and P. Venkatesu *Int. J. Biol. Macromol.* **47**, 540 (2010).

83. G. Graziano *Chem. Phys. Lett.* **556** 292 (2013).

84. N. Zhang, F. F. Liu, X. Y. Dong and Y. Sun *J. Phys. Chem. B* **116**, 7040 (2012).

85. C. Wu, H. Lei, Z. Wang, W. Zhang and Y. Duan *Biophys J.* **91**, 3664 (2006).

86. C. Wu, Z. Wang, H. Lei, W. Zhang and Y. Duan *J. Am. Chem. Soc.* **129** 1225 (2007).

87. F.-F. Liu, X.-Y. Dong, L. He, A. P. J. Middelberg and Y. Sun *J. Phys. Chem. B* **115**, 11879 (2011).

88. J. W. Ponder and D. A. Case *Adv. Prot. Chem.* **66**, 27 (2003).

89. D. A. Case, T. A. Darden, T. E. Cheatham III, C. L. Simmerling, J. Wang, R. E. Duke, R. Luo, M. Crowley, R. C. Walker, W. Zhang, K. M. Merz, B. Wang, S. Hayik, A. Roitberg, G. Seabra, I. Kolossváry, K. F. Wong, F. Paesani, J. Vanicek, X. Wu, S. R. Brozell, T. Steinbrecher, H. Gohlke, L. Yang, C. Tan, J. Mongan, V. Hornak, G. Cui, D. H. Mathews, M. G. Seetin, C. Sagui, V. Babin and P. A. Kollman, AMBER 10, University of California, San Francisco (2008).

90. D.A. Case, T.A. Darden, T.E. Cheatham, III, C.L. Simmerling, J. Wang, R.E. Duke, R. Luo, R.C. Walker, W. Zhang, K.M. Merz, B. Roberts, S. Hayik, A. Roitberg, G. Seabra, J. Swails, A.W. Gtz, I. Kolossvry, K.F. Wong, F. Paesani, J. Vanicek, R.M. Wolf, J. Liu, X. Wu, S.R. Brozell, T. Steinbrecher, H. Gohlke, Q. Cai, X. Ye, J. Wang, M.-J. Hsieh, G. Cui, D.R. Roe, D.H. Mathews, M.G. Seetin, R. Salomon-Ferrer, C. Sagui, V. Babin, T. Luchko, S. Gusarov, A. Kovalenko and P.A. Kollman, AMBER 12, University of California, San Francisco (2012).

91. J. E. Lennard-Jones *Proc. R. Soc. London, Ser. A* **106**, 463 (1924).

92. J. D. van der Waals *Verhandelingen der Koninklijke Akademie der Wetenschappen* **1**, 1 (1893).

93. C. A. Coulomb *Collection de ḿemoires relatifs à la physique* pages 569638, Gauthier-Villars, 1884.

94. L. Verlet *Phys. Rev.* **159**, 98 (1967).

95. R. W. Hockney *Meth. Comp. Phys.* **9**, 136 (1970).

96. C. Tanford *The Hydrophobic Effect: Formation of Micelles and Biological Membranes*; Wiley: New York, 1973.

97. D. Chandler *Nature* **437**, 640 (2005).

98. N. Choudhury and B. M. Pettitt *J. Am. Chem. Soc.* **129**, 4847 (2007).

99. K. A. Dill *Biochemistry* **29**, 7133 (1990).

100. C. Narayanan and C. L. Dias *J. Chem. Phys.* **139**, 115103 (2013).

101. W. Wang *Int. J. Pharm.* **185**, 129 (1999).

102. R. A. Dimitrov and R. R. Crichton *Proteins Struct. Funct. Genet.* **27**, 576 (1997).

103. H. Li, C. Tang and N. S. Wingreen *Phys. Rev. Lett.* **79**, 765 (1997).

104. R. L. Baldwin *Proc. Natl. Acad. Sci. USA* **83**, 8069 (1986).

105. N. T. Skipper *Chem. Phys. Lett.* **207**, 424 (1993).

106. R. L. Mancera and A.D. Buckingham *Chem. Phys. Lett.* **234**, 296 (1995).

107. S. Shimizu and H. S. Chan *J. Chem. Phys.* **113**, 4683 (2000).

108. S. Lüdemann, H. Schreiber, R. Abseher and O. Steinhauser *J. Chem. Phys.* **104**, 286 (1996).

109. S. Lüdemann, R. Abseher, H. Schreiber and O. Steinhauser *J. Am. Chem. Soc.* **119**, 4206 (1997).

110. L. R. Pratt and D. Chandler *J. Chem. Phys.* **67**, 3683 (1977).

111. L. R. Pratt and D. Chandler *J. Solution Chem.* **9**, 1 (1980).

112. L. R. Pratt and D. Chandler *J. Chem. Phys.* **73**, 3434 (1980).

113. G. Ravishanker, M. Mezei and D. L. Beveridge *Faraday Symp. Chem. Soc.* **17**, 79 (1982).

114. A. Wallqvist and B. J. Berne *Chem. Phys. Lett.* **145**, 26 (1988).

115. T. Head-Gordon *Chem. Phys. Lett.* **227**, 215 (1994).

116. S. Swaminathan and D. L. Beveridge *J. Am. Chem. Soc.* **101**, 5832 (1979).

117. C. Pangali, M. Rao and B. J. Berne *J. Chem. Phys.* **71**, 2982 (1979).

118. K. Watanabet and H. C. Andersen *J. Phys. Chem.* **90**, 795 (1986).

119. A. Bartosik, M. Wiśniewska and M. Makowski *J. Phys. Org. Chem.* **28**, 10 (2015).

120. K. N. Kirschner, A. B. Yongye, S. M. Tschample, J. Gonzaález-Outeiriño, C. R. Daniels, B. L. Foley and R. J. Woods *J. Comput. Chem.* **29**, 622 (2008).

121. H. J. C. Berendsen, J. R. Grigera and T. P. Straatsma *J. Phys. Chem.* **91**, 6269 (1987).

122. W. L. Jorgensen, D. S. Maxwell and J. Tirado-Rives *J. Am. Chem. Soc.* **118**, 11225 (1996).

123. R. Sarma and S. Paul *J. Chem. Phys.* **135**, 174501 (2011).

124. X. Huang, C. J. Margulis and B. J. Berne *J. Phys. Chem. B* **107**, 11742 (2003).

125. C. A. Stortz, P. G. Jhonson, A. D. French and G. I. Csonka *Carbohydr. Res.* **344**, 2217 (2009).

126. F. Corzana, M. S. Motawia, C. H. Du Oenhoat, S. Perez, S. M. Tschampel, R. J. Woods and S. B. Engelsen *J. Comput. Chem.* **25**, 573 (2004).

127. P. Mark and L. Nilsson *J. Phys. Chem. A* **105**, 9954 (2001).

128. V. A. Verde and R. K. Campen *J. Phys. Chem. B* **115**, 7069 (2011).

129. L. Martínez, R. Andrade, E. G. Birgin and J. M. Martínez *J. Comput. Chem.* **30**, 2157 (2009).

130. H. J. C. Berendsen, J. P. M. Postma, W. F. van Gunsteren, A. DiNola and J. R. Haak *J. Chem. Phys.* **81**, 3684 (1984).

131. J.-P. Ryckaert, G. Ciccotti and H. J. C. Berendsen *J. Comput. Phys.* **23**, 327 (1977).

132. W. Humphrey, A. Dalke and K. Schulten *J. Molec. Graphics.* **14**, 33 (1996).

133. R. Sarma and S. Paul, *J. Chem. Phys.* **136**, 114510 (2012).

134. R. Sarma and S. Paul *J. Phys. Chem. B* **116**, 2831 (2012).

135. H. L. Martinez, R. Ravi and S. C. Tucker *J. Chem. Phys.* **104**, 1067 (1996).

136. G. Bonanno, R. Noto and S. L. Fornili *J. Chem. Soc., Faraday Trans.* **94**, 2755 (1998).

137. M. C. Donnamaria, E. I. Howard and J. R. Grigera *J. Chem. Soc., Faraday Trans.* **90**, 2731 (1994).

138. M. Sakurai, M. Murata, Y. Inoue, A. Hino and S. Kobayashi *Bull. Chem. Soc. Jpn.* **70**, 847 (1997).

139. P. B. Conrad and J. J. de Pablo *J. Chem. Phys. A* **103**, 4049 (1999).

140. Y. Choi, K. W. Cho, K. Jeong and S. Jung *Carbohydr. Res.* **341**, 1020 (2006).

141. S. Magazù, P. Migliardo, A. M. Musolino and M. T. Sciortino *J. Phys. Chem. B* **101**, 2348 (1997).

142. S. B. Engelsen and S. Pérez *J. Phys. Chem. B* **104**, 9301 (2000).

143. S. Chowdhuri and A. Chandra *J. Chem. Phys.* **115**, 3732 (2001).

144. R. Sarma and S. Paul *J. Phys. Chem. B* **117**, 677 (2013).

145. H. Inoue and S. N. Timasheff *Bioploymers* **11**, 737 (1972).

146. J. A. Schellman *Annu. Rev. Biophys. Biophys. Chem.* **16**, 115 (1987).

147. V. A. Parsegian, R. P. Rand and D. C. Rau *Proc. Natl. Acad. Sci.* **97**, 3987 (2000).

148. R. Giangiacomo *Food Chem.* **96**, 371 (2006).

149. L. Sapir and D. Harries *J. Phys. Chem. B* **115**, 624 (2011).

150. A. Luzar and D. Chandler *Phys. Rev. Lett.* **76**, 928 (1996).

151. A. Chandra *Phys. Rev. Lett.* **85**, 768 (2000).

152. A. Chandra *J. Phys. Chem. B* **107**, 3899 (2003).

153. Q. Liu, R. K. Schmidt, B. Teo, P. A. Karplus and J. W. Brady *J. Am. Chem. Soc.* **119**, 7851 (1997).

154. B. Guillot and Y. Guissani *J. Chem. Phys.* **99**, 8075 (1993).

155. A. Lerbret, P. Bordat, F. Affouard, M. Descamps and F. Migliardo *J. Phys. Chem. B* **109**, 11046 (2005).

156. V. Molinero, T. Çağin and W. A. Goddard III *Chem. Phys. Lett.* **377**, 469 (2003).

157. N. Ekdawi-sever, J. J. de Pablo, E. Feick and E. von Meerwall *J. Phys. Chem. A* **107**, 936 (2003).

158. D. P. Miller, J. J. de Pablo and H. Corti *Pharm. Res.* **14**, 578 (1997).

159. S. L. Lee, P. G. Debenedetti and J. R. Errington *J. Chem. Phys.* **122**, 204511 (2005).

160. S. Magazu, G. Maisano, H. D. Middendorf, P. Migliardo, A. M. Musolino and V. Villari *J. Phys. Chem. B* **102**, 2060 (1998).

161. E. Iannilli, E. Tettamanti, L. Galantini and S. Magazù *J. Phys. Chem. B* **105**, 12143 (2001).

162. M. Rampp, C. Buttersack and H. D. Lüdemann *Carbohydr. Res.* **328**, 561 (2000).

163. J. A. Rupley *J. Phys. Chem.* **68**, 2002 (1964).

164. G. G. Hammes and P. R. Schimmel *J. Am. Chem. Soc.* **89**, 442 (1967).

165. S. Shimizu and H. S. Chan *Proteins* **49**, 560 (2002).

166. D. Trzesniak, N. F. A. van der Vegt and W. F. van Gunsteren *Phys. Chem. Chem. Phys.* **6**, 697 (2004).

167. M. V. Athawale, J. S. Dordick and S. Garde *Biophys. J.* **89**, 858 (2005).

168. S. Paul and G. N. Patey *J. Phys. Chem. B* **111**, 7932 (2007).

169. S. Paul and G. N. Patey *J. Phys. Chem. B* **112**, 11106 (2008).

170. L. J. Smith, H. J. C. Berendsen and W. F. van Gunsteren *J. Phys. Chem. B* **108**, 1065 (2004).

171. G. Cottone, S. Giuffrida, G. Ciccotti and L. Cordone *Proteins* **59**, 291 (2005).

172. S. A. Galema and H. Hoeiland *J. Phys. Chem.* **95**, 5321 (1991).

173. A. M. Massari, I. J. Finkelstein, B. L. McClain, A. Goj, X. Wen, K. L. Bren, R. F. Loring and M. D. Fayer *J. Am. Chem. Soc.* **127**, 14279 (2005).

174. A. Caballero-Herrera, K. Nordstrand, K. D. Berndt, and L. Nilsson *Biophys. J.* **89**, 842 (2005).

175. C. Tanford *J. Am. Chem. Soc.* **86**, 2050 (1964).

176. Y. Liu and D. W. Bolen *Biochemistry* **34**, 12884 (1995).

177. M. Auton and D. W. Bolen *Proc. Natl. Acad. Sci. U.S.A.* **102**, 15065 (2005).

178. C. Tanford *Adv. Protein Chem.* **24**, 1 (1970).

179. D. W. Bolen and I. V. Baskakov *J. Mol. Biol.* **310**, 955 (2001).

180. M. Auton and D. W. Bolen *Biochemistry* **43**, 1329 (2004).

181. R. Zhang, H. Li, Y. Lei, S. Han *J. Mol. Struct.* **693**, 17 (2004).

182. M. Buck and M. Karplus *J. Phys. Chem. B* **105**, 11000 (2001).

183. N. S. Myshakina, Z. Ahmed and S. A. Asher *J. Phys. Chem. B* **112**, 11873 (2008).

184. L. C. Mayne, L. D. Ziegler and B. Hudson *J. Phys. Chem.* **89**, 3395 (1985).

185. G. P. Harhay and B. S. Hudson *J. Phys. Chem.* **97**, 8158 (1993).

186. Y. Wang, R. Purrello, T. Jordan and T. G. Spiro *J. Am. Chem. Soc.* **113**, 6359 (1991).

187. Y. Wang, R. Purrello, S. Georgiou and T. G. Spiro *J. Am. Chem. Soc.* **113**, 6368 (1991).

188. N. G. Mirkin and S. Krimm *J. Am. Chem. Soc.* **113**, 9742 (1991).

189. T. Köddermann and R. Ludwig *Phys. Chem. Chem. Phys.* **6**, 1867 (2004).

190. J. N. Spencer, S. K. Berger, C. R. Powell, B. D. Henning, G. S. Furman, W. M. Loffredo, E. M. Rydberg, R. A. Neubert, C. E. Shoop and D. N. Blauch *J. Phys. Chem.* **85**, 1236 (1981).

191. J. B. O. Mitchell and S. L. Price *Chem. Phys. Lett.* **180**, 517 (1991).

192. J. Kaminský, P. Bouř and J. Kubelka *J. Phys. Chem. A* **115**, 30 (2011).

193. G. Kaminski and W. L. Jorgensen *J. Phys. Chem.* **100**, 18010 (1996).

194. L. R. Pratt and D. Chandler *J. Chem. Phys.* **73**, 3430 (1980).

195. R. Sarma and S. Paul, *J. Phys. Chem. B* **117**, 569 (2013).

196. M. Auton, L. M. F. Holthauzen and D. W. Bolen *Proc. Natl. Acad. Sci. U.S.A.* **104**, 15317 (2007).

197. D. K. Klimov, J. E. Straub and D. Thirumalai *Proc. Natl. Acad. Sci. U.S.A.* **101**, 14760 (2004).

198. M. C. Stumpe and H. Grubmüller *J. Am. Chem. Soc.* **129**, 16126 (2007).

199. Z. Yang, P. Xiu, B. Shi, L. Hua and R. Zhou *J. Phys. Chem. B* **116**, 8856 (2012).

200. F. Rodríguez-Ropero and N. F. A. van der Vegt *J. Phys. Chem. B* **118**, 7327 (2014).

201. A. Hédoux, J.-F. Willart, L. Paccou, Y. Guinet, F. Affouard, A. Lerbret and M. Descamps *J. Phys. Chem. B* **113**, 6119 (2009).

202. P. Carninci, Y. Nishiyama, A. Westover, M. Itoh, S. Nagaoka, N. Sasaki, Y. Okazaki, M. Muramatsu and Y. Hayashizaki *Proc. Natl. Acad. Sci. U.S.A.* **95**, 520 (1998).

203. T. Y. Lin, S. N. Timasheff *Protein Sci.* **5**, 372 (1996).

204. G. F. Xie and S. N. Timasheff *Biophys Chem.* **64**, 25 (1997).

205. G. Xie and S. N. Timasheff *Protein Sci.* **6**, 211 (1997).

206. M. V. Fedorov, J. M. Goodman, D. Nerukh and S. Schumm *Phys. Chem. Chem. Phys.* **13**, 2294 (2011).

207. E. E. Kim, R. Varadarajan, H. W. Wyckoff and F. M. Richards *Biochemistry* **31**, 12304 (1992).

208. J. Tirado-Rives and W. L. Jorgensen *Biochemistry* **30**, 3864 (1991).

209. Z. Zhang, Y. Zhu and Y. Shi *Biophys. Chem.* **89**, 145 (2001).

210. W. Kabsch *Biopolymers* **22**, 2577 (1983).

211. S. Marqusee and R. L. Baldwin *Proc. Natl. Acad. Sci. U.S.A.* **84**, 8898 (1987).

212. S. Padmanabhan, S. Marqusee, T. Ridgeway, T. M. Laue and R. L. Baldwin *Nature* **344**, 268 (1990).

213. L. M. Crowe, R. Mouradian, J. H. Crowe, S. A. Jackson and C. Womersley *Biochim. Biophys. Acta* **769**, 141 (1984).

214. R. Sarma and S. Paul *J. Chem. Phys.* **139**, 034504 (2013).

215. R. Sarma and S. Paul, *J. Phys. Chem. B* **117**, 9056 (2013).

216. R. Walser, A. E. Mark and W. F. van Gunsteren *Biophys. J.* **78**, 2752 (2002).

217. R. Day, B. J. Bennion, S. Ham and V. Daggett *J. Mol. Biol.* **322**, 189 (2002).

218. E. S. Courtenay, M. W. Capp, C. F. Anderson and M. T. Record Jr. *Biochemistry* **39**, 4455 (2000).

219. C. Camilloni, A. Guerini Rocco, I. Eberini, E. Gianazza, R.A. Broglia and G. Tiana *Biophys. J.* **94**, 4654 (2008).

220. A. Das and C. Mukhopadhyay *J. Phys. Chem. B* **112**, 7903 (2008).

221. E. P. O'Brien, G. Ziv, G. Haren, B. R. Brooks and D. Thirumalai *Proc. Natl. Acad. Sci. U.S.A.* **105**, 13403 (2008).

222. J. Tirado-Rives, M. Orozco and W. L. Jorgensen *Biochemistry* **36**, 7313 (1997).

223. M. Gao, Z.-S. She and R. Zhou *J. Phys. Chem. B* **114**, 15687 (2010).

224. M. Eleftheriou, R. S. Germain, A. K. Royyuru and R. Zhou *J. Am. Chem. Soc.* **128**, 13388 (2006).

225. H. Kokubo, C. Y. Hu and B. M. Pettitt *J. Am. Chem. Soc.* **133**, 1849 (2011).

226. H. T. Tran, A. Mao and R. V. Pappu *J. Am. Chem. Soc.* **130**, 7380 (2008).

227. N. Kumar and N. Kishore *Biophys. Chem.* **189**, 16 (2014).

228. M. Torrent, T. Vreven, D. G. Musaev and K. Morokuma *J. Am. Chem. Soc.* **124**, 192 (2002).

229. A. Idrissi, M. Gerard, P. Damay, M. Kiselev, Y. Puhovsky, E. Cinar, P. Lagant and G. Vergoten *J. Phys. Chem. B* **114**, 4731 (2010).

230. S. Funkner, M. Havenith and G. Schwaab *J. Phys. Chem. B* **116**, 13374 (2012).

231. P. Bordat, A. Lerbret, J.-P. Demaret, F. Affouard and M. Descamps *Europhys. Lett.* **65**, 41 (2004).

232. M. Lindgren and P.-O. Westlund *Phys. Chem. Chem. Phys.* **12**, 9358 (2010).

233. Y. Karino and N. Matubayasi *Phys. Chem. Chem. Phys.* **15**, 4377 (2013).

234. B. J. Bennion and V. Daggett *Proc. Natl. Acad. Sci. U.S.A.* **101**, 6433 (2004).

235. Q. Zou, B. J. Bennion, V. Daggett and K. P. Murphy *J. Am. Chem. Soc.* **124**, 1192 (2002).

List of Publications

1. Subrata Paul and Sandip Paul, The Influence of Trehalose on Hydrophobic Interactions of Small Nonpolar Solute: A Molecular Dynamics Simulation Study. *J. Chem. Phys.* **139**, 044508 (2013).

2. Subrata Paul and Sandip Paul, Trehalose Induced Modification in the Solvation Pattern of N-Methylacetamide. *J. Phys. Chem. B* **118**, 1052 (2014).

3. Subrata Paul and Sandip Paul, Effects of the temperature and trehalose concentration on the hydrophobic interactions of a small nonpolar neopentane solute: a molecular dynamics simulation study. *RSC Advances* **4**, 34267 (2014).

4. Subrata Paul and Sandip Paul, Molecular Insights into the Role of Aqueous Trehalose Solution on Temperature-Induced Protein Denaturation. *J. Phys. Chem. B* **119**, 1598 (2015).

5. Subrata Paul and Sandip Paul, Exploring the Counteracting Mechanism of Trehalose on Urea Conferred Protein Denaturation: Molecular Dynamics Simulation Study. *J. Phys. Chem. B* **119**, 9820 (2015).

6. Subrata Paul and Sandip Paul, Investigating the Counteracting Effect of Trehalose on Urea Induced Protein Denaturation Using Molecular Dynamics Simulation. *J. Phys. Chem. B* **119**, 10975 (2015).

7. Subrata Paul and Sandip Paul, Influence of Temperature on The Solvation of N-methylacetamide in Aqueous Trehalose Solution: A Molecular Dynamics Simulation Study. *J. Mol. Liq.* **211**, 986 (2015).

8. Subrata Paul and Sandip Paul, Trehalose Induced Protection of Chymotrypsin Inhibitor from Temperature Conferred Denaturation: A Molecular Dynamics Simulation Study. (Manuscript under preparation).

Conferences Attended

1. Attended a workshop entitled *Understanding Molecular Simulation :Theory and Application* Organised by *International Center For Theoretical studies (ICTS), TIFR* held at IIT Kanpur from 3-13 November 2010.

2. Presented a poster entitled *Investigating the Influence of Trehalose on Interaction of Small Hydrophobic Solute* in the conference *Current Trends in Computational Chemistry (CTCC)* held at Department of Chemistry, North-Eastern Hill University, Shillong from 16-17 March 2012.

3. Presented a poster entitled *Investigation of Effect of Urea on Protecting Ability of Trehalose-Water Solution* in the conference *Theoretical Chemistry Symposium (TCS)* held at Department of Chemistry, IIT Guwahati from 19-22 December 2012.

4. Presented a poster entitled *The Influence of Trehalose on Hydrophobic Interactions of Small Nonpolar Solute: A Molecular Dynamics Simulation Study* in the conference *Current Trends in Theoretical Chemistry (CTTC)* held at BARC, Mumbai from 26-28 September 2013.